Zoological Journal of the Linnean Society, 2022, **196**, 845–884. With 24 figures.

Systematics and phylogeography of western Mediterranean tarantulas (Araneae: Theraphosidae)

JAN KORBA[1,2,*], VERA OPATOVA[2], ARNAU CALATAYUD-MASCARELL[1], ALBA ENGUÍDANOS[3,4], ADRIÀ BELLVERT[3,4], SILVIA ADRIÁN[3,4], ALBERTO SÁNCHEZ-VIALAS[5] and MIQUEL A. ARNEDO[3,4]

[1]*Department of Evolutionary Biology, Ecology and Environmental Sciences (Arthropods), and Biodiversity Research Institute (IRBio), Universitat de Barcelona, Av. Diagonal 643, 08028 Barcelona, Spain*
[2]*Department of Zoology, Faculty of Science, Charles University, Viničná 7, 128 43 Prague, Czech Republic*
[3]*Department of Evolutionary Biology, Ecology and Environmental Sciences (Arthropods), Universitat de Barcelona, Av. Diagonal 643, 08028 Barcelona, Spain*
[4]*Institut de Recerca de la Biodiversitat (IRBio), Universitat de Barcelona (UB), Barcelona, Spain*
[5]*Museo Nacional de Ciencias Naturales (MNCN-CSIC), Calle de José Gutiérrez Abascal, 2, 28006 Madrid, Spain*

Received 7 July 2021; revised 25 March 2022; accepted for publication 24 April 2022

Theraphosidae is the most diversified family of mygalomorph spiders, commonly known as tarantulas. Two genera inhabit the Mediterranean region: *Chaetopelma* in the east and *Ischnocolus* mostly in the western part of the Basin. Their phylogenetic position and the validity of some *Ischnocolus* species remain unclear. We implemented a multilocus target approach to shed new light on the position of both genera and further integrated molecular data with additional lines of evidence (morphology and ecology) to explore species boundaries in western Mediterranean *Ischnocolus*. Our results reveal that *Ischnocolus* and *Chaetopelma* are not closely related. *Chaetopelma* formed a clade with the African subfamily Eumenophorinae and *Ischnocolus* was recovered in a clade comprising all remaining theraphosids. The western Mediterranean *Ischnocolus* comprises two deeply divergent clades that separated during the Early Miocene and differ in both morphology and lifestyle. We found molecular, morphological and ecological evidence to restore the name *Ischnocolus mogadorensis* and revalidate this species. We also uncovered distinct allopatric lineages in *Ischnocolus elongatus*. However, the lack of males, the uniform morphology of females and low within-clade support hampered the assessment of their status and boundaries. Finally, our data support that *I. elongatus* should be considered a senior synonym of *Ischnocolus hancocki* and *Harpactirella insidiosa*.

ADDITIONAL KEYWORDS: *Chaetopelma* – Iberian Peninsula – integrative taxonomy – *Ischnocolus* – Morocco – Mygalomorphae.

INTRODUCTION

Research in systematics has become essential in the age of global biodiversity decline (Grooten & Almond, 2018). Clear species definition and correct delimitation is paramount for biodiversity assessment and conservation planning. Even though the species category is the main operational unit in biology, an agreement over its definition remains elusive (Mayr, 1982; Mayden, 1997; de Queiroz, 1998). The unified species concept proposed by de Queiroz (2007) offered an elegant solution to this situation by defining species as 'independently evolving metapopulations'. The evolutionary uniqueness of a candidate lineage should be determined based on an agreement of different lines of evidence, which attenuates the risk of confounding interspecific divergence with population structure (Carstens *et al.*, 2013; Cicero *et al.*, 2021). The current advance in molecular techniques has greatly facilitated the acquisition of molecular data in non-model organisms (Hamilton *et al.*, 2016a; Starrett *et al.*, 2017), which can be integrated along with other lines of evidence, such as morphology (Adams *et al.*, 2020), ecology and behavioural data (Caeiro-Dias

*Corresponding author. E-mail: korbajan91@gmail.com

et al., 2018), to provide grounds for species delimitation and diagnosis in an integrative taxonomic framework (Schlick-Steiner *et al.*, 2010).

The use of DNA-based methods for recognizing candidate species has greatly increased in popularity within the last two decades (e.g. Pons *et al.*, 2006; Cao *et al.*, 2016; Lukhtanov, 2019). In animals, the most used marker for species discovery and identification is the mitochondrial cytochrome *c* oxidase subunit I (*COI*), given its informativeness at shallow divergence levels, easiness of amplification and sequencing, and representation across all eukaryotes (Hebert *et al.*, 2003). However, due to the high mutational rates and extremely low rate of recombination of mitochondrial markers (Pappalardo *et al.*, 2015), the species delimitation process can easily overestimate diversity by confounding population structure with interspecific divergence. This issue is particularly acute in sedentary organisms (Vences *et al.*, 2005; Cooper *et al.*, 2011), where deep population structure can evolve even in the absence of geographic barriers (Irwin, 2002). Because of the maternal inheritance of the mitochondrial markers, gene flow may also go unrecognized in organisms with male-mediated dispersal, such as mygalomorph spiders (Hedin *et al.*, 2013; Satler *et al.*, 2013; Ortiz & Francke, 2016). Despite these limitations, *COI* sequences are widely used and considered informative for generating the initial species hypotheses (i.e. species discovery) that can be subsequently validated by additional information (Bond & Stockman, 2008; Hamilton *et al.*, 2014; Mendoza & Francke, 2017; Xu *et al.*, 2019; Rix *et al.*, 2020). The nuclear ribosomal internal transcribed spacers (ITS1, ITS2) are a valuable complement to *COI*, sometimes referred to as the second animal barcode (Yao *et al.*, 2010; Kress *et al.*, 2015). Although they are not exempt from important drawbacks (e.g. paralogy and indel mutations; Yao *et al.*, 2010), ITS markers have been successfully used for systematics in animal groups such as fish (Ali *et al.*, 2019), nematodes (Adams *et al.*, 1998; Schoch *et al.*, 2012), springtails (Anslan & Tedersoo, 2015), termites (Roy *et al.*, 2014) and mygalomorph spiders (Ortiz & Francke, 2016; Ferretti *et al.*, 2019).

The Mediterranean Basin of southern Europe, northern Africa and western Asia is a biodiversity hotspot (Mittermeier *et al.*, 2011). Its exceptional species richness is usually attributed to its dynamic geological history and to the fact that the region served as a refugium for many taxa during Pleistocene glaciations (Hewitt, 2000). Spiders of the infraorder Mygalomorphae are among the terrestrial organisms with a long evolutionary history in the Mediterranean (Opatova *et al.*, 2013; Mora *et al.*, 2017). Theraphosidae, commonly known as the 'tarantulas', are one of the eight mygalomorph families occurring in the region (WSC, 2021). They are often ground-dwelling and build silk-lined burrows. Some species are colourful, which, along with their large size, have made them popular in the exotic pet trade, bringing some species to the verge of extinction in their natural habitats (Mendoza, 2016; Mendoza & Francke, 2017). Although the family includes more than 1000 species world-wide, only three genera have been reported in the Mediterranean region (WSC, 2021). *Chaetopelma* Ausserer, 1871 includes seven species distributed in the eastern Mediterranean and the Middle East, *Harpactirella* Purcell, 1902, comprising 11 species restricted to South Africa and a single Moroccan species, and *Ischnocolus* Ausserer, 1871, which includes some of the smallest theraphosids and is represented by eight species, mostly distributed across the western Mediterranean, the Middle East, eastern Africa and the Arabian Peninsula (Montemor *et al.*, 2020).

The clarification of the systematic position of *Ischnocolus* in Theraphosidae has long been hampered by the lack of clear synapomorphies. *Ischnocolus* is the type genus of the subfamily Ischnocolinae (Simon, 1892), which were originally defined based on the presence of a divided tarsal scopula, a trait now considered plesiomorphic (Guadanucci, 2014). Subsequently, the subfamily became a dumping ground for theraphosid genera that could not be placed elsewhere and, therefore, it was considered polyphyletic (Raven, 1985). The Ischnocolinae were delimited again by Guadanucci (2014), based on a quantitative phylogenetic analysis of morphological characters. Guadanucci's newly defined 'Ischnocolinae *sensu stricto*' contains the New World genera *Acanthopelma* F.O.Pickard-Cambridge, 1897, *Reichlingia* Rudloff, 2001, *Trichopelma* Simon, 1888, part of *Holothele* Karsch, 1879 and the Old World *Ischnocolus*, suggesting closer affinities of the last to New World taxa. However, a mitochondrial analysis of theraphosid relationships (Turner *et al.*, 2018) did not recover the monophyly of *Ischnocolus* with one unidentified New World Ischnocolinae specimen. Recent multilocus molecular analyses examining relationships within Theraphosidae (target gene approach, Lüddecke *et al.*, 2018; transcriptomics, Foley *et al.*, 2019) only included single representatives of Ischnocolinae *s.s.*, preventing the corroboration of the limits of the subfamily. *Ischnocolus* was included in the phylogenomic revision of Mygalomorphae relationships (Opatova *et al.*, 2020), where it was inferred as sister to the Asian genus *Cyriopagopus* Simon, 1887. However, the limited taxon sampling (nine taxa included) hampers any conclusion about its phylogenetic placement. The close relationship between *Ischnocolus* and New World Ischnocolinae *s.s.* was recently questioned by Longhorn & Hamilton (2020), who instead hypothesized either a closer relationship to African Harpactirineae/Stromatopelminae, as potentially suggested by molecular data (Opatova *et al.*, 2020), or, alternatively, an early diverging position for *Ischnocolus*, placing it closer to Eumenophorinae. Additionally, they suggested a close relationship between *Ischnocolus* and *Chaetopelma* based on their Afro-European distribution, which had been first proposed by Smith (1990).

The genus *Ischnocolus* is represented by three currently recognized species in the western Mediterranean, namely: *I. elongatus* (Simon, 1873), *I. hancocki* Smith, 1990 and *I. valentinus* (Dufour, 1820). Guadanucci & Wendt (2014) synonymized several poorly described species to *I. valentinus*, which resulted in a broad distribution range for this taxon, spanning across Libya, Tunisia, Algeria, Western Sahara, Morocco up to the Iberian Peninsula, as well as some Mediterranean islands, such as Sicily and Lampedusa (Caporiacco, 1937; R. Kaderka & F. Polakovič, pers. obs.). This species excavates or opportunistically inhabits natural cavities between or under rocks and tree roots and lines them with silk. *Ischnocolus elongatus* (Simon, 1873), described from Ksar el Kebir (north-western Morocco), differs from *I. valentinus* in lifestyle. The original description mentioned its unusual burrow entrance, consisting of a prolonged silk tube connected with grass above the ground (Simon, 1873: 33–34). The third valid species, *I. hancocki* Smith, 1990, was described from female material from Larache (NW Morocco), approximately 30 km from the type locality of *I. elongatus*. Zonstein (2018) added the description of a male, from El Jadida (Moroccan central coast) and suggested the possible synonymy between *I. hancocki* and *I. elongatus*, based on the proximity of the localities and the possession of an unusually short apical segment of the posterior lateral spinnerets (PLS).

Interestingly, the same type of unique burrow architecture observed in *I. elongatus* was also reported in the genus *Luphocemus* Denis, 1960 (type species *Luphocemus insidiosus* Denis, 1960), described from two females from north-western Morocco (Sokhrat Nemra and Boulhaut/Benslimane). This monotypic genus was subsequently considered a junior synonym of *Harpactirella* (Benoit, 1965), a genus otherwise restricted to South Africa (WSC, 2021). A recent study has provided additional information on the natural history of *Harpactirella insidiosa* and expanded its range (Calatayud-Mascarell & Sánchez-Vialas, 2020) without critically evaluating its generic placement.

The aim of the present study is to: (1) shed new light on the phylogenetic position of the Mediterranean genera *Ischnocolus* and *Chaetopelma* within the family Theraphosidae by using a multilocus target gene approach; (2) infer the phylogeographic patterns and temporal diversification of western Mediterranean *Ischnocolus*; and (3) explore its species boundaries by integrating genetic, morphological and ecological data. Our results will provide a better understanding of a unique yet poorly known component of the Mediterranean spider fauna.

MATERIAL AND METHODS

Taxon sampling and species identification

We collected *Ischnocolus* specimens from 43 localities (Fig. 1; Supporting Information, Table S1). Two additional *Ischnocolus* sequences were retrieved from GenBank. *Tliltocatl vagans* (Ausserer, 1875) sequences from GenBank (Longhorn *et al*., 2007), along with two newly sequenced *Chaetopelma* samples from Cyprus and Israel, were used to root the tree in the phylogeographic analyses. To assess the monophyly of *Ischnocolus*, its position within Theraphosidae and its relationship with the Mediterranean *Chaetopelma*, we combined representatives of the main lineages identified within *Ischnocolus* (see phylogeographic analysis), the two Chaetopelma samples and all sequences from Lüddecke *et al*. (2018). Further, we complemented the matrix by two additional sequences from Wheeler *et al*. (2017) (see Supporting Information, Table S1 for GenBank accession numbers), representing the families Bemmeridae and Barychelidae, recovered as the closest relatives to Theraphosidae by Opatova *et al.* (2020).

The specimens were pre-sorted into two distinct groups in the field based on their different lifestyles. Specimens living under stones, inhabiting cavities among rocks and tree roots and sometimes constructing funnel-like webs, hereafter referred to as '*valentinus* morphotype', were later identified as *I. valentinus* based on morphological characters described in Guadanucci & Wendt (2014). Specimens displaying a strictly burrowing lifestyle, more robust body and shorter posterior lateral spinnerets (PLS) with triangular apical segment, hereafter referred to as '*elongatus* morphotype', were later identified as *I. elongatus* based on published information (Simon, 1873; Ausserer, 1875; Smith, 1990; Zonstein 2018) (see Taxonomy section for justification).

Specimens were examined under a Leica MZ16A dissection stereomicroscope. Digital images were taken with a high-resolution digital camera LEICA DFC 450 attached to the microscope and controlled by the software Leica Application Suite v.4.4 (Leica Microsystems Ltd, Switzerland). Legs III and IV were removed and stored in 96% ethanol –20 °C for subsequent DNA analyses. The remaining parts were preserved in 70% ethanol for morphological analysis and as voucher specimens and stored at the Centre de Recursos de Biodiversitat Animal in the University of Barcelona (CRBA), Catalonia, Spain. The map of localities was created with QGIS (QGIS Development Team, 2020).

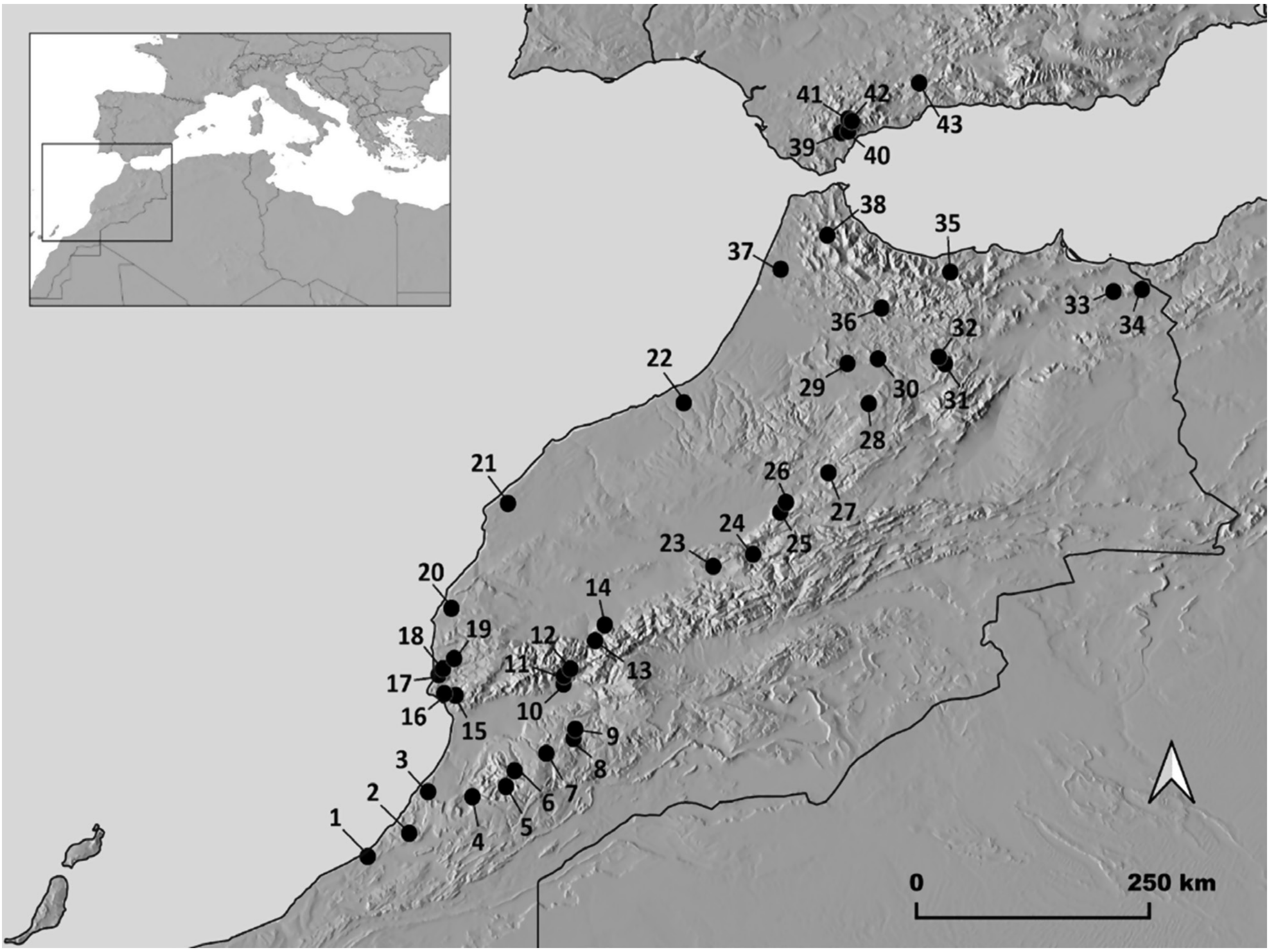

Figure 1. Map of sampled localities in Morocco and the Iberian Peninsula. Numbers correspond to localities as in the Supporting Information, Table S1.

Table 1. Maximum intra-lineage (diagonal, bold) and minimum inter-lineage uncorrected genetic distances calculated with *COI* sequences for *Ischnocolus*

Lineage	valen_north	valen_south	elong_north	elong_south	elong_central	elong_north-east
valen_north	**0.1667**					
valen_south	0.1337	**0.1185**				
elong_north	0.1443	0.1276	**0.1260**			
elong_south	0.1275	0.1292	0.1003	**0.1324**		
elong_central	0.1387	0.1172	0.9960	0.8790	**0.1292**	
elong_north-east	0.1259	0.1284	0.1058	0.9570	0.8060	**0.1475**

Molecular procedures

Whole genomic DNA was extracted from leg III or IV using the SpeedTools Tissue Extraction Kit (Biotools B&M Labs SA, Spain) following the manufacturer's protocol. The 5′ half of the mitochondrial cytochrome *c* oxidase I (*COI*) was amplified in 94 *Ischnocolus* (approx. two per locality) and the two *Chaetopelma* specimens.

One to two specimens per locality/*COI* lineages identified in the preliminary *COI_96* data matrix analyses (see below, tree not shown), totalling 49 specimens, were selected for subsequent amplification of the nuclear internal transcribed spacer (ITS2). Finally, the remaining mitochondrial and nuclear regions targeted in Lüddecke *et al.* (2018) (12S, 16S, 18S, 28S and *H3*) were amplified in eight specimens representing the six main *Ischnocolus COI* lineages (see Results) and the two *Chaetopelma* specimens. All polymerase chain reactions (PCRs) were carried out in 20 µL reaction volume, which included 12.4 µL of distilled H_2O, 5 µL of buffer, 0.2 µL of Taq DNA polymerase (Bioline) and 0.2 µL of respective primers (Supporting Information, Table S2). The purified PCR products were sequenced in both directions at Macrogen Inc. (Madrid, Spain).

Sequence editing, alignment and matrix construction

Raw sequences were edited, assembled and manipulated in GENEIOUS v.10.1.2. (Biomatters Ltd). Sequences were automatically aligned with the MAFFT v.7.309 (Katoh *et al.*, 2002) plugin available in GENEIOUS, using the G-INS-i algorithm. Protein-coding sequences were translated to amino acids to rule out the presence of stop codons. Individual gene sequences were concatenated in GENEIOUS. Four different matrices were built for downstream phylogenetic analyses. The *COI_96* data matrix contained 94 *Ischnocolus* (including two sequences from GenBank) and two *Chaetopelma COI* haplotypes. The *ITS2_50* data matrix contained 49 ITS2 sequences of *Ischnocolus* and a single one of *T. vagans*, which was used as an outgroup, because *Chaetopelma* specimens did not amplify the ITS2 successfully. The *All_Ischnocolus* data matrix included the concatenation of the *COI_96* matrix and *ITS2_50*, with an additional *COI* sequence of *T. vagans*. Finally, *All_Theraphosidae* contained the concatenation of six genes for a total of 61 taxa: 51 taxa (49 theraphosids + two outgroups) retrieved from Lüddecke *et al.* (2018), eight *Ischnocolus* and two *Chaetopelma* specimens sequenced in this study and samples of *Homostola pardalina* (Hewitt, 1913) and *Synothele arrakis* Raven, 1994 from Wheeler *et al.* (2017) as outgroups for rooting the tree.

Phylogenetic analyses

Phylogenetic analyses were conducted under maximum parsimony (MP) (only for the *All_Theraphosidae* matrix), maximum likelihood (ML) and Bayesian inference (BI). MP analysis was performed in PAUP* v.4.0a (Swofford, 2003) with 2000 bootstrap replicates, each with ten random-addition sequence replicates and tree bisection and reconnection branch swapping. For model-based analyses, the best partition scheme and evolutionary model for each partition was selected with PartitionFinder v.2.1.1 (Lanfear *et al.*, 2017). ML analyses were conducted with IQ-TREE v.1.6 (Nguyen *et al.*, 2015) starting from 100 independently inferred parsimony trees with the best-fit model of the matrix determined using ModelFinder (Kalyaanamoorthy *et al.*, 2017), as implemented in IQTREE; support values were assessed from 1000 replicates of ultrafast bootstrap (Hoang *et al.*, 2018).

Bayesian analyses were conducted with MrBayes v.3.2.6 (Ronquist & Huelsenbeck, 2003), and models and partitions were set as proposed by PartitionFinder. For each dataset, the analyses consisted of two independent runs of 10 million generations with four Markov chain Monte Carlo (MCMC) each, starting from random trees and sampling every 1000 generations. The first 25% of the runs were discarded as burn-in. Chain convergence and mixing was assessed by monitoring the standard deviation of split frequencies (< 0.01) and ESS values (< 200) in TRACER v.1.7 (Rambaut *et al.*, 2018). All trees were manipulated in FigTree (Rambaut, 2009, http://tree.bio.ed.ac.uk/software/figtree/) and edited in INKSCAPE (https://inkscape.org/) for aesthetic purposes.

Estimation of divergence times

Divergence-time estimation analyses were performed in BEAST v.1.8.2 (Drummond, 2012) both for *Ischnocolus* (using the concatenated *All_Ischnocolus* matrix) and for all Theraphosidae (*All_Theraphosidae* matrix). We implemented the time estimates inferred in Opatova *et al.* (2020) for calibrating the *All_Theraphosidae* matrix as follows: the split between Barychelidae and Theraphosidae inferred at 107 million years ago (Mya) (118–103, 95% HPD) was assigned a normal distribution (mean = 107, standard deviation = 7); split between Bemmeridae and Barychelidae + Theraphosidae inferred at 134 Mya (139–126), normal distribution (134, 5); Nemesioidina inferred at 115 Mya (120–107), normal distribution (115, 5). The *Cretamygale chasei* Selden, 2002 fossil, dated at 125 Mya (Selden, 2002), currently classified as Nemesiidae, was conservatively assigned as the minimum bound for the split between Bemmeridae + Barychelidae + Theraphosidae and 'Nemesioidina' clades. The maximum bound was assigned 242 Mya, corresponding to the age of *Rosamygale* Selden & Gall, 1992, the oldest mygalomorph fossil. Due to lack of fossils, and to avoid circular reasoning in using internal biogeographic events as calibration points, we relied on informative priors on the substitution rates of the *COI*. Although recent estimates of *COI* substitution rates for theraphosids are available in the literature (e.g. Ortiz *et al.*, 2018), we inferred values from the *All_Theraphosidae* analyses. We implemented the rate information as a normal distributed prior assigned to the *COI* ucld.mean parameter of the log-normal relaxed clock. A wide uniform prior to ucld.mean with lower and upper bounds 0.0001 and 0.199, respectively, was assigned to the nuclear fragment to reduce the parameter space.

In both analyses, partitions and models were set as proposed by PartitionFinder. Unlinked, relaxed, log-normal clocks were assigned for each fragment, and the birth–death speciation process was set as a tree prior. Three independent runs of 150 and 10 million generations each were conducted for the *All_Theraphosidae* and the *All_Ischnocolus* matrices, respectively. Chain convergence and correct mixing of chains was checked in TRACER. Individual runs were combined in LogCombiner, discarding the first 10% of generations of each run as burn-in. A consensus chronogram was obtained with TreeAnnotator (Drummond, 2012).

Species delimitation

Both distance and tree-based delimitation methods were employed. The distance-based automatic barcode gap discovery (ABGD) (Puillandre *et al.*, 2012) was applied to the *COI_96* and *ITS2_50* datasets, independently. The same parameters used in former delimitation studies on mygalomorphs (Hamilton *et al.*, 2014; Leavitt *et al.*, 2015) were used for comparative purposes (Pmin = 0.0001, Pmax = 0.200, Steps = 10, X = 1, Nb bins = 20, simple distance). Similarly, we applied the general mixed Yule coalescent (GMYC) method (Fujisawa & Barraclough, 2013) to the *COI* and ITS2 datasets, separately. Ultrametric gene trees were inferred with BEAST, assigning the best partition scheme and model as suggested by PartitionFinder, a constant coalescence tree prior and ucld.mean fixed to 1. Outgroups were removed before GMYC analyses using the drop.tip function in R package 'APE' (Paradis *et al.*, 2004). GMYC models were estimated with the R package 'SPLITS' (Fujisawa & Barraclough, 2013). Analyses were conducted in R Studio (RStudio Team, 2019). Multi-rate Poisson tree processes (mPTP) (Kapli *et al.*, 2017) analyses were conducted on gene trees obtained with IQTREE, using 1000 iterations. The command line version of mPTP was used to implement a MCMC approach to estimate support values for the delimitations, using three runs of 50 million generations each and discarding the first two million as burn-in. The uncorrected pairwise genetic distances for each gene were estimated in MEGA v. 7 (Kumar *et al.*, 2015).

Morphological analyses

Male copulatory bulbus and spination on tibia I, constituting the main diagnostic characters used in *Ischnocolus* taxonomy (Guadanucci & Wendt, 2014), were examined in the males available for this study. The shape of the spermatheca is the most widely used diagnostic trait in theraphosid females (Hamilton *et al.*, 2011; de Oca *et al.*, 2016; Ortiz & Francke, 2017). The vulva of adult females representing the six most divergent lineages observed (see below) was dissected and enzymatically digested in pancreatin and borax solution, following Álvarez-Padilla & Hormiga (2008), and photographed with a THORLABS C-mount CML15 lens attached to a ZEISS Axio LAB.A1 (Carl Zeiss Microscopy GmbH, Germany) stereomicroscope. Images for stacking were mounted with the software Helicon Focus (Helicon Soft, Ltd). Descriptions of leg spination followed Bertani (2001). All measurements were recorded in millimetres. Lengths of leg segments were taken from the mid-proximal point of articulation to the mid-distal point of the article (Bond, 2012). Appendage measurements were based on left appendages in retrolateral view. Width of carapace, labium and sternum corresponded to the maximum values obtained. The following abbreviations are used: ALE, anterior lateral eyes; AME, anterior median eyes; AP, apical; D, dorsal; P, prolateral; PLE, posterior lateral eyes; PLS, posterior lateral spinnerets; PME, posterior median eyes; R, retrolateral; V, ventral.

The following institutional abbreviations are used: CRBA, Centre de Recursos de Biodiversitat Animal at the University of Barcelona, Catalonia, Spain; BMNH, British Museum of Natural History, London, United Kingdom; MNHN, Muséum National d´Histoire Naturelle, Paris, France; SMNS, Staatliches Museum für Naturkunde Stuttgart, Germany.

Additional morphological traits other than genitalia were investigated by means of geometric morphometric (GM) methods. Based on the observation made during the sorting process, the prosoma shape in dorsal view, the height of the cephalic region in lateral view and the apical segment of the posterior lateral spinnerets (PLS) were considered as potentially informative to delimit the main lineages. Due to sex dimorphism in prosoma shape and the limited number of males, GM analyses were only performed on females. For the carapace analysis, 29 subadult and adult female specimens, representing the main groups found in the phylogenetic analyses (see Results), were included. Legs were removed before imaging to facilitate lateral placement and spiders were submerged into silica gel to secure homologous view. Two pictures (dorsal and lateral views) were taken from each specimen. For the dorsal view, three fixed landmarks and 50 semi-landmarks were recorded. All landmarks were placed in homologous structures: two in each anterior margin, where the carapace joins the chelicerae, and one in the middle of the opposite margin of the carapace, where it connects with the abdomen (see section Geometric morphometric analyses). All semi-landmark points were spaced equidistantly between them. For the lateral view, the same number of landmarks and semi-landmarks were used, i.e. one landmark in the posterior margin of the prosoma, where it joins the abdomen, one on the most anterior point of the prosoma ventral side and one on the top of the clypeus (see section Geometric morphometric analyses). The GM analyses of the PLS shape were restricted to the *elongatus* morphotype as we lacked sufficient adult females of the *valentinus* morphotype with well-conserved PLS. Two pictures (lateral and dorsal) were taken for each PLS of the 28 females sampled, belonging to the six lineages. Five fixed landmarks were defined and recorded: four on each margin of the median segment and one at the top of the apical segment of the PLS (see section Geometric morphometric analyses).

TPSUTIL v.178 and TPSDIG2 v.2.30 (Rohlf, 2008) software were used to digitize the landmarks. Digitized files were analysed using the 'geomorph' package (Adams *et al.*, 2021; Baken *et al.*, 2021) in the R environment (R Core Team, 2021). For removing the non-shape variation, each dataset was subjected to a generalized Procrustes analysis (GPA: Gower 1975; Rohlf & Slice, 1990) using the function *gpagen* and the coordinates of each dataset were retained for the subsequent analysis of shape variation. Principal component analysis (PCA) was performed using the function *gm.prcomp* and the two first principal components (PC) were used to visualize the shape variation. To test for significant shape differences between distinct clades, a Procrustes ANOVA using distributions generated from a resampling procedure based on 1000 permutations using the function *procD.lm* (Adams *et al.*, 2021; Baken *et al.*, 2021) was performed. Plots generated in R were edited for aesthetic purposes in INKSCAPE.

Species distribution modelling

The potential geographic distribution range of five different lineages of *Ischnocolus* (see Results) was inferred with MAXENT 3.4.0 (Phillips *et al.*, 2017), which estimates the interaction between environmental variables and species presence in a geographic area in order to create suitability models. The analyses were based on all known localities from Morocco and the Iberian Peninsula (Guadanucci & Wendt, 2014; Tamajón Gómez *et al.*, 2020; this study) for lineages where at least six records were available.

Nineteen bioclimatic layers were retrieved from the WorldClim 2.1 database (www.worldclim.org) at 2.5 minutes resolution (Fick & Hijmans, 2017). A subset of bioclimatic variables was selected based on the results of a correlation analysis using the R package 'corrgram' (Wright, 2006), namely annual mean temperature = Bio1, mean diurnal range [mean of monthly (max. temp.–min. temp.)] = Bio2, max. temperature of warmest month = Bio5, annual precipitation = Bio12, precipitation of driest quarter = Bio17. Analyses in MAXENT software were conducted with 25 replicates for each lineage using the cross-validation testing procedure recommended for small datasets (Philips *et al.*, 2006). MAXENT output was set to Cloglog, which gives an estimate between 0 and 1 for probability of presence. The MAXENT outputs were further edited with QGIS 3.8.3 Zanzibar (www.qgis.org) to generate distribution maps.

Potential ecological interchangeability among the different lineages within the two main clades, measured as niche overlap, was evaluated with the Schoener's D-metrics (Wooten & Gibbs, 2012) by conducting pairwise comparisons. Niche identity tests were performed using 100 randomized pseudoreplicates to determine if the Schoener's D-values from the species distribution models were statistically different (one-tailed test) than expected under the null distribution. Niche conservatism or divergence was inferred by comparing the niche overlap values with the null distribution of overlap values. Niche divergence is supported when the niche overlap values are smaller than the null distribution. Analyses were conducted with ENMTOOLS 1.3 (Warren *et al.*, 2010).

RESULTS

Data matrices

The *COI_96* matrix included 658 bp, 125 variable (v) and 105 parsimony informative sites (pi). The *ITS2_50* matrix included 686 aligned positions (28 v, 22 pi). The concatenation of the two former matrices (*All_Ischnocolus)* resulted in 1354 characters. The concatenated supermatrix *All_Theraphosidae* contained in total 4419 aligned positions (658 bp of the *COI*, 1077 positions of 16S, 431 of 12S, 841 of 28S, 1072 of 18S and 340 bp of *H3*, respectively).

Phylogeny and diversification timeline of the family Theraphosidae

The best partitions with their respective evolutionary models are listed in the Supporting Information, Table S3. The consensus chronogram recovered in BEAST, with mapped support values from trees inferred in time-stamped (BEAST) and unconstrained (MRBAYES) Bayesian inference, maximum likelihood (IQTREE) and parsimony (PAUP*), is shown in Figure 2 (see Supporting Information, Figs S1–S4 for trees from each analysis separately).

The inclusion of the *Ischnocolus* and *Chaetopelma* samples, along with the representatives of the families Barychelidae and Bemmeridae, did not have a significant impact on the results reported by Lüddecke *et al.* (2018). Major differences corresponded to relationships that already received low support in the original analyses, including the position of the

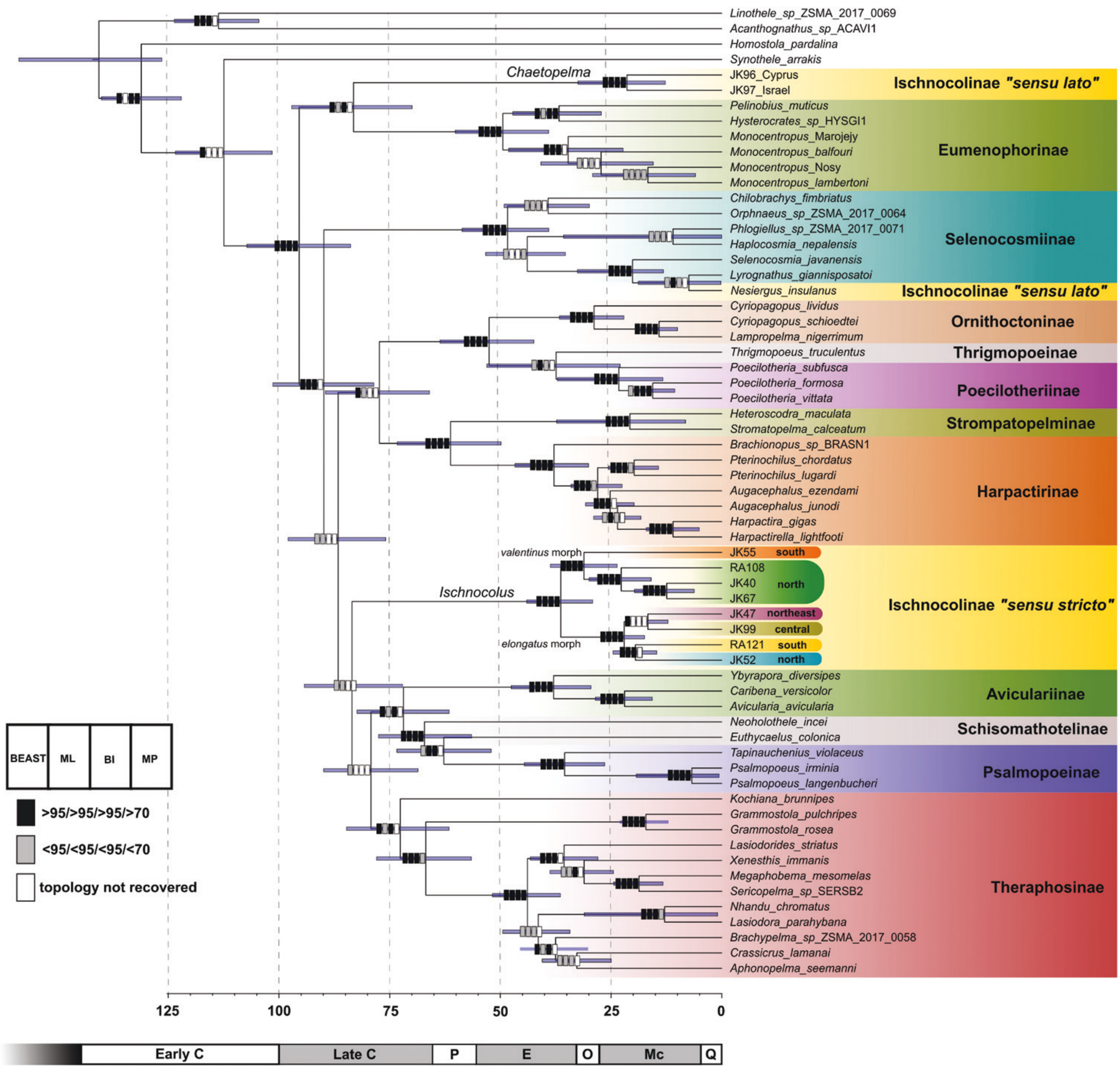

Figure 2. Time-calibrated phylogeny of family Theraphosidae inferred by BEAST using six genes (12S, 16S, *COI*, 18S, 28S and *H3*). Boxes indicate node supports from BEAST (posterior probability, PP), maximum likelihood (ML, ultrafast bootstrap proportions UFBoot), MrBayes (BI, posterior probability) and parsimony (MP, bootstrap proportions BS). Supports are summarized as follows: black = supported (PP > 0.95, UFBoot > 0.95, BS > 0.70), grey = recovered but support values below thresholds, white = not recovered. The axis is in millions of years.

Theraphosinae and the Selenocosmiinae – our results recovered all Neotropical subfamilies as a monophyletic group (including Theraphosinae, Aviculariinae, Schisomatohotelinae and Psalmopoeinae) and the subfamily Selenocosmiinae as a sister-group to all the remaining Theraphosidae, except *Chaetopelma* and Eumenophorinae.

The phylogenetic trees inferred from the *All_Theraphosidae* matrix did not recover a sister-group relationship between *Ischnocolus* and *Chaetopelma*. The position of *Ischnocolus* differed among the analyses; supports were generally low – posterior probability (PP) = 0.69, ultrafast bootstrap support (UFBoot) = 40, not recovered in MrBayes or maximum parsimony (MP) – but all agree on placing it close to Neotropical taxa (see Figs S1–S4). On the other hand, *Chaetopelma* was recovered as sister to the subfamily Eumenophorinae in model-based analyses with high support (PP = 1, UFBoot = 94, PP = 1 for BEAST, IQTREE and MrBayes, respectively). A close relationship between the sampled *Ischnocolus* and the South African genus *Harpactirella* was not recovered in any of our analyses, highlighting the erroneous classification of *I. elongatus* as *Harpactirella* (Benoit, 1965; Calatayud-Mascarell & Sánchez-Vialas, 2020). We inferred the monophyly of western Mediterranean *Ischnocolus* and main morphotype clades with high support across all inference methods, but internal relationships within *I. elongatus* differed.

Our results suggest that Theraphosidae separated from its sister-family Barychelidae during the Early Cretaceous and subsequently diversified into several monophyletic clades following continental drift. The earliest branching lineage is subfamily Eumenophorinae along with genus *Chaetopelma* today inhabiting mainly eastern Africa, Madagascar and the Middle East. All subsequent main splits occurred during the Late Cretaceous (100.5–66.0 Mya). Fossil-based calibrations on the theraphosid tree suggest an old split of the two *Ischnocolus* lineages, which would trace back to the Late Eocene to Oligocene (44–29 Mya).

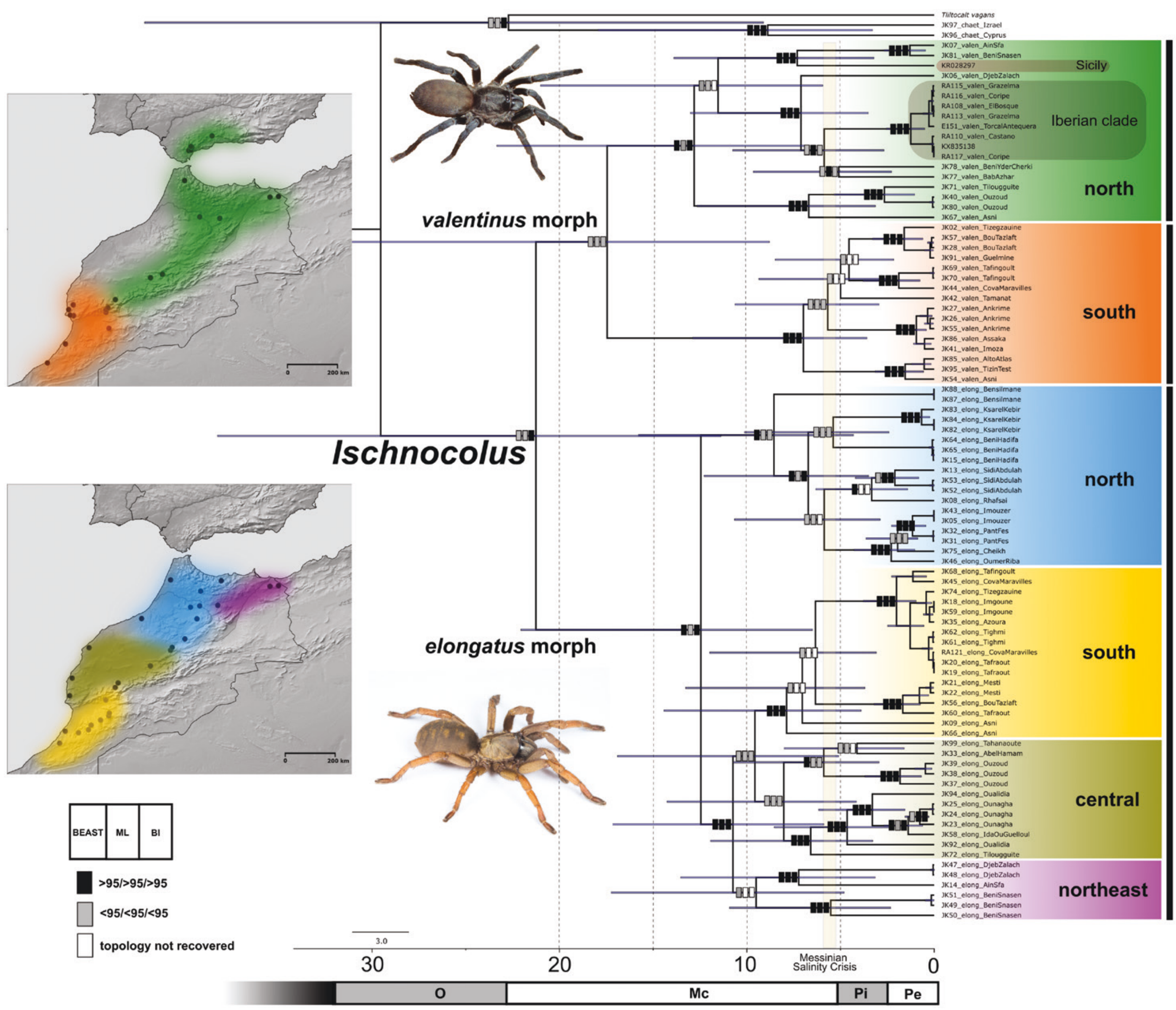

Figure 3. Time calibrated phylogeny of western Mediterranean *Ischnocolus* inferred by BEAST using two concatenated genes (*COI* + ITS2) and values inferred from Theraphosidae analysis as *COI* rate priors. Boxes indicate node supports from BEAST (posterior probability, PP), maximum likelihood (ML, ultrafast bootstrap proportions UFBS) and MrBayes (BI, posterior probability). Black = supported (PP > 0.95, UFBS > 0.95), grey = recovered with support values below thresholds, white = not recovered. Scale axis is in millions of years. Photo credits: *valentinus* morphotype – T. Romanov, *elongatus* morphotype – J. Korba. The *Ischnocolus* lineages are named and coloured as in Figure 2.

PHYLOGEOGRAPHY OF *ISCHNOCOLUS*

Analysis of the *All_Ischnocolus* matrix (Fig. 3) recovered *Ischnocolus* monophyly with different levels of support, depending on the method (PP = 0.90, UFBoot = 91, PP = 1, for BEAST, IQTREE and MrBayes, respectively; see Supporting Information, Figs S5–S7 for trees from each analysis separately). *Ischnocolus* specimens were split into two main clades, corresponding to the two morphotypes defined in the initial sorting. The clade formed by the *valentinus* morphotype received low support (PP = 0.88, UFBoot = 82, PP = 0.91), while the clade comprising the *elongatus* morphotype was supported in all analyses except ML (PP = 1, UFBoot = 94, PP = 1). Both clades showed strong internal geographic structuring.

Two lineages were recovered with high support in all analyses (except 'north' lineage in ML) within the *valentinus* clade: a lineage corresponding to the High Atlas, Anti-Atlas and southern Morocco populations (hereafter referred as 'south') and a lineage comprising the Middle Atlas, northern Morocco, as well as the Iberian populations and the single sample from Sicily (hereafter referred as 'north'). The Iberian specimens always formed a clade (PP = 1, UFBoot = 100, PP = 1) placed as sister to the northern Morocco diversity, rendering the Moroccan populations paraphyletic. The *I. valentinus* sample from Sicily (KR028297) was sister to populations from north-eastern Morocco. The 'north' and 'south' lineages were mostly allopatric, except in a single locality on the northern slopes of the High Atlas (Asni).

Similarly, the internal relations of *I. elongatus* also reflected a clear geographic structure. Support at deeper nodes was generally low, but the recovered lineages were consistent across the different methods and datasets. Four lineages were recovered, grossly corresponding to the northernmost Morocco populations ('north'), northern High Atlas and central coastal populations ('central'), Atlas and Anti-Atlas populations, including one locality north of the High Atlas ('south'), and populations from north-eastern Morocco close to the Algerian border ('north-east'). Relationships among the four lineages differed among the analyses and datasets (see Species delimitation below), but supports were generally low. The 'south' lineage was the only one with consistently high support (PP = 1, UFBoot = 99, PP = 1). All four lineages were strictly allopatric.

DIVERGENCE-TIME ESTIMATION BASED ON SUBSTITUTION RATES

Estimated posterior mean values for the *COI* obtained from the *All_Theraphosidae* were 0.0124 and 0.008, respectively. We used these values to define the mean and standard deviation of a normal distributed prior of a log-normal relaxed clock on the *COI* for *Ischnocolus*.

The split between the two morphotypes was dated to the Early Miocene 21.3 Mya (95%HPD = 11.4–38.2). Subsequent split of the 'north' and 'south' lineages of the *valentinus* clade was dated at 17.45 Mya (8.8–31.6). Divergence of north Moroccan and Iberian lineages was dated at 5.88 Mya (2.7–10.9). Divergence between north Moroccan samples and the sample from Sicily was dated at 7.3 Mya (3.2–13.9). The first split within the *elongatus* clade was dated at 12.45 Mya (6.5–22.0), which separated the well-supported 'north' lineage from the rest. The split between the 'south' and the 'central'/'north-east' lineages was estimated at 10.75 Mya (5.9–19.3).

SPECIES DELIMITATION

Results of the single-locus delimitation methods performed on each gene tree are summarized in Figure 4. The ABGD method delimited 35 groups (prior maximal distance P = 0.00369) for the *COI* and 18 groups (prior maximal distance P = 0.001260) for the ITS2.

The mPTP analysis yielded the most conservative results on the mitochondrial marker, as it recovered 22 clusters (minimum threshold = 0.60). The ITS2 supported the split between both morphotype clades and between the 'south' and 'north' *valentinus* lineages (0.99). Subsequently, the 'north-east' sample of *I. valentinus* from Beni Snassen received support of 0.50. Similar support (0.55) received the split between 'north' and 'south'/'central' *elongatus* lineages.

The GMYC model provided a significantly better fit than the null model (LR test: 1.354472e-14) and partitioned the *COI* dataset into 57 clusters. Conversely, the GMYC performed on the ITS2 dataset did not significantly fit the data better than the null model (LR test: 0.8657888) and did not separate more than two entities corresponding to the two main clades.

GENETIC DISTANCES

The maximum intra-lineage distances of *COI* (16.67 %), as well as of ITS2 (7.38 %), were found in the 'north' *valentinus* lineage (Tables 1, 2). The minimum inter-lineage distance was found between *elongatus* 'central' and *elongatus* 'north' linages in *COI* (8.06%) and between *elongatus* 'central' and *elongatus* 'south' in ITS2 (1.61%). Comparing three delimited species, we found similar maximum intraspecific distances in *I. valentinus* and *I. elongatus* (16.67% and 16.12%, respectively) for *COI* and for ITS2 (7.20% and 7.38%, respectively), while the lowest interspecific distance was found between *I. elongatus* and *I. mogadorensis* sp. reval. in both markers (11.72% for *COI* and 6.17% for ITS2) (Tables 3, 4).

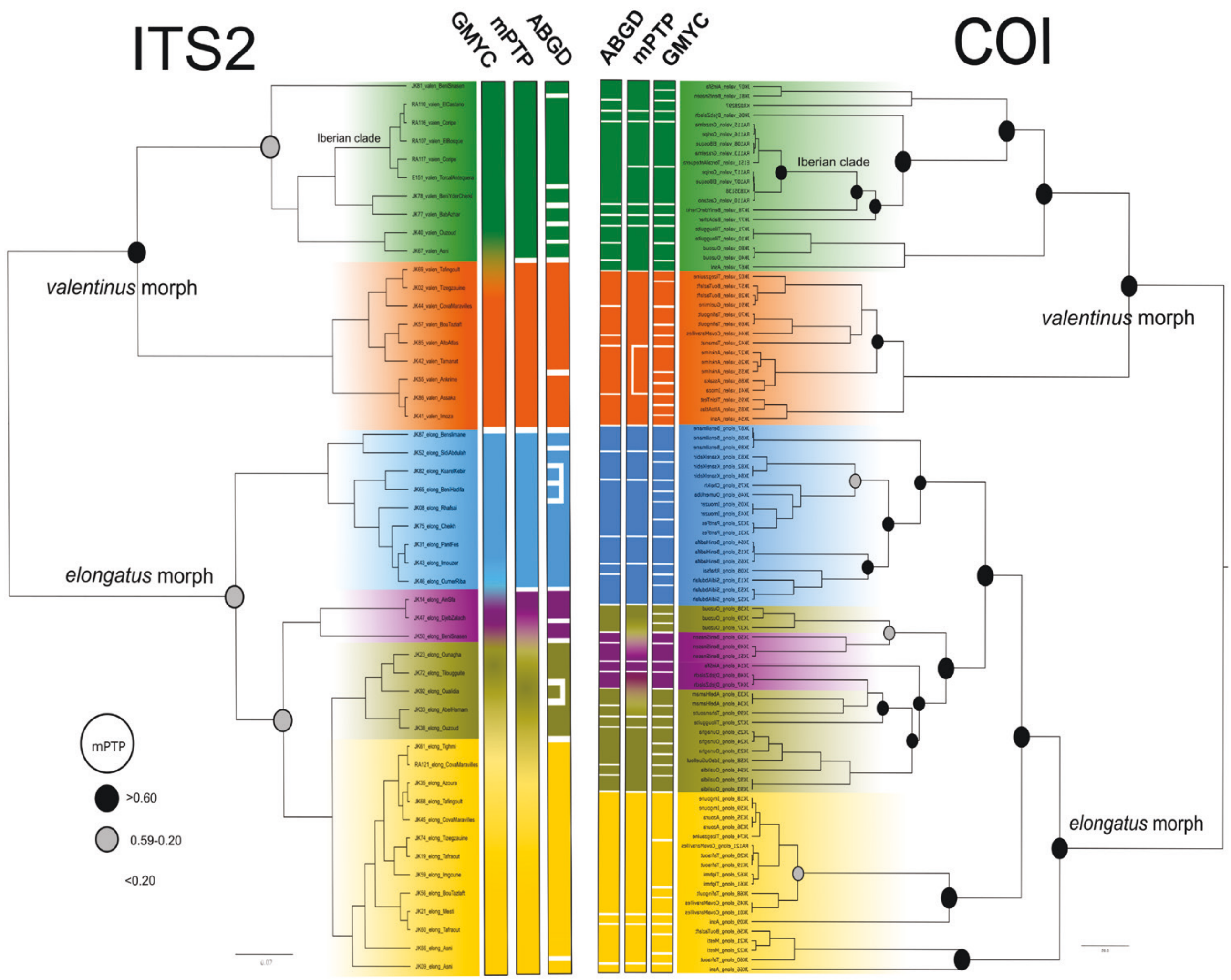

Figure 4. *COI* and ITS2 gene trees inferred by BEAST with bars representing three species delimitation methods: ABGD, mPTP and GMYC, respectively. Each individual block represents a delimited unit. Split blocks within ABGD and mPTP analyses indicate incongruences among phylogenetic inference and species delimitation analysis. Circles indicate support levels for the corresponding split in mPTP: black > 0.60, grey = 0.59–0.20 and no circle < 0.20.

Table 2. Maximum intra-lineage (diagonal, bold) and minimum inter-lineage uncorrected genetic distance calculated with ITS2 sequences for *Ischnocolus*

Lineage	valen_north	valen_south	elong_north	elong_south	elong_central	elong_north-east
valen_north	**0.0739**					
valen_south	0.0290	**0.0296**				
elong_north	0.8670	0.0541	**0.0264**			
elong_south	0.9750	0.0893	0.0328	**0.0457**		
elong_central	0.1028	0.0860	0.0301	0.0161	**0.0233**	
elong_north-east	0.1000	0.0887	0.0326	0.0299	0.0244	**0.0475**

Morphology

The examination of morphological characters revealed profound differences between the two morphotype clades. Females of *valentinus* lineages are generally less robust compared to *elongatus* (Figs 16, 20 vs. Fig. 23). The carapace in dorsal view is wider with short straight to slightly recurved fovea (Figs 11A, 15A, 19A), the cephalic region is not raised (Figs 11B,

Table 3. Maximum intraspecific (diagonal, bold) and minimum interspecific *COI* uncorrected genetic distances for three species of *Ischnocolus*

Species	*valentinus*	*elongatus*	*mogadorensis*
valentinus	**0.1667**		
elongatus	0.1259	**0.1612**	
mogadorensis	0.1324	0.1172	**0.1185**

Table 4. Maximum intraspecific (diagonal, bold) and minimum interspecific ITS2 uncorrected genetic distances for three species of *Ischnocolus*

Species	*valentinus*	*elongatus*	*mogadorensis*
valentinus	**0.0720**		
elongatus	0.0886	**0.0738**	
mogadorensis	0.0737	0.0617	**0.0300**

15E, 19E) and the eye tubercle is low. Chelicerae possess few long bristles on the margin (Figs 14N, 15D, 18N, 19D). Tarsus IV is always pseudosegmented. PLS are long (Fig. 9A, B) and their apical segment is always digitiform (Fig. 10A, B).

On the other hand, females of *I. elongatus* lineages are more robust (Fig. 23), the carapace from the dorsal view is longer than wide with slightly procurved fovea (Figs 11A, 22A) with significantly more raised cephalic region and eye tubercle (Figs 11B, 22E). Chelicerae possess strong, black bristles on the margin (Figs 21N, 22D). Tarsus IV is not pseudosegmented. PLS are shorter and thick (Fig. 9C, D) with a triangular apical segment (Fig. 10C–F).

Conversely, there are subtle differences in external female morphology between the 'north' and 'south' *valentinus* lineages. The 'south' lineage has a slightly deeper golden-pink colour and reduced overall measurements of PLS. Similarly, female external morphology differences among *elongatus* lineages were also minimal. They vary in colour (Fig. 23) and in the overall length of PLS (Fig. 9C, D). A north–south cline in the reduction of apical segment of PLS was observed (Fig. 10C–F) but significant differences were only detected between the 'south' and 'north-east', and the 'south' and 'north' lineages (see also Geometric morphometric analyses).

Genital morphology

Both morphotypes also differ in the morphology of female spermathecae as *valentinus* possess apical lobes, while *elongatus* spermathecae are without or with few (one or two) lobes (Figs 5, 6). Potential differences in the shape of the spermatheca within the *valentinus* clade (Fig. 5) were also observed between specimens from the 'south' lineage and the 'north' lineage, although a limited number of specimens were available (only one adult female from the 'south' lineage). The vulva of the 'south' lineage is formed by two separated spermathecae, longer than wide, each with three apical lobes in a cross-like disposition, while the 'north' lineage spermathecae are ventrally connected, as wide as long, with more than three apical lobes aligned on a single plane (Fig. 5). The 'north' lineage spermathecae type is the one reported in literature for *I. valentinus* (Guadanucci & Wendt, 2014).

The spermathecae shape also varied across the *elongatus* lineages, with 'north' and 'south' lineages showing the largest differences (Fig. 6). Unfortunately, only a limited number of specimens were available to assess within-lineage variation.

The assessment of male morphological differences between both morphotypes was hampered by the limited sample size (one *elongatus* and seven *valentinus*). However, it was possible to observe some significant differences. In *elongatus* male the palpal tibia is almost the same length as the tarsus (Fig. 21F–H) and lacks the sigmoid ventral furrow (Fig. 21G), the bulbus is larger with a moderately long, straight, flattened and apically twisted embolus with a pointed tip (Fig. 7) and possesses few spines on ventral tibia I (Fig. 8). On the other hand, the *valentinus* morphotype shows a longer male palpal tibia (Figs 14F–H, 18F–H), a smaller bulbus with a curved to straight embolus and a flattened tip (Fig. 7) and tibia I displays many spines ventrally (Fig. 8).

Furthermore, within the *valentinus* morphotype, it was possible to observe differences between 'north' and 'south' lineages (Figs 7, 8), where three males for *I. mogadorensis* and four males for *I. valentinus* were available for comparison. Males of the 'south' lineage showed an S-shaped embolus (Fig. 7) and bore two strong spines on the distal margin of ventral tibia I, while the rest of the spines were scattered through the ventral side, whereas in the 'north' lineage the embolus showed a simple curvature, tibia I bore a single prolateral-terminal ventral spine and the rest of spines were concentrated on the proximal margin of the pro-ventral side (Fig. 8).

Geometric morphometric analyses

GM analysis of the carapace clearly distinguished the two main morphotypes, but did not separate any of the internal lineages. The 'Prosoma Lateral' PC1 accounted for 48.87% of variability and the PC2, for 33.44% (Fig. 11). The two-dimensional plot clearly separated the two main morphotypes (Fig. 11). Five out of eight between-morphotype comparisons were statistically significant (ANOVA, $P < 0.05$), but all of the

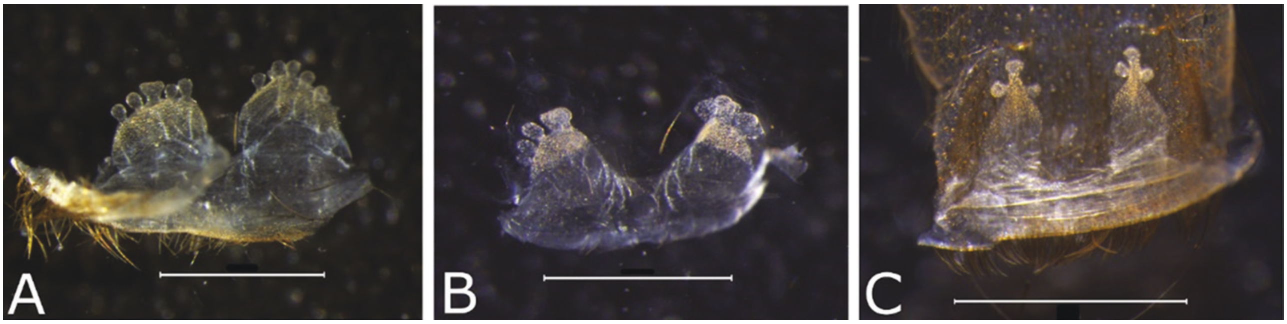

Figure 5. Spermathecae shape variation across the *valentinus* morphotype. A, B, 'north' lineage (*I. valentinus*); C, 'south' lineage (*I. mogadorensis*). Scale bar = 1 mm.

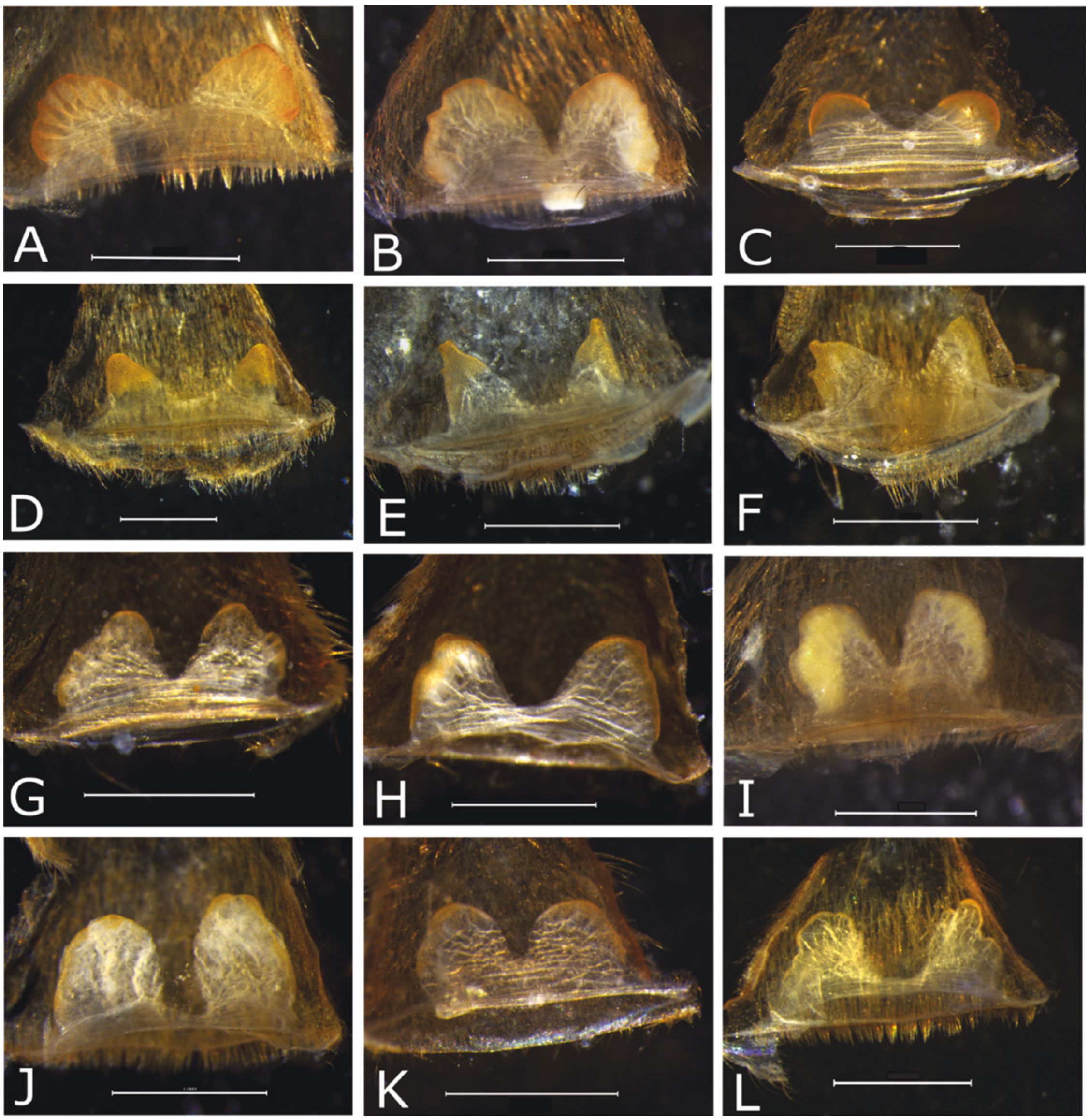

Figure 6. Spermathecae shape variation across lineages of the *elongatus* morphotype. Lineages are grouped as follows: A-C, 'north-east'; D-F, 'north'; G-I, 'central'; J-L, 'south'. Scale bar = 1 mm.

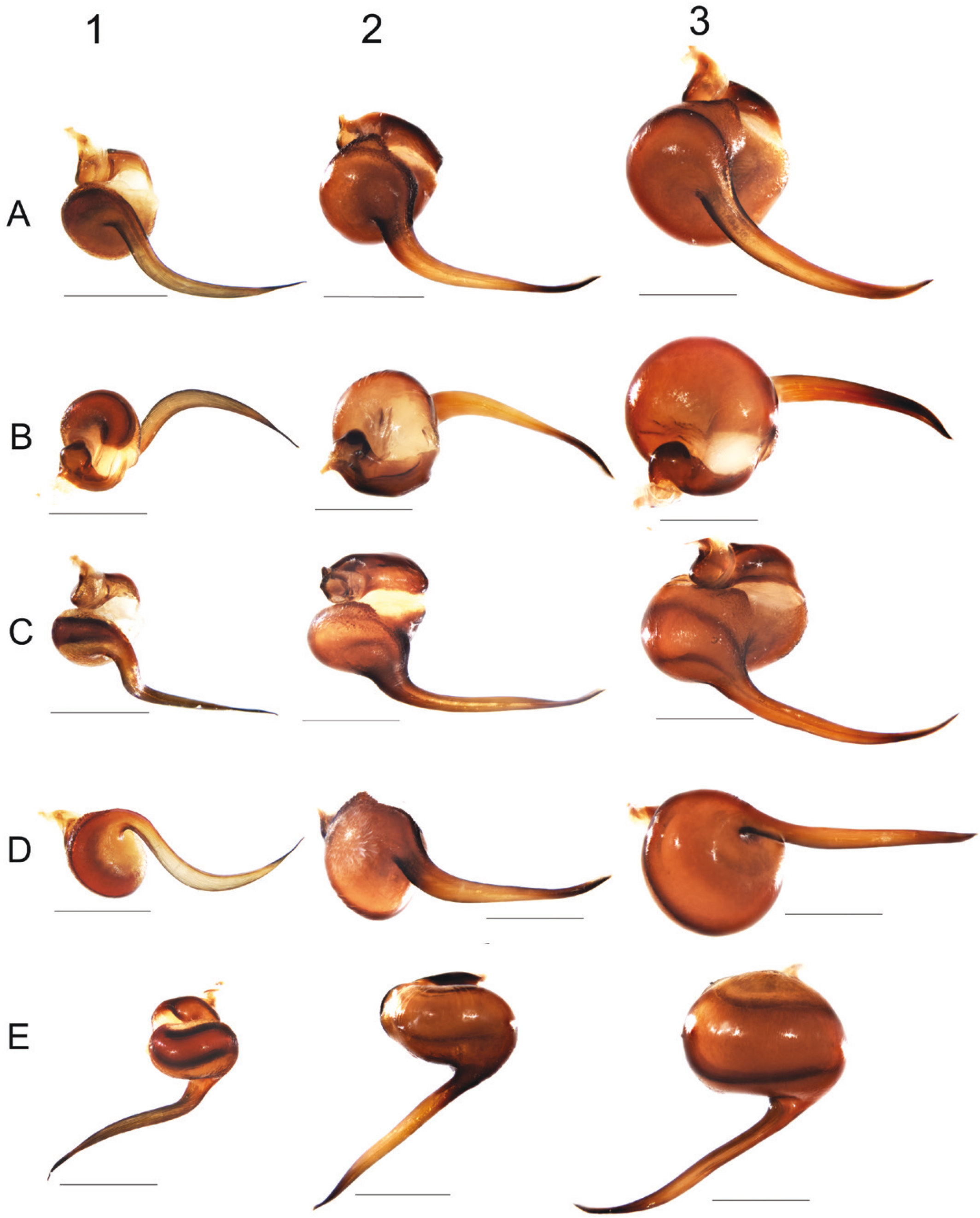

Figure 7. Bulbus shape comparison between males. 1, *I. mogadorensis*; 2, *I. valentinus*; 3, *I. elongatus.* A, proventral; B, dorsal; C, prolateral; D, ventral; E, retrolateral. Scale bar = 1 mm.

within-morphotype comparisons were not (Supporting Information, Table S5). The 'Prosoma Dorsal' PC1 accounted for 54.71% and PC2 for 18.32% (Fig. 11). Six out of eight between-morphotype comparisons were statistically significant (ANOVA: $P < 0.05$); the within-morphotype comparisons were not significant (Supporting Information, Table S6).

Within *I. elongatus*, 'Lateral PLS' and 'Dorsal PLS' views identified significant differences in the shape of the PLS apical segment and its relative length regarding the medial segment between the 'south' and both the 'north' and 'north-east' lineages (Fig. 12; ANOVA: $P < 0.05$), but not from the 'central' lineage (Supporting Information, Tables S7, S8). A similar north–south reduction of overall length of spinnerets, and especially of the apical segment, was also observed in *I. valentinus*, but the lack of adult females prevented statistical analysis.

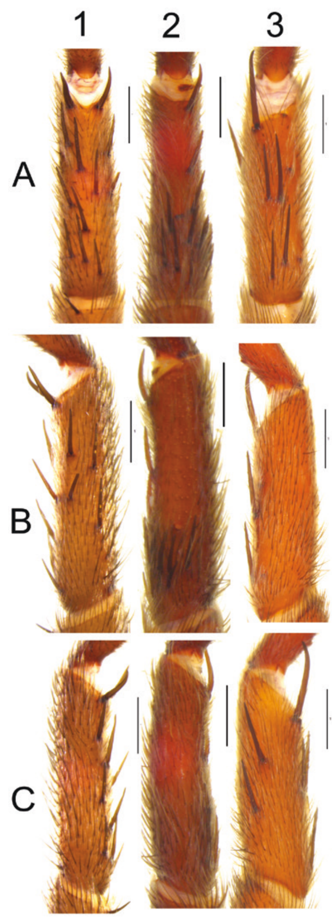

Figure 8. Comparison of the spine pattern on tibia I among males. 1, *I. mogadorensis*; 2, *I. valentinus*; 3, *I. elongatus.* A, ventral; B, prolateral; C, retrolateral. Scale bar = 1 mm.

Species distribution modelling

The species distribution models (SDM) performed well for *I. mogadorensis* (AUC = 0.937, SD = 0.086) and for *I. valentinus* [area under curve (AUC) = 0.871, SD = 0.116]. The variables 'Precipitation of the Driest Quarter' (Bio17, 66%) and 'Annual Precipitation' (Bio12, 25.3%) contributed most to *I. valentinus* and 'Max Temperature of the Warmest Month' (Bio5, 51.57%) and 'Precipitation of the Driest Quarter' (Bio17, 43.2%) to *I. mogadorensis* (Fig. 13A, B).

For *I. elongatus* lineages, the SDM also performed well: *I. elongatus* 'north' (AUC = 0.851, SD = 0.199), *I. elongatus* 'south' (AUC = 0.948, SD = 0.063) and *I. elongatus* 'central' (AUC = 0.823, SD = 0.153). Similarly, variables that made a major contribution were 'Precipitation of the Driest Quarter' (Bio17, 62%) and 'Annual Precipitation' (Bio12, 37.4%) for the 'north' lineage, 'Max. Temperature of the Warmest Month' (Bio5, 55,3%) and 'Precipitation of the Driest Quarter' (Bio17, 37,8%) for the 'south' and 'Precipitation of the Driest Quarter' (Bio17, 78.6%) and 'Max. Temperature of the Warmest Month' (Bio5, 16.9%) for the 'central' lineage (Fig. 13C–E). The *I. elongatus* 'north-east' lineage was not included in the analyses, because only three localities were available.

There was relatively low niche overlap, as assessed by Schoener's D-metric, between both *I. valentinus* lineages (D = 0.35) (Supporting Information, Table S4). Conversely, there was a large overlap between the *I. elongatus* 'north' and 'central' lineages (D = 0.85) and moderate between 'south' and 'central' (D = 0.60) and 'north' and 'south' (D = 0.55) lineages. All comparisons were statistically significant (i.e. species are not ecologically interchangeable), except for *I. elongatus* 'north' and 'central' (Supporting Information, Fig. S8).

Taxonomy

Our integrative approach combining morphological characters, molecular and ecological data and extensive geographic sampling, including material from type localities, allowed us to evaluate the current status of the western Mediterranean *Harpactirella* and *Ischnocolus* diversity. As a result, we remove *Ischnocolus mogadorensis* Simon, 1909 from the synonymy of *Ischnocolus valentinus* (Dufour, 1820) and synonymize *Harpactirella insidiosa* (Denis, 1960) and *Ischnocolus hancocki* Smith, 1990 with *Ischnocolus elongatus* (Simon, 1873) on the basis of the molecular phylogenetic evidence reported herein and morphological differences described below (see Remarks on *I. elongatus* for details).

Family Theraphosidae Thorell, 1869

Subfamily Ischnocolinae Simon, 1892

Genus *Ischnocolus* Ausserer, 1871

Type species: Ischnocolus holosericeus Koch, in Ausserer (1871) by original designation, syn. of *Ischnocolus valentinus* (Dufour, 1820).

Diagnosis: See Guadanucci & Wendt (2014) for a recent diagnosis of the genus.

Species included: Ischnocolus elongatus (Simon, 1873); *Ischnocolus ignoratus* Guadanucci & Wendt, 2014; *Ischnocolus jickelii* L. Koch, 1875; *Ischnocolus mogadorensis* Simon, 1909; *Ischnocolus rubropilosus* Keyserling, 1891 (note: taxonomic allocation of *I. rubropilosus* in *Ischnocolus* is dubious because it lies far outside the zoogeographical range of the genus); *Ischnocolus tomentosus* Thorell, 1899 (probably belongs to *Myostola* Simon, 1903, according to Guadanucci & Wendt, 2014, who considered it as *incertae sedis*); *Ischnocolus valentinus* (Dufour, 1820) (type species).

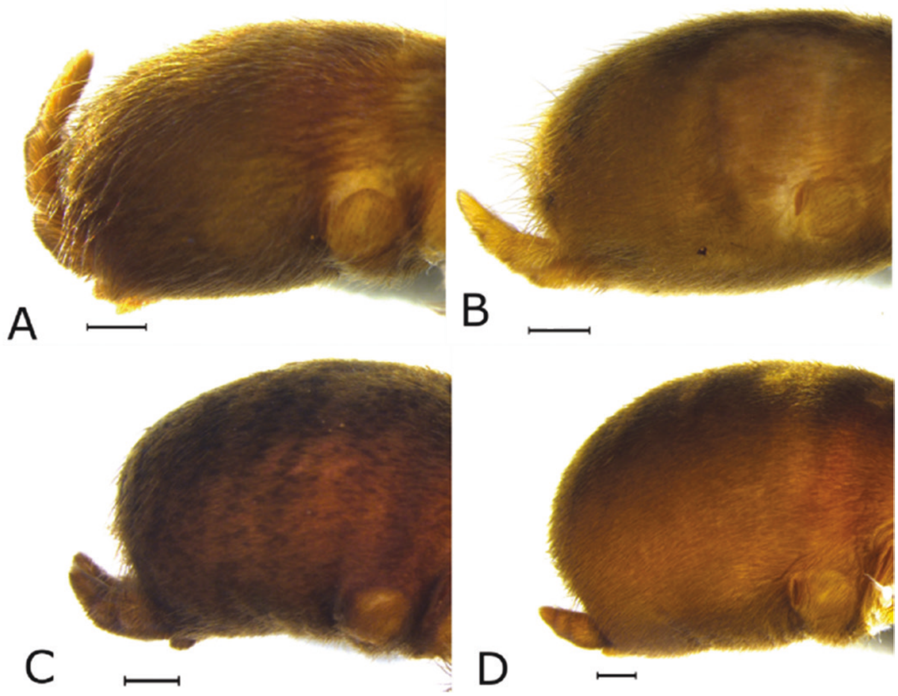

Figure 9. Lateral view of abdomen showing variability in PLS length. A, *I. valentinus*; B, *I. mogadorensis*; C, *I. elongatus* 'north'; D, *I. elongatus* 'south'. Scale bar = 1 mm.

ISCHNOCOLUS JICKELII L.KOCH, 1875

Ischnocolus jickelii L.Koch, 1875: 58, pl. 6, fig. 2 (♀). Guadanucci & Wendt [2014: 395, fig. 4B (♀)]. Zonstein [2018: 110, fig. 914: 3 (♂)]. *Chaetopelma adenense* Simon [1890: 83 (♀)]. Synonymized with *I. jickelii* by Guadanucci & Gallon (2008: 42).

Type material: Holotype, female Eritrea: Hamasien (BMNH 19-9-18-5698-99), Guadanucci & Wendt (2014), not examined.

Material examined: Somaliland: 2♂♂ 5♀♀, Daallo forest park; 10°45′38″N, 47°18′13″E; 4.ix.17 (P. Just, D. Král, P. Frýdlová, D. Frynta, F. Kovařík, T. Mazuch & M. Häckel leg.).

Diagnosis description and distribution: See Montemor *et al.* (2020).

ISCHNOCOLUS VANANDALAE MONTEMOR *ET AL.*, 2020

Type material: Holotype: Male, Oman, Dhofar, Salalah, Wadi Darbat, near Tawi Atayr, 17°06′12″N, 54°21′10″E, x.2000, S. Huber leg. (SMNS-Aran-003439). Not examined.

Material examined: 1♂ (SMNS-Aran-002581), Ad Dakhiliyah Governorate, Muhafazat ad Dakhiliyah, Dar Sawda', flank of Jebel Shams, 23°14′19″N, 57°11′37″E, 03.ix.2016. 1♂ (SMNS-Aran-002587), Al Wusta Governorate, Ras Madrakah, near coast, 18°58′29″N, 57°23′38″E), 05.ix.2016.

Diagnosis, description and distribution: See Montemor *et al.* (2020).

ISCHNOCOLUS MOGADORENSIS SIMON, 1909, SP. REVAL.

(FIGS 5C, 7, 8, 9B, 10B, 13B, 14A–N, 15A–G, 16A–D, 17A–F)

Ischnocolus mogadorensis Simon (1909, description of female, p. 10).
Ischnocolus valentinus: Guadanucci & Wendt (2014: 391, as senior synonymy of *I. mogadorensis).*

Type material: Female holotype. Morocco: Mogador (Essaouira), Martínez de la Escalera leg., presumably deposited in MNHN in Paris, lost (Guadanucci & Wendt, 2014). Not examined.

Material examined: Morocco: 1♂, 2♀♀ (CRBA004988, CRBA004989, CRBA004990), province of Agadir, Ankrime, 30°37′25″N, 9°34′50″W, 26.ii.2020 (J. Korba leg.). 1♂, 3 juv. (CRBA004981, CRBA004982, CRBA004983, CRBA004984), province of Tiznit, Bou

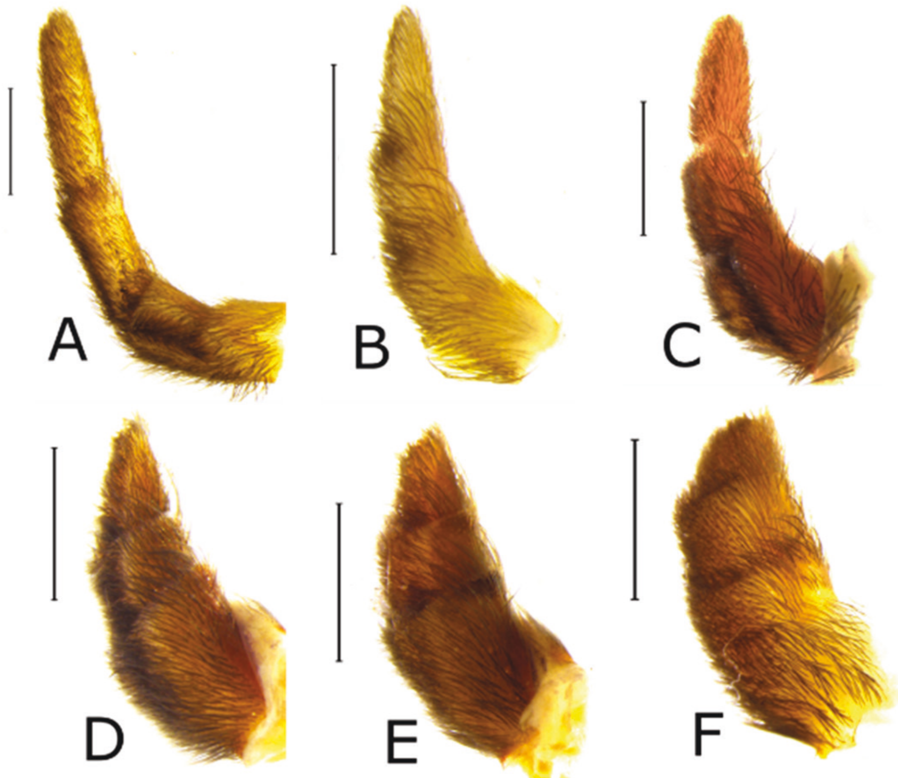

Figure 10. Lateral view of PLS showing shape variability of apical segment in: A, *I. valentinus*; B, *I. mogadorensis*; C, *I. elongatus* 'north-east'; D, *I. elongatus* 'north'; E, *I. elongatus* 'central'; F, *I. elongatus* 'south'. Scale bar = 1 mm.

Tazlaft, 29°37′40″N, 9°52′52″W, 24.ii.2020 (J. Korba leg.), 1 juv. (CRBAMM000346), province of Agadir, Imoza, 30°38′34″N, 9°42′20″W, 7.iv.2010 (V. Opatova & M. Arnedo leg.). 1♀ (CRBAMM000342), province of Essaouira, Tamanat, 31°00′21″N, 9°35′49″, 7.iv.2010 (V. Opatova & M. Arnedo leg.). 1 juv. (CRBAMM000348), province of Taroudant, Cova Maravilles, 30°10′40″N, 8°17′38″W, 8.iv.2010 (V. Opatova & M. Arnedo leg.). 1♀, 1 juv. (CRBAMM000370, CRBAMM000366), province Al Haouz, Asni, 31°11′22″N, 8°03′27″W, 9.iv.2010 (V. Opatova, M. Arnedo leg.). 2 juv. (CRBAMM000358, CRBAMM000359), province of Taroudant, Tafingoult, 30°44′31″N, 8°24′06″W, 9.iv.2010 (V. Opatova, M. Arnedo leg.). 1♀ (CRBA005025), province of Taroudant, Tizi n′Test 30°49′40″N, 8°23′57″W, 24.ii.2010 (A. Calatayud-Mascarell & A. Sánchez-Vialas leg.). 1 juv. (CRBA005026), province of Agadir, Assaka, 30°50′18″N, 9°45′53″W, 28.xii.2018 (A. Sánchez-Vialas leg.). 1♂, 1 juv, (CRBA005030, CRBA005031), province of Guelmim, Playa Blanca, 28°57′39″N, 10°33′03″W, 23.iv.2019 (A. Sánchez-Vialas leg.). 1 juv. (CRBA005037), province of Taroudant, Alto Atlas, 30°53′59″N, 8°19′35″W, 24.ii.2020 (A. Calatayud-Mascarell & A. Sánchez-Vialas leg.), 1♂ (SMNS-Aran-3824), province of Azilal, Demnate, 31°45′03″N, 7°05′33″W.

Justification for the revalidation of the species: Integration of evidence provided in this work has revealed that the 'south' lineage of the *valentinus* morphotype clade represents a different species from the 'north' lineage, which corresponds to the nominal *I. valentinus*. Simon (1909) described the female of *I. mogadorensis* from the surroundings of Essaouira (Mogador), but the type material could not be examined because it is presumably lost (Guadanucci & Wendt, 2014). The original description lacks any diagnostic traits other than a 'pinkish-brown coloration' (Simon, 1909: 10). The type locality is Mogador (today Essaouira) but can refer broadly to the surroundings of the city. We lacked samples from the direct vicinity of Essaouira, but our nearest locality, Tamanat, is just 60 km south. Additionally, the SDM of *I. valentinus* 'south' lineage predicted its distribution well into coastal plains up to Essaouira (see Fig. 13B). Therefore, we propose restoring the name *I. mogadorensis* and revalidating the species.

Diagnosis: Males can be distinguished from their congeners by the presence of two short, strong spines apically on the ventral part of tibia I and a moderate number of remaining spines distributed equally across tibia I (Figs 8, 14B–D). They further differ from

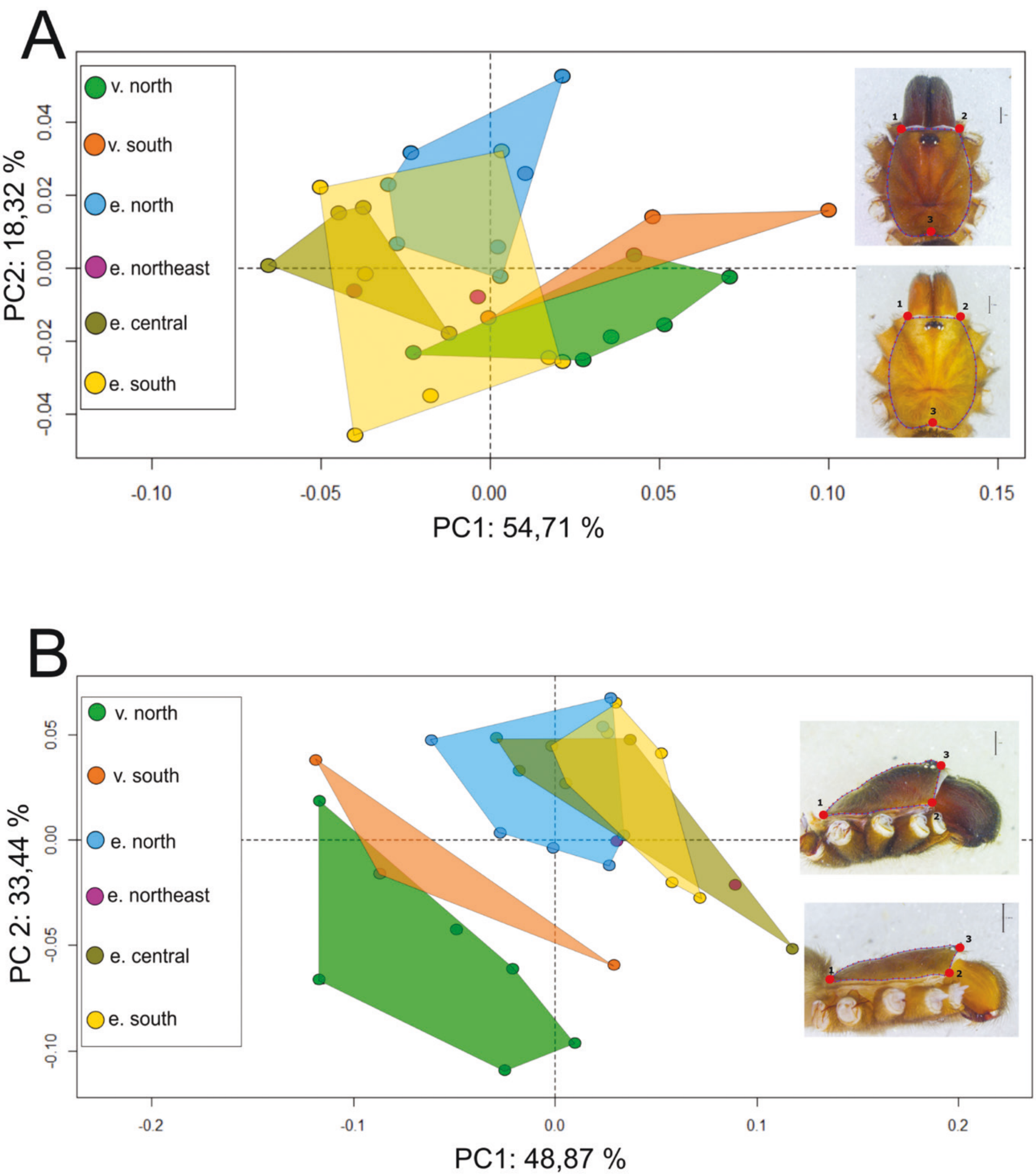

Figure 11. Principal component analysis of prosoma from dorsal (A) and lateral (B) views. Images show placement of landmarks and semi-landmarks. Upper image belongs to the *elongatus* morphotype and the image below to the *valentinus* morphotype.

I. valentinus by their smaller size ($N = 3$) and markedly S-shaped embolus (Figs 7, 14F–J, L, M).

Females differ from all other *Ischnocolus* species, except *I. jickelii*, by the spermatheca shape, which is longer than wide, narrowing apically and having three cross-like shaped apical lobes (Figs 5, 15F).

Description: Male (CRBA004987, Ankrime): total length 12.93. **Colour pattern**: *Colour in ethanol:* legs and carapace light yellow-brown. Carapace with silver hairs (Fig. 14A). Abdomen darker brown with dorsal light, striped pattern. *Colour of live specimen (Fig. 16):* variable, depending on the life stage. Legs and carapace golden brown, chelicerae golden grey, abdomen dark with lighter striped pattern (Fig 14B, C). After moulting, specimens can be dark. **Carapace:** 5.32 long, 4.46 wide; cephalic region almost flat from lateral view; eye tubercle low 0.49 long, 0.85 wide;

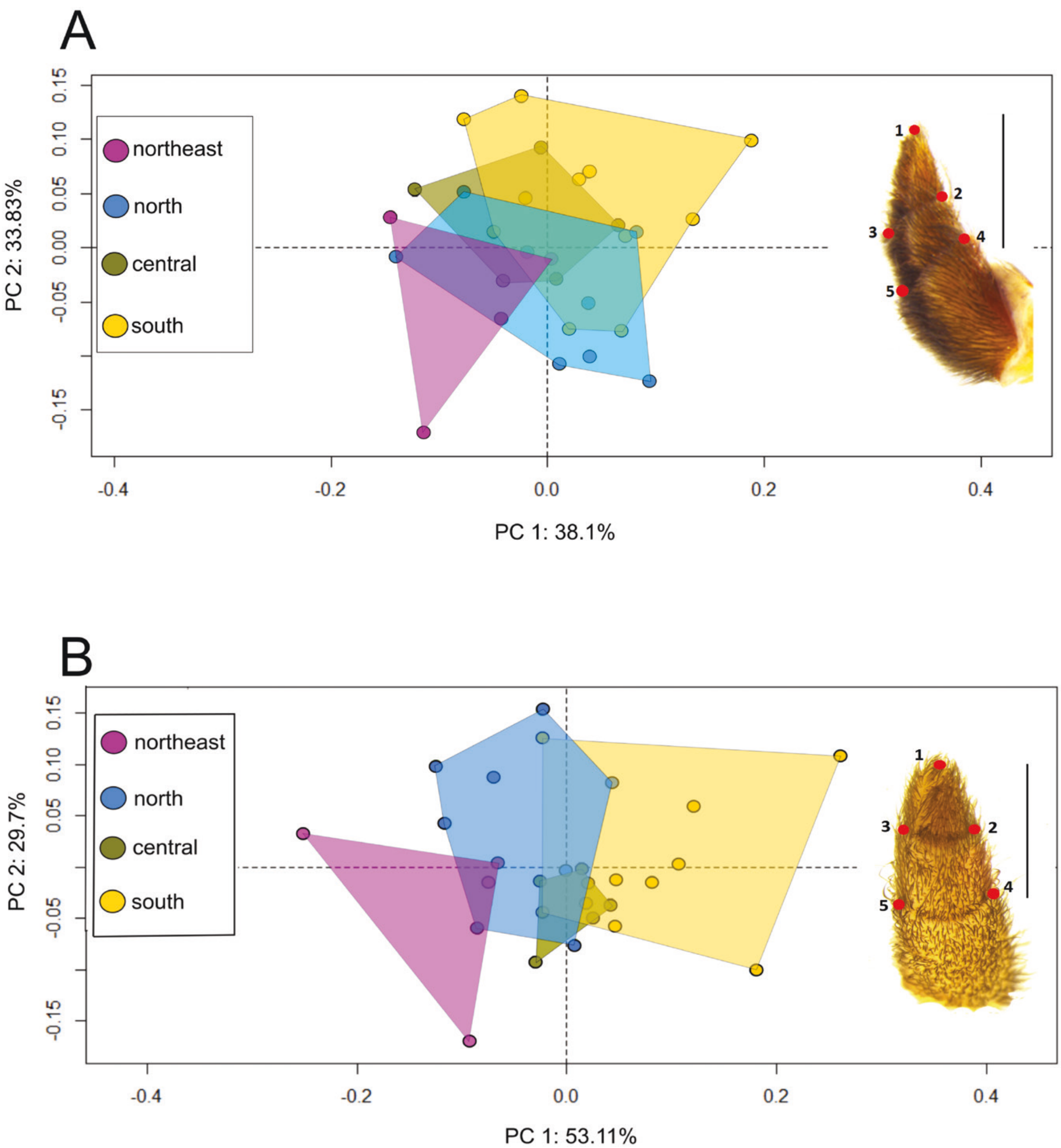

Figure 12. Principal component analysis of the shape of the apical segment of PLS from lateral (A) and dorsal (B) views among four lineages of the *elongatus* morphotype clade.

fovea with shallow depression, slightly recurved (Fig. 14A). Clypeus 0.15 wide. **Eyes** (Fig. 14E): AME 0.15, PME 0.16, ALE 0.27, PLE 0.17; PME-PME 0.46, ALE-AME 0.23, ALE-PLE 0.26, AME-PLE 0.34, AME-AME 0.27, ALE-ALE 0.67. **Sternum, labium and maxillae**: sternum 2.4 long, 2.02 wide, setose, with three inconspicuous sigilla on each margin opposite to coxa I, II and III. Labium twice as wide as long, 0.37 long, 0.86 wide, with two cuspules. Maxillae with approx. 40 cuspules (Fig. 14K). **Abdomen**: 6.30 long, 3.23 wide; long setae scattered across the dorsal part of abdomen with a group of long black setae in the anterior part. PLS basal segment 0.87 long, median segment 0.67 long, apical segment digitiform 0.75 long. **Chelicerae:** 2.31 long, basal article with nine teeth interchelicéral tumescence present, few long bristles along the margin. **Pedipalps:** length: 7.76 (femur 2.71, patella 1.80, tibia 2.12, tarsus 1.13). Furrow on ventral tibia short, slightly sigmoid. Spination: femur (p)1ap. **Copulatory bulb:** small bulb with remarkably S-shaped embolus with flattened tip (Figs 7, 14). **Legs:** scopula on all tarsi divided by a

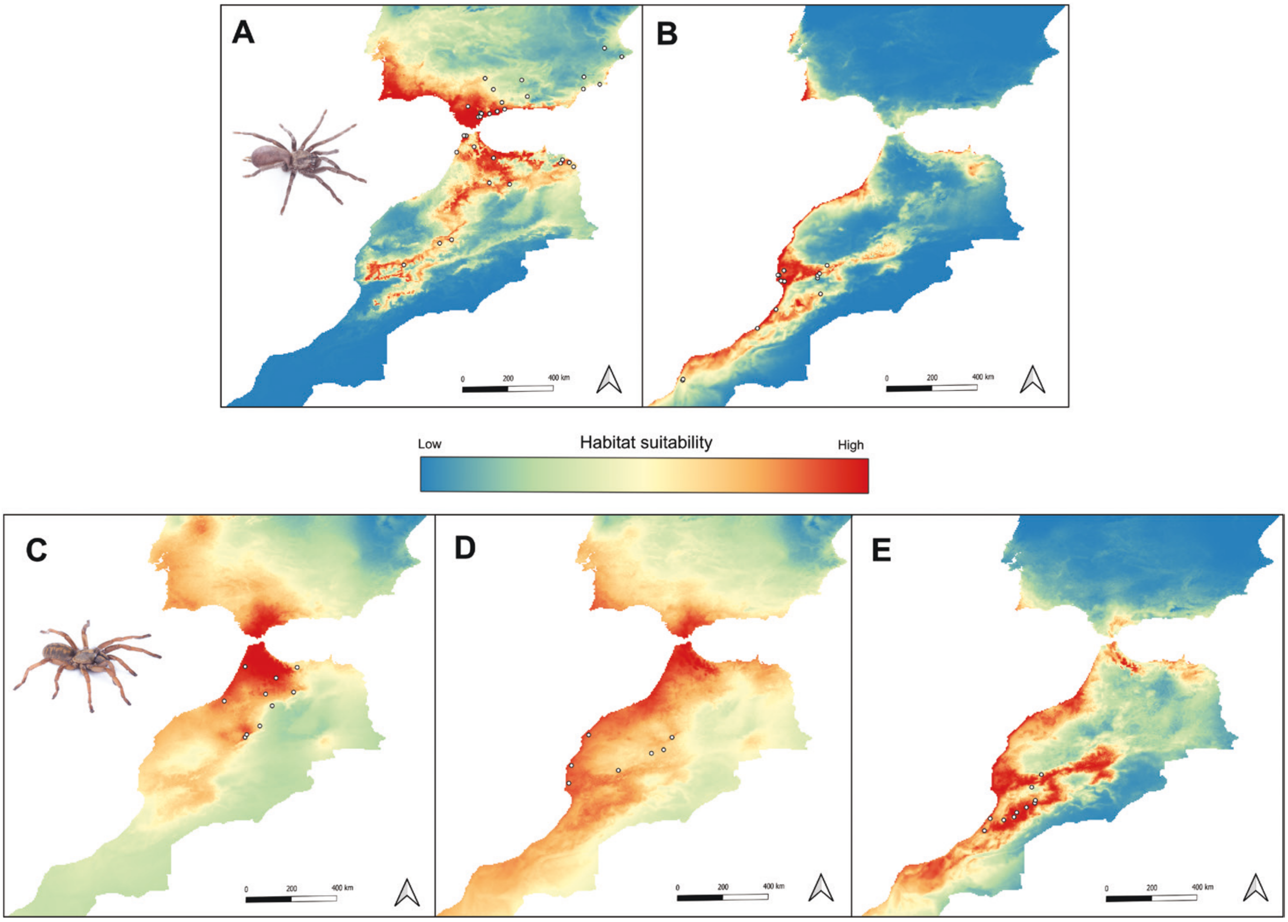

Figure 13. Suitability maps obtained with MaxEnt for *I. valentinus* (A), *I. mogadorensis* (B), *I. elongatus* 'north' (C), *I. elongatus* 'central' (D) and *I. elongatus* 'south' (E) for Morocco and the Iberian Peninsula.

thick band of setae. Scopula on ventral metatarsus I nearly totally occupied, II half occupied, III and IV < half occupied. *Leg measurement:* length of legs IV > I > II > III; leg I: 15.98 (femur 4.72, patella 2.14, tibia 3.64, metatarsus 3.18, tarsus 2.23), leg II: 15.12 (femur 4.13, patella 2.09, tibia 3.61, metatarsus 3.16, tarsus 2.13), leg III: 14.30 (femur 3.78, patella 1.83, tibia 3.51, metatarsus 3.12, tarsus 2.04), leg IV: 19.15 (femur 4.93, patella 2.04, tibia 4.50, metatarsus 4.90, tarsus 2.76). *Spines:* I femur (p)1, tibia (p)2-2, (v)3-1-1-ap2, tarsus(v)1-1. II femur (r)1, tibia (r)1-1-1, (v)1-1-1-2, metatarsus(r)1-0-0, (p)1-0-0, (v)1-1; III femur (r)1, tibia (r)1-1,(v)1-1-1-3, metatarsus (r)1-0-1, (v)1-1; IV femur (r)1, (p)1, patella (p)2, tibia (r)1-2-1-1, (p)1-1-1, (v)1-1-2, metatarsus (r)1-1-2-1-1-1, (p)1-1-1-1-1, (v)1-1-2; tarsus IV pseudosegmented.

Female (CRBA004989, Ankrime): Total length 15.86. **Colour pattern**: *Colour in ethanol:* carapace, chelicerae and legs light orange, abdomen grey-brown with light striped pattern (Fig. 15A, E). *Colour of live specimen:* body uniformly dark-brown-pinkish. Abdomen with light, striped pattern (Fig. 15A–C). **Carapace:** 5.51 long, 4.34 wide; cephalic region almost flat from lateral view (Fig. 15E); eye tubercle low, 0.50 long, 0.87 wide. Fovea with shallow depression slightly recurved (Fig. 15A). Clypeus 0.22. **Eyes** (Fig. 15C): AME 0.14, PME 0.13, ALE 0.26, PLE 0.19; PME-PME 0.50, ALE-AME 0.23, ALE-PLE 0.29, AME-PLE 0.35, AME-AME 0.28, ALE-ALE 0.68. **Sternum, labium and maxillae:** sternum 2.69 long, 2.18 wide; labium twice as wide as long, 0.45 long, 0.97 wide, with four cuspules; maxillae with approx. 40 cuspules (Fig. 15B). **Abdomen:** 8.35 long, 4.14 wide; PLS basal segment 0.82 long, median segment 0.51 long, apical segment 0.75 long, digitiform (Fig. 15G). **Vulva:** spermathecae longer than wide, each with three apical lobes in a cross-like disposition (Fig. 15F). **Chelicerae**: 2.93 long; basal article with 10 teeth; few long bristles on the margin (Fig. 15D). **Pedipalps:** length: 9.06 (femur 3.05, patella 1.89, tibia 2.20, tarsus 1.92). *Spination:* without spines. **Legs:** Scopula on all tarsi divided by a thick band of setae. Scopula on ventral metatarsus I and II entirely

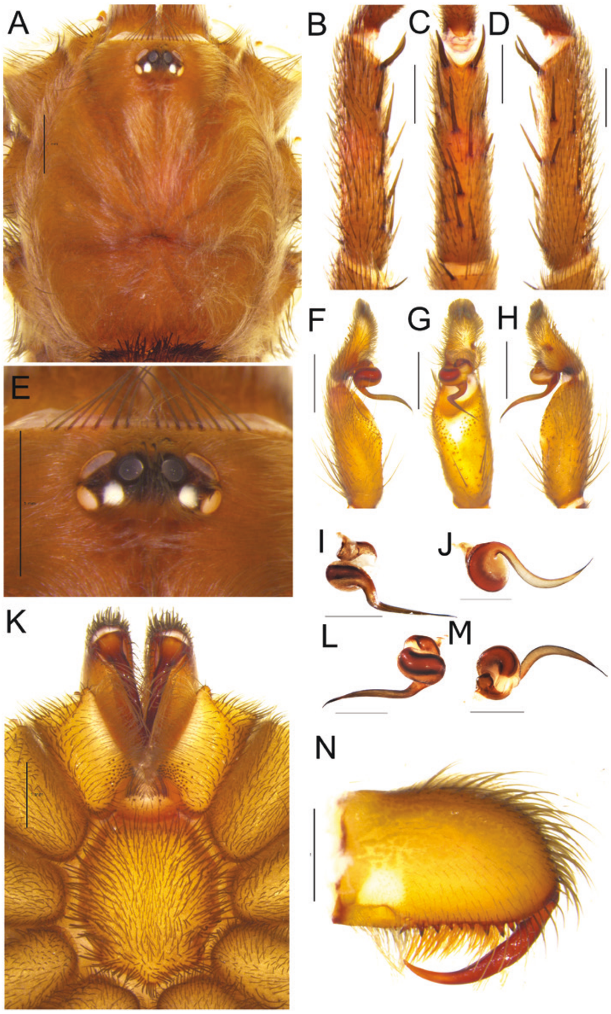

Figure 14. *Ischnocolus mogadorensis*, male, A–N (CRBA004987). A, prosoma, dorsal view. B, tibia I, prolateral view. C, tibia I, ventral view. D, tibia I, retrolateral view. E, eye tuberlce, dorsal view. F, palpal bulbus, prolateral view. G, palpal bulbus, ventral view. H, palpal bulbus, retrolateral view. I, sternum, maxillae, labium and chelicerae, ventral view. J, bulbus, prolateral view. K, bulbus, ventral view. L, bulbus, retrolateral view. M, bulbus, dorsal view. N, chelicerae, prolateral view. Scale bar = 1 mm.

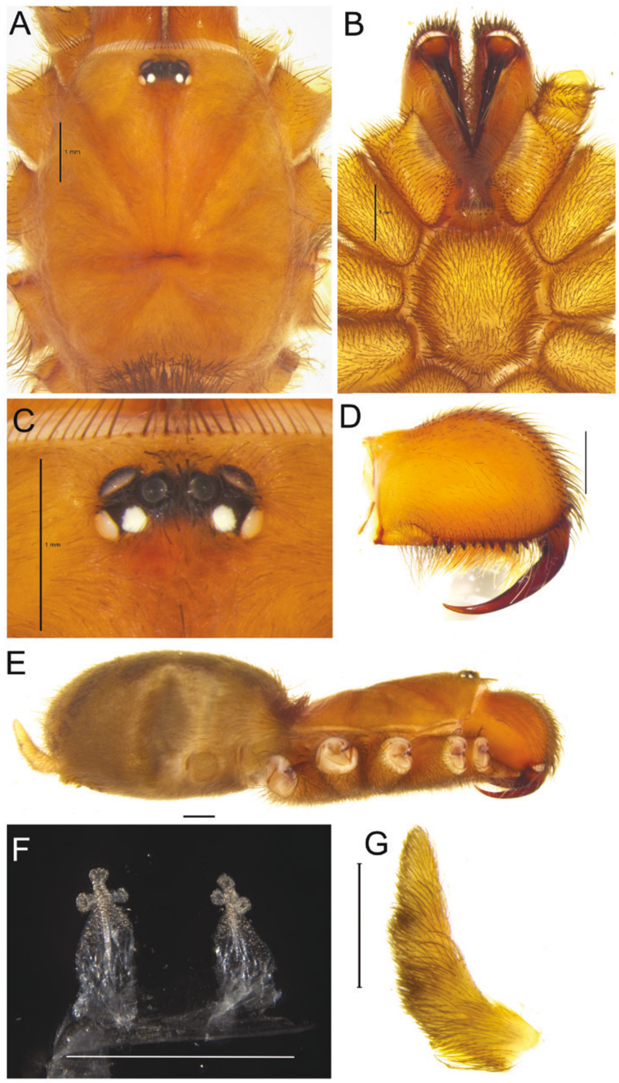

Figure 15. *Ischnocolus mogadorensis*, female, A–G (CRBA004989). A, prosoma, dorsal view. B, sternum, maxillae and chelicerae, ventral view. C, eye tubercle, dorsal view. D, chelicerae, prolateral view. E, whole body, lateral view. F, spermathecae. G, posterior lateral spinneret, retrolateral view. Scale bar = 1 mm.

occupied, III three-quarter occupied, IV half occupied. *Leg measurement:* length of legs IV > I > II > II. Leg IV: 17.93 (femur 4.63, patella 2.54, tibia 4.09, metatarsus 4.28, tarsus 2.39); leg III: 12.45 (femur 3.28, patella 1.92, tibia 2.50, metatarsus 2.89, tarsus 1.86), leg II: 12.65 (femur 3.62, patella 2.20, tibia 2.64, metatarsus 2.40, tarsus 1.79); leg I: 14.24 (femur 4.12, patella 2.69, tibia 3.16, metatarsus 2.58, tarsus 1.69). *Spines:* I femur (p)0-0-1, tibia (p)0-1-1, (v)1-1-2, (p)1-2-1, (v)1-2-2; II femur (p)0-0-1, tibia (p)1-1-1, (v)1-1-2, metatarsus (v)1-1; III femur (d)0-0-1r., tibia (r)1-1, (p)2-2-1, (v)1-1-2, metatarsus (r)2-2, (p)2-2-2, (v)1-1-1, patella (p)2; IV femur (r)0-0-1, (p)0-0-1, tibia (r)1-2-2-1, (p)1-2-1-2, (v)1-1-2, metatarsus (r)1-1-1-1-1-1-1, (p)3-2-2-2, (v)1-1-1, patella (p)2; tarsus IV pseudosegmented.

Distribution: The species is endemic to southern Morocco and northern Western Sahara. Actual distribution includes western High Atlas (either the southern and northern slopes east to Demnate) and Anti-Atlas Mountain ranges (up to 2000 m a.s.l.), the coastal region south from Essaouira and the coastal part of southern Morocco down to Western Sahara (Fig. 13B)

Figure 16. *Ischnocolus mogadorensis*, habitus of living specimens. A, subadult female from Souss Massa region; B, adult female from Imsoane; C, subadult male from Boutazlaft; D, adult female from Souss Massa NP. Photo credits: E. Hijmensen (A), P. Fabiánek (B), J. Korba (C), R. Cavalcante (D).

Natural history: The lifestyle is similar to that of *I. valentinus* and could be described as opportunistic. Some specimens were found to excavate shallow chambers under rocks covered with loose, sheet web, whereas others were found in deeper holes under rocks, or they inhabited the cavities between rocks and stones (Fig. 17E, F). Habitat preferences range from coastal forests of Barbary thuja, *Tetraclinis articulata* (Vahl) Mast., habitats with dwarf fan palm (*Chamaerops humilis* L.) (Fig. 17A), coastal *Euphorbia* L. communities (Fig. 17D), High Atlas *Juniperus* L. communities (Fig. 17C) to semi-desert habitats. The distribution model for this species overlaps with the extension of the Mediterranean *Acacia–Argania* Dry Woodland and Succulent Thicket ecoregion (PA1212), defined by the WWF (2021).

Ischnocolus valentinus (Dufour, 1820)

(Figs 5A–B, 7, 8, 9A, 10A, 13A, 18A–N, 19A–G, 20A–F)

Mygale valentina Dufour (1820: 101; description of male).
Mygale valenciana: Walckenaer (1837: 228).
Trechona valentina: Thorell (1870: 168).
Ischnocolus holosericus L.Koch, in Ausserer (1871: 186; description of juvenile); Simon (1892: 136, fig. 119); Bacelar (1932: 171); Smith (1990: 129, figs 819–829; description of female).
Ischnocolus triangulifer Ausserer (1871: 186; description of juvenile); Bacelar (1932: 171).
Avicularia andalusiaca Simon (1873: 197, pl. 1, fig. 2; description of male and female); Bacelar (1932: 171, figs. 3–5).
Ischnocolus algericus Thorell (1875: 123, description of male). Simon (1903: 925, figs. 1070–1071, m).
Ischnocolus fuscostriatus Simon (1885: 41; description of male).
Leptopelma cavicola Simon (1889: 396; description of male and female, burrow structure; 1909: 8); Reimoser (1919: 7); Roewer (1942: 222); Bonnet (1957: 2395); Benoit (1964: 414, figs 1, 2; male and female).
Ischnocolus maroccanus Simon (1873: 199; description of male and female).
Ischnocolus numidus Simon (1909: 9; description of male).
Ischnocolus tripolitanus Caporiacco (1937: 57; description of female).
Ischnocolus valentinus: Ausserer (1871: 186); Guadanucci & Wendt (2014: 391; description of male and female); Zonstein (2018: 114; description of male) (synonymy of *Nemesia cavicola*); Montemor *et al.* (2020: 89, fig. 9C, D); Tamajón Gómez *et al.* (2020: 165).

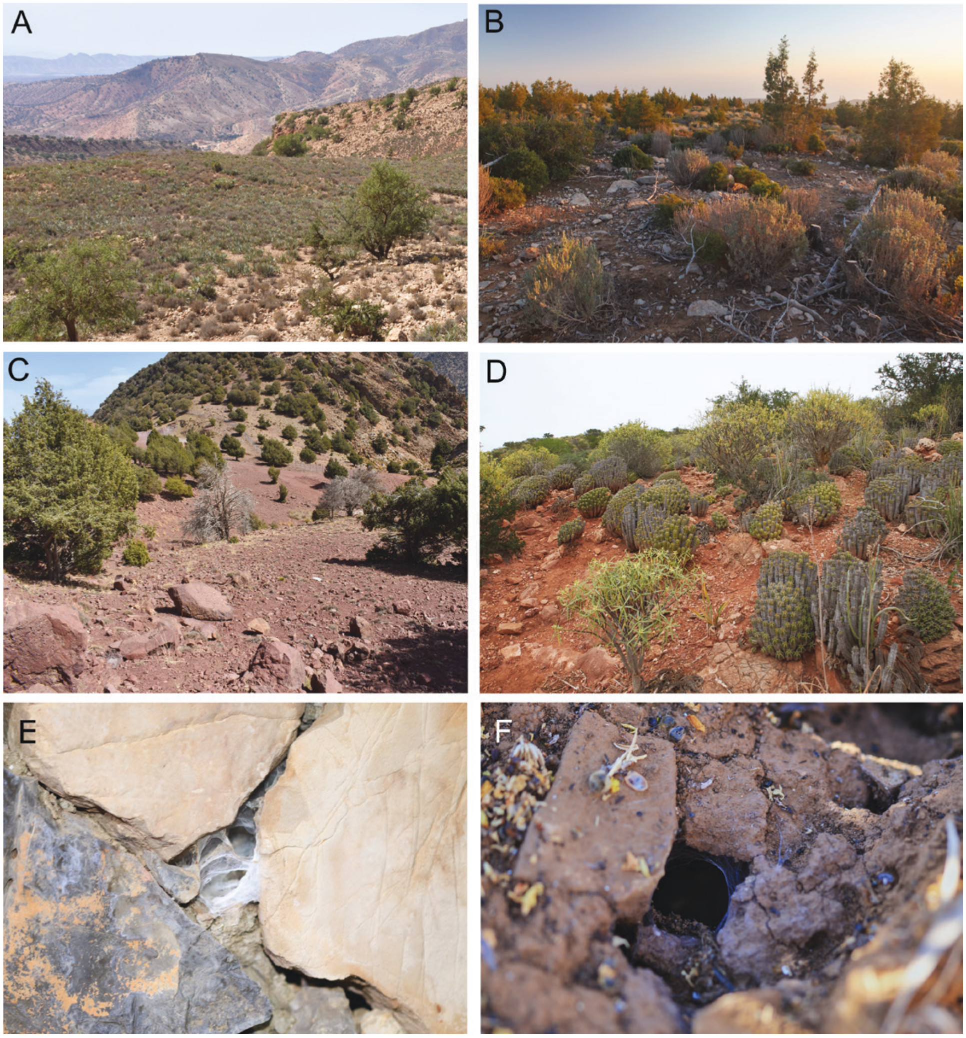

Figure 17. The habitats and burrows of *I. mogadorensis*. A, locality Alto Atlas, 1310 m a.s.l., shrubby vegetation with *Chamaerops humilis.* B, mountains near Ankrime, 1150 m a.s.l., shrubby vegetation with *Juniperus phoenicea.* C, locality Tizi n′Test, 2010 m a.s.l., rocky habitat with *Juniperus oxycedrus.* D, locality Bou Tazlaft, semi-arid Macaronesian vegetation with *Euphorbia balsamifera* and *E. officinarum.* E, burrow between stones. F, entrance to subterranean burrow with only slight web cover. Photo credits: A. Sánchez-Viallas (A, C), J. Korba (B, D), E. Hijmensen (E, F).

Type material: Type locality Moixent, Valencian Community, Spain. Female neotype deposited at BMNH, examined.

Material examined: Spain: 1♂, 1♀ (CRBAMM000941, CRBAMM000930), province of Cádiz, El Bosque, 36°26′50″N, 5°22′19″W, 27.iii.2010 (M. A. Ferrández leg.). 3♀♀ (CRBAMM000965, CRBAMM000966, CRBAMM000967), province of Cádiz, Grazalema, 36°27′28″N, 5°17′34″W, 28.iii.2010 (M. A. Ferrández leg.). 1♀ (CRBAMM000948), province of Sevilla, Castaño, 36°33′58″N, 5°15′14″W, 27.iii.2010 (M. A. Ferrández leg.). 1♂, 1♀ (CRBAMM000980, CRBAMM000986), province of Sevila, Coripe, 36°35′20″N, 5°17′34″W, 27.iii.2010 (M. A. Ferrández leg.). 1♀ (CRBAMM000141), province of Almería, La Rambla del Aljibe, 37°16′20″N, 2°02′24″W, 21.XI.2009 (E. Planas & V. Opatova leg.). 1 juv. (CRBAME000858), province of Málaga, Torcal de Antequera, 36°57′43″N, 4°31′06″W, 12.VI.2011 (E. Mora, V. Opatova & P. Sousa leg.). Morocco: 2♀♀, 5 juv. (CRBAMM000386, CRBAMM000387, CRBAMM000388, CRBAMM000389, CRBAMM000390, CRBAMM000391, CRBAMM000392), province of Azilal, near Ouzoud falls, 31°57′35″N, 6°46′05″W, 10.IV.2010 (V. Opatova & M. Arnedo leg.). 2♀♀, 1♂, 3 juv. (CRBAMM000393, CRBAMM000395, CRBAMM000396, CRBAMM000398, CRBAMM000399, CRBAMM000400), province of Azilal, Tilouguite, 32°05′04″N, 6°20′00″W,

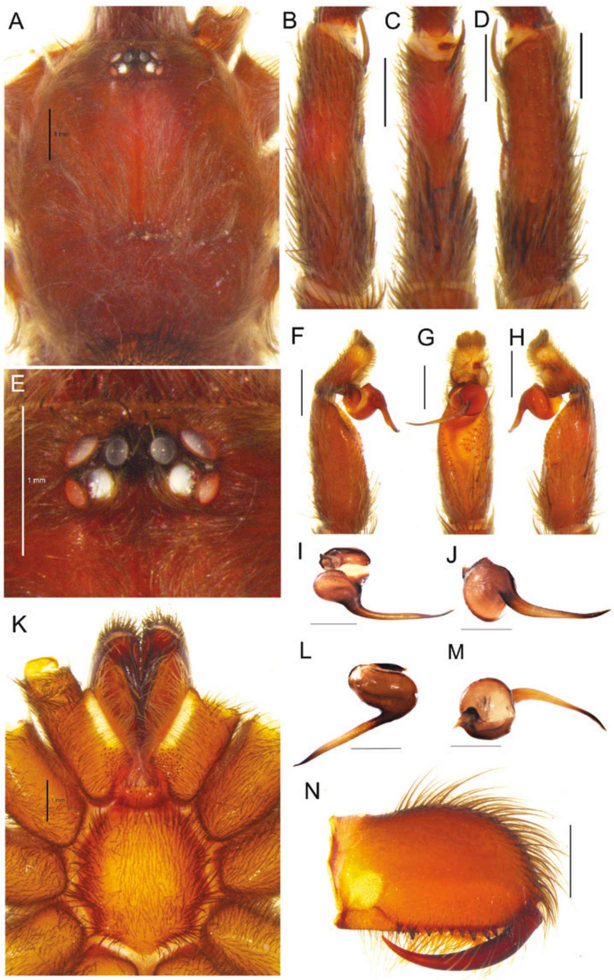

Figure 18. *Ischnocolus valentinus*, male, A–N (CRBAMM000941). A, prosoma, dorsal view. B, tibia I, prolateral view. C, tibia I, ventral view. D, tibia I, retrolateral view. E, eye tubercle, dorsal view. F, palpal bulbus, prolateral view. G, palpal bulbus, ventral view. H, palpal bulbus, retrolateral view. I, sternum, maxillae, labium and chelicerae, ventral view. J, bulbus, prolateral view. K, bulbus, ventral view. L, bulbus, retrolateral view. M, bulbus, dorsal view. N, chelicerae, prolateral view.

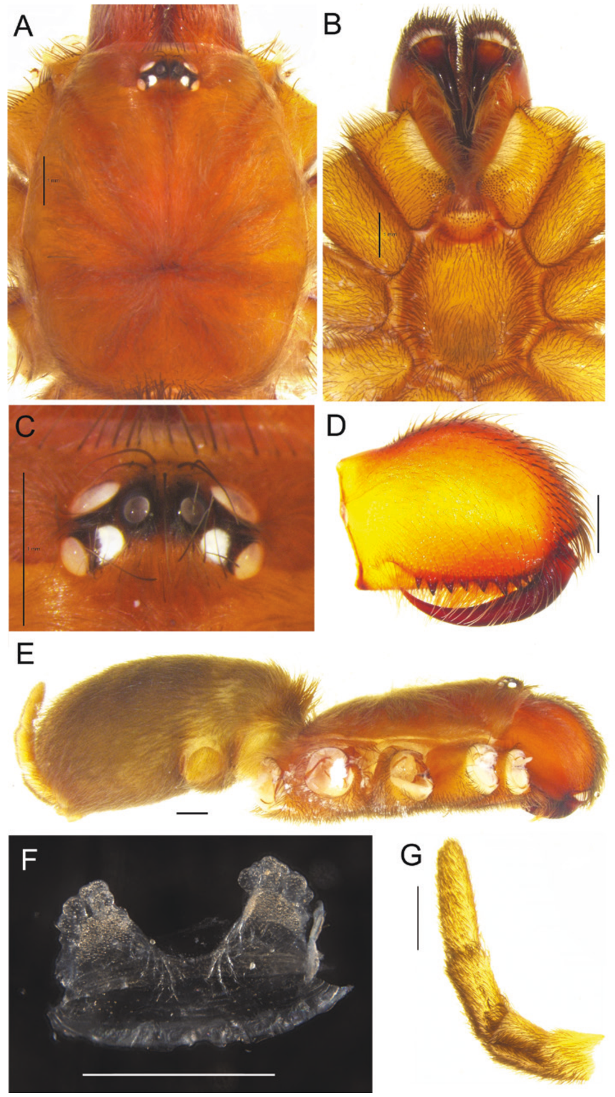

Figure 19. *Ischnocolus valentinus*, female, A–G (CRBAMM00387). A, prosoma, dorsal view. B, sternum, maxillae and chelicerae, ventral view. C, eye tubercle, dorsal view. D, chelicerae, prolateral view. E, whole body, lateral view. F, spermathecae. G, posterior lateral spinneret, retrolateral view. Scale bar = 1 mm.

10.IV.2010 (V. Opatova & M. Arnedo leg.). 1 juv. (CRBAMM000450), province of Fés, Djebel Zalach, 34°06′23″N, 4°58′10″W, 12.IV.2010 (V. Opatova & M. Arnedo leg.). 1 juv. (CRBAMM000485), province of Oujda, Ain Sfa, 34°49′28″N, 2°05′12″W, 14.IV.2010 (V. Opatova & M. Arnedo leg.). 3 juv. (CRBAMM000564, CRBAMM000565, CRBAMM000566), province of Tetuán, Beni Yder Cherki, 35°23′08″N, 5°31′20″W, 17.IV.2010 (V. Opatova, M. Arnedo leg.). 2 juv. (CRBAMM000493, CRBAMM000583), province of Berkane, Beni Snassen, 34°48′12″N, 2°23′48″W, 14.IV.2010 (V. Opatova & M. Arnedo leg.). 1♀ (CRBAMM000366), province of Al Haouz, Asni, 31°11′22″N, 8°03′27″W, 9.IV.2010 (V. Opatova & M. Arnedo leg.). 1♂ (SMNS-Aran-1376), province of Murcia, Mula, 38°03′41″N, 1°31′05″W, 2005. 1♂ (CRBA) province of Berkane, Taforalt, Grotte des Pigeons, 34°48′52″N, 2°24′10″W, 15.iv.2002 (M. Arnedo & C. Hernando leg.).

Diagnosis: Males can be distinguished from their congeners, except *I. jickeli*, by bearing only one spine apically along with dense concentration of spines on pro-ventral tibia I (Figs 8, 18B–D). They further differ

Figure 20. *Ischnocolus valentinus*, habitus of living specimens and burrow. A, adult male from Ouzoud, northern Morocco; B, adult female from Ouzoud, northern Morocco; C, adult female from Ouzoud, northern Morocco; D, adult female from Alhurin del Grande, Andalucia, southern Spain; E, burrow entrance under tree; F, burrow under the stone. Photo credits: J. Korba (A, B, C, E, F), T. Romanoff (D).

from all other *Ischnocolus* species by having straight embolus with narrowing tip (Figs 7, 18J–M). Females differ from their congeners by having spermathecae as wide as long with several (> four) apical lobes (Figs 5A, B, 19F).

Description: A detailed redescription is provided by Guadanucci & Wendt (2014) with male and female reproductive organ drawings and male spine pattern on tibia I. Additional photos and drawings of male bulbus are shown by Zonstein (2018), Tamajón Gómez *et al.* (2020) and Decae (in: Nentwig *et al.*, 2020).

Distribution: Following our circumscription of *I. valentinus* to the 'north' lineage, the distribution of the species is more restricted than previously thought, as it only includes the Iberian Peninsula and northern Morocco (Fig. 13A). The northernmost current localities are near Benidorm, in Alacant, Spain and the southernmost ones are located on the northern slopes of the High Atlas Mountains in Morocco. Previous studies have suggested the species occurrence extending as far east as Sicily, Tunisia and Libya (Guadanucci & Wendt, 2014). Although the only Sicilian sample included in our phylogeny was recovered within the 'north' lineage (i.e. *I. valentinus*), detailed morphological and molecular analyses of a more thorough specimen sampling in Algeria, Tunisia and Sicily will be required to confirm the status of the easternmost populations.

Natural history: Similar to *I. mogadorensis*, *I. valentinus* is an opportunistic species inhabiting natural cavities under and between rocks and tree roots. It usually covers the entrance with a dense, sheet web, sometimes resembling that of a funnel-web spider *Macrothele calpeiana* Walckenaer, 1805 or some Agelenidae. The burrow entrance can also sometimes resemble that made by *I. elongatus*, but the web of *I. valentinus* is less dense and more sheet-like (Fig. 20E, F). The burrow of *I. valentinus* never forms a proper tube, but continues as an irregular hole connecting one or several natural underground cavities. Habitat preferences range from Mediterranean open grasslands to dense Aleppo pine (*Pinus halepensis* Mill.) or Barbary thuja (*Tetraclinis articulata*) forests.

Ischnocolus elongatus (Simon, 1873)
(Figs 6A-L, 7, 8, 9C, D, 10C–F, 13C–F, 21A–N, 22A–G, 23A–F, 24A–H)

Cyrtauchenius elongatus Simon, 1873: 32 (description of female). Moggridge (1874: 182, 189, 248, pl. XIII, fig. B; burrow entrance); Savory (1928: 290). Presumably deposited in MNHN, not found by Zonstein (2018), not examined. Topotypes (Ksar el Kebir) were included in this study.

Leptopelma africana Ausserer, 1875: 167 (description of female). Synonymized with *Cyrtauchenius elongatus* Simon, 1873 by Simon (1889: 396).

Leptopelma elongata Simon 1889: 395, pl. XIII, fig. 2 (female, burrow entrance), Simon (1909: 9); Reimoser (1919: 7); Berland (1932: 110, fig. 219; burrow entrance).

Luphocemus insidiosus Denis, 1960: 186–189 (description of female), illustration of burrow (fig. 2, p.187). Deposition place unknown. Type not examined. Topotypes (Benslimane) were included in this study. **New synonymy**.

Harpactirella insidiosa Benoit, 1965: 297; Calatayud-Mascarell & Sánchez-Vialas (2020: figs 2–4, adult female and burrow).

Ischnocolus hancocki Smith, 1990: 127, figs 803–818 (female); Guadanucci & Wendt (2014: 394, fig. 4A; female); Zonstein (2018: 107, figs 1–8; male). Deposited in BMNH, type not examined. Topotypes (Larache) were morphologically examined. **New synonymy**.

Ischnocolus elongatus: Zonstein (2018: 106).

Type material: Type locality Ksar el Kebir (Morocco), female holotype presumably in MNHN, not found by Zonstein (2018), not examined. Topotypes were included in this study.

Material examined: Morocco: 9♀♀ (CRBAMM000430, CRBAMM000432, CRBAMM000424, CRBAMM000425, CRBAMM000426, CRBAMM000427, CRBAMM000428, CRBAMM000429, CRBAMM000431), province of Fés, Imouzer, 33°38′39″N, 5°04′09″W, 12.iv.2010 (V. Opatova, M, Arnedo leg.). 1♀, 2 juv. (CRBAMM000351, CRBAMM000350), province of Taroudant, Cova Maravilles, 30°10′40″N, 8°17′38″W, 8.iv.2010 (V. Opatova & M. Arnedo leg.). 3♀♀, 3 juv. (CRBAMM000372, CRBAMM000363, CRBAMM000371, CRBAMM000364, CRBAMM000365, CRBAMM000367), province Al Haouz, Asni, 31°11′22″N, 8°03′27″W, 9.iv. 2010 (V. Opatova, M. Arnedo leg.). 1♀ (CRBAMM000534), province of Taounate, Rhafsai, 34°37′55″N, 4°55′52″W, 16.iv.2010 (V. Opatova, M. Arnedo leg.). 1♂, 1 juv. (CRBAMM000397, CRBAMM000403), province of Azilal, Tilouguite, 32°05′04″N, 6°20′00″W, 10.IV.2010 (V. Opatova & M. Arnedo leg.). 3♀♀, 4 juv. (CRBAMM000411, CRBAMM000406, CRBAMM000407, CRBAMM000408, CRBAMM000410, CRBAMM000412, CRBAMM000413), province of Béni-Mellal, Ab el Hamam, 32°31′19″N, 4°55′52″W, 11.iv.2010 (V. Opatova & M. Arnedo leg.). 3♀♀ (CRBAMM000468, CRBAMM000467, CRBAMM000470), province of Taza, Sidi Abdulah, 32°31′20″N, 6°02′02″W, 13.iv.2010 (V. Opatova & M. Arnedo leg.). 1♀, 1 juv. (CRBAMM000483, CRBAMM000484), province of Oujda, Ain Sfa, 34°49′28″N, 2°05′12″W, 14.IV.2010 (V. Opatova & M. Arnedo leg.). 4♀♀, 4 juv. (CRBAMM000501, CRBAMM000502, CRBAMM000503, CRBAMM000504, CRBAMM000506, CRBAMM000507, CRBAMM000508, CRBAMM000509), province of Al Hoceima, Bni Hadifa, 35°00′19″N, 4°10′44″W, 15.iv.2010 (V. Opatova & M. Arnedo leg.). 1♀, 2 juv. (CRBA004970, CRBA004971, CRBA004972), province of Taroudant, Imgoune, 30°16′29″N, 8°16′26″W, 22.ii.2020 (J. Korba leg.). 2♀♀, 3 juv. (CRBA004973, CRBA004974, CRBA004975, CRBA004976, CRBA004977), province of Tiznit, Tafraout, 29°40′54″N, 9°01′54″W, 23.ii.2020 (J. Korba leg.). 2 juv. (CRBA004985, CRBA004986), province of Guelmim, Mesti, 29°11′52″N, 10°05′15″W, 25.ii.2020 (J. Korba leg.). 5♀♀, 2 juv. (CRBA004992, CRBA004993, CRBA004994, CRBA004995, CRBA004996, CRBA004997, CRBA004998), province of Essaouira, Ounagha, 31°31′32″N, 9°37′38″W, 28.ii.2020 (J. Korba leg.). 2♀♀ (CRBAMM000446, CRBAMM000447), province of Fés, Pantano, 34°03′33″N, 5°18′12″W, 12.iv.2010 (V. Opatova, M. Arnedo leg.). 2 juv. (CRBAMM000352, CRBAMM000353), province of Taroudant, Azoura, 30°01′31″N, 8°35′24″W, 8.iv.2010 (V. Opatova, M. Arnedo leg.). 4 juv. (CRBAMM000373, CRBAMM000374, CRBAMM000375, CRBAMM000376), province of Azilal, near Ouzoud falls, 31°57′35″N, 6°46′05″W, 10.IV.2010 (V. Opatova & M. Arnedo leg.). 1♀ (CRBAMM000419), province of Khénifra, Oumer Riba, 32°55′41″N, 5°30′34″W, 11.iv.2010 (V. Opatova, M. Arnedo leg.). 2♀♀ (CRBAMM000448, CRBAMM000449), province of Fés, Djebel Zalach, 34°06′23″N, 4°58′10″W, 12.IV.2010 (V. Opatova & M. Arnedo leg.). 3♀♀, 1 juv. (CRBAMM000488, CRBAMM000489, CRBAMM000490, CRBAMM000491), province of Berkane, Beni Snassen, 34°48′12″N, 2°23′48″W, 14.IV.2010 (V. Opatova & M. Arnedo leg.). 1♀ (CRBA004980), Bou Tazlaft, 29°37′40″N, 9°52′52″W, 24.ii.2020 (J. Korba leg.). 1♀ (CRBA004991), province of Essaouira, Ida Ou Guelloul, 30°54′00″N, 9°43′04″W, 27.ii.2020 (J. Korba leg.). 2♀♀ (CRBA004978, CRBA004979), province of Tiznit, Tighmi, 29°34′32″N, 9°23′51″W, 24.ii.2020 (J. Korba leg.). 1 juv. (CRBAMM000357), province of Taroudant, Tafingoul, 30°44′32″N, 8°24′06″W, 9.iv.2010 (V. Opatova & M. Arnedo leg.). 1 juv. (CRBAMM000356), province of Tiznit, Tizegzauine, 29°50′42″N, 8°56′14″W, 8.iv.2010 (V. Opatova & M. Arnedo leg.). 1♀ (CRBAMM000415), province of Beni Mellal, Cheikh, 32°37′23″N, 5°58′27″W, 11.iv.2010 (V. Opatova & M. Arnedo leg.). 3♀♀ (CRBA005022, CRBA005023, CRBA005024), province of Larache, Ksar el Kebir, 35°02′03″N, 6°01′50″W, 26.ii.2010 (A. Calatayud-Mascarell & A. Sánchez-Vialas leg.). 3♀♀ (CRBA005027, CRBA005028, CRBA005029), province of Benslimane, Benslimane, 33°39′06″N, 7°05′23″W, 26.ii.2020 (A. Calatayud-Mascarell & A. Sánchez-Vialas leg.). 5♀♀ (CRBA005032, CRBA005033, CRBA005034, CRBA005035, CRBA005036), province of Sidi Bennour, Oualidia, 32°36′38″N, 9°00′34″W, 25.ii.2020 (A. Calatayud-Mascarell & A. Sánchez-Vialas leg.). 1♀ (CRBAMM000222), province of Al Haouz, Tahanaoute, 31°21′15″N, 7°57′06″W, 9.iii.2007 (M. Arnedo & C. Ribera leg.). 4♀♀ (deposited in Department of Zoology, Charles University), province of Larache, 35°12′08″N, 6°06′03"W, 12.ix.2021 (J. Korba & V. Opatova leg.)

Remarks: Originally described as *Cyrtauchenius elongatus* Simon, 1873, this species has been recently transferred to the genus *Ischnocolus* by Zonstein (2018) based on Ausserer's description of *Leptopelma africana*, which clearly pointed to Theraphosidae ('… two toothless claws bearing two tufts of hairs in each tarsi'). The three samples from the type locality analysed in our study (JK82, JK83, JK84, see Fig. 3) were recovered within the *elongatus* clade, which is clearly defined by its distinct morphology. Similarly, we included individuals from the type locality of *H. insidiosa* (JK87, JK88, see Fig. 3), which were shown to belong to the same clade as the remaining species identified as *I. elongatus*.

In the case of *I. hancocki*, we could not examine the holotype female nor add samples from Larache (type locality) to the molecular analyses. However, we examined the morphology of specimens from the type locality, which fit the redescription by Guadanucci & Wendt (2014) and turned out to be indistinguishable from the rest of the *elongatus* morphotype samples. Moreover, the type locality Larache is located within the estimated (SDM) range of occurrence, only 30 km north-west from the topotype locality of *I. elongatus*. The putative synonymy of *I. elongatus* and *I. hancocki* was already suggested by Zonstein (2018).

Based on these arguments and the detailed examination of topotypes of each taxon, we herein propose *I. elongatus* as senior synonym of both *I. hancocki* and *Harpactirella insidiosa*.

Diagnosis: Ischnocolus elongatus differs from all its congeners by the following combination of characters: robust appearance (Fig. 23), apical segment of PLS triangular (Figs 9C, D, 10C–F, 22D), cephalic region and eye tubercle elevated (Figs 11B, 22E), presence of black bristles on cheliceral margin (Fig. 22D) and tarsus IV without pseudosegmentation. Females further differ from other *Ischnocolus* species, except *I. vanandalae*, by possessing 0–2 apical lobes on spermathecae (Figs 6A–L, 22F). Males differ from other *Ischnocolus* species by having reduced spination on ventral tibia I (Figs 8, 21B–D) and having a shorter palpal tibia in comparison to the tarsus and patella (Fig. 21F–H). The lifestyle of *I. elongatus* is unique among its congeners [see Montemor *et al.* (2020) for natural history of Middle Eastern species], as it excavates deep tube-like burrows (see Natural history section).

Description: Male, (CRBAMM000397, Tilougguite): Total length 14.12. **Colour pattern:** *Colour in ethanol:* legs and carapace light yellow-brown. Carapace with silver hairs (Fig. 21A). Abdomen darker brown with dorsal light striped pattern. **Carapace:** 5.43 long, 4.72 wide (Fig. 21A); cephalic region raised from lateral view; eye tubercle elevated, 0.68 long, 1.08 wide; fovea slightly procurved (Fig. 21A). Clypeus 0.23 wide. **Eyes** (Fig. 21E): AME 0.18, PME 0.17, ALE 0.23, PLE 0.20; PME-PME 0.67, ALE-AME 0.26, ALE-PLE 0.34, AME-PLE 0.38, AME-AME 0.35, ALE-ALE 0.81. **Sternum, labium and maxillae:** sternum 2.60 long, 2.47 wide, setose; labium 0.58 long, 1.02 wide, with approx. 20 cuspules; maxillae with approx. 40 cuspules (Fig. 21I). **Abdomen**: 6.30 long, 3.23 wide; PLS basal segment 0.84 long, median segment 0.51 long, apical segment 0.52 long, triangular. **Chelicerae:** 2.27 long; basal article with nine teeth; intercheliceral tumescence present (Fig. 21N). Rastellum *sensu* Raven (1994) absent, but a group of strong black bristles in front of the fang base is present (Fig. 21N). **Pedipalps:** spination: femur (p)1ap., ventral furrow on tibia not sigmoid, broad. Length: 7.76 (femur 3.12, patella 1.82, ≤ tibia 2.09, tarsus 1.59). **Copulatory bulb:** bulb globular, embolus curved with pointed tip (Figs 7, 21F–H, J–M). **Legs:** scopula on all tarsi divided by a thick

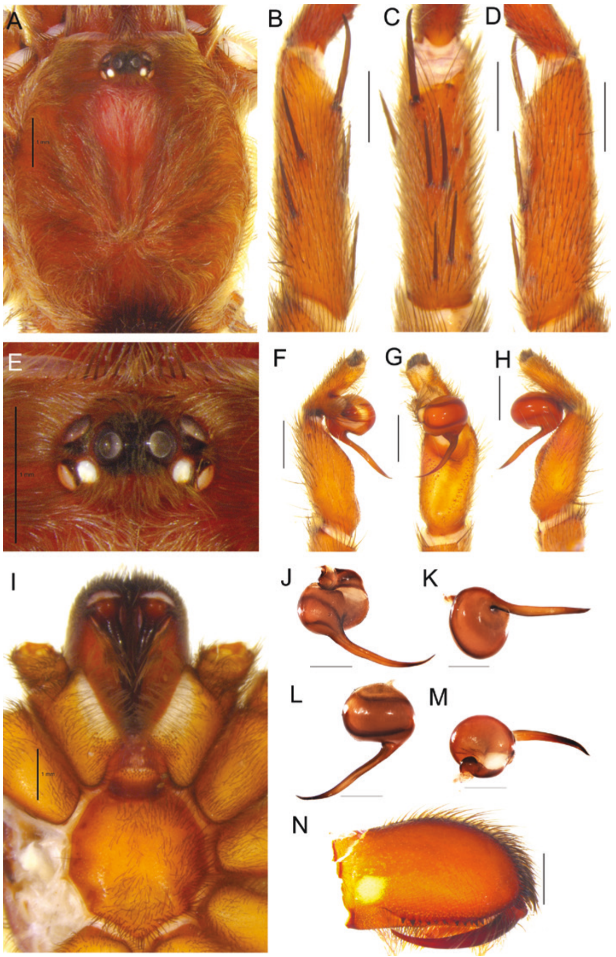

Figure 21. *Ischnocolus elongatus*, male, A–N (CRBAMM000397). A, prosoma, dorsal view. B, tibia I, prolateral view. C, tibia I, ventral view. D, tibia I, retrolateral view. E, eye tubercle, dorsal view. F, palpal bulbus, prolateral view. G, palpal bulbus, ventral view. H, palpal bulbus, retrolateral view. I, sternum, maxillae, labium and chelicerae, ventral view. J, bulbus, prolateral view. K, bulbus, ventral view. L, bulbus, retrolateral view. M, bulbus, dorsal view. N, chelicerae, prolateral view. Scale bar = 1 mm.

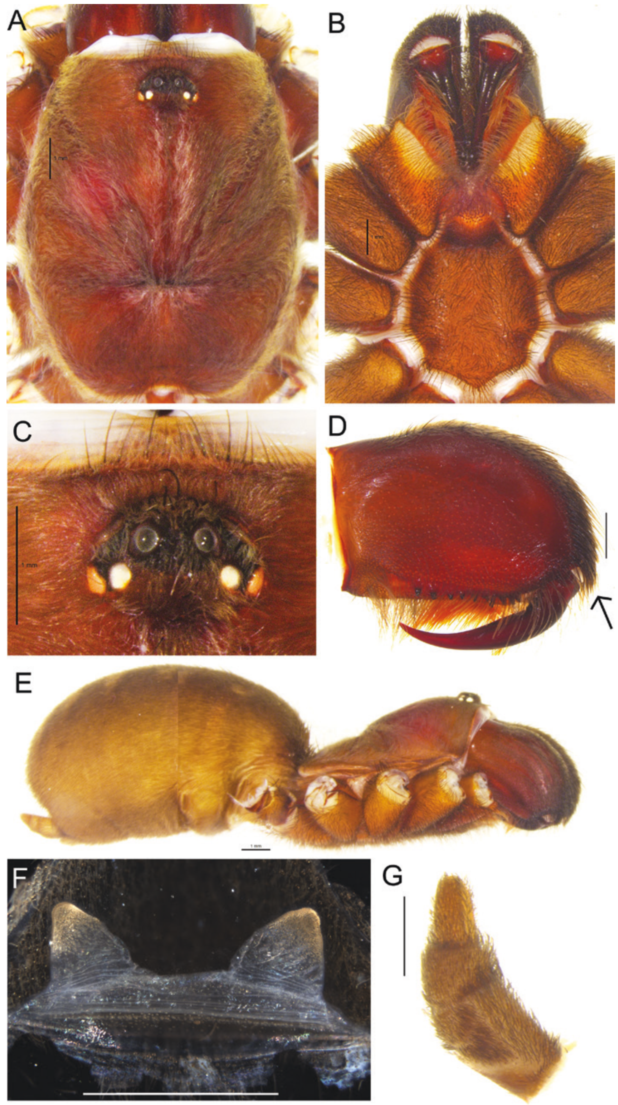

Figure 22. *Ischnocolus elongatus*, female, A–G (CRBA005027). Prosoma, dorsal view. B, sternum, maxillae and chelicerae, ventral view. C, eye tubercle, dorsal view. D, chelicerae, prolateral view (arrow indicates dense strong black bristles). E, whole body, lateral view. F, spermathecae. G, posterior lateral spinneret, retrolateral view. Scale bar = 1 mm.

band of setae. Scopula on ventral metatarsus I nearly totally occupied, II half occupied, III and IV < half occupied. Paired claws on tarsi I–IV, bipectinate, with two rows of five teeth. Leg measurement: length of legs IV > I > II > III. Leg I: 15.98 (femur 4.76, patella 2.62, tibia 3.39, metatarsus 3.01, tarsus 1.94), leg III: 14.30 (femur 3.54, patella 2.06, tibia 2.27, metatarsus 3.22, tarsus 2.04), leg IV: 19.15 (femur 4.98, patella 2.55, tibia 3.78, metatarsus 4.26, tarsus 2.49). Spines: I femur (p)ap1, (r)ap1, patella (r)1, tibia (r)1-1, (v)2-2-2, metatarsus (v)1-1; III femur (p)ap1, patella (p)1, tibia (r)1-1, (p)2-2, (v)1-1-2, metatarsus (r)0-1-1, (p)2-2-2, (v)1-1-1-1; IV femur (r)ap1, (d)ap1, patella (p)1, tibia (r)1-1-1-1-1-1, (p)2-1-1-1, (v)1-1-2, metatarsus (r)1-1, (p)1-2-1-1-2, (v)1-1. Tarsus IV without pseudosegmentation.

Female (CRBA005027, Benslimane): Total length 25.07. **Colour pattern:** *Colour in ethanol:* carapace, chelicerae and legs dark orange-brown, abdomen grey-brown with light striped pattern. *Colour of live specimens:* northern populations have beige-golden setae on carapace, legs and chelicerae. Basal part of the chelicerae is black without setae, black stripe on

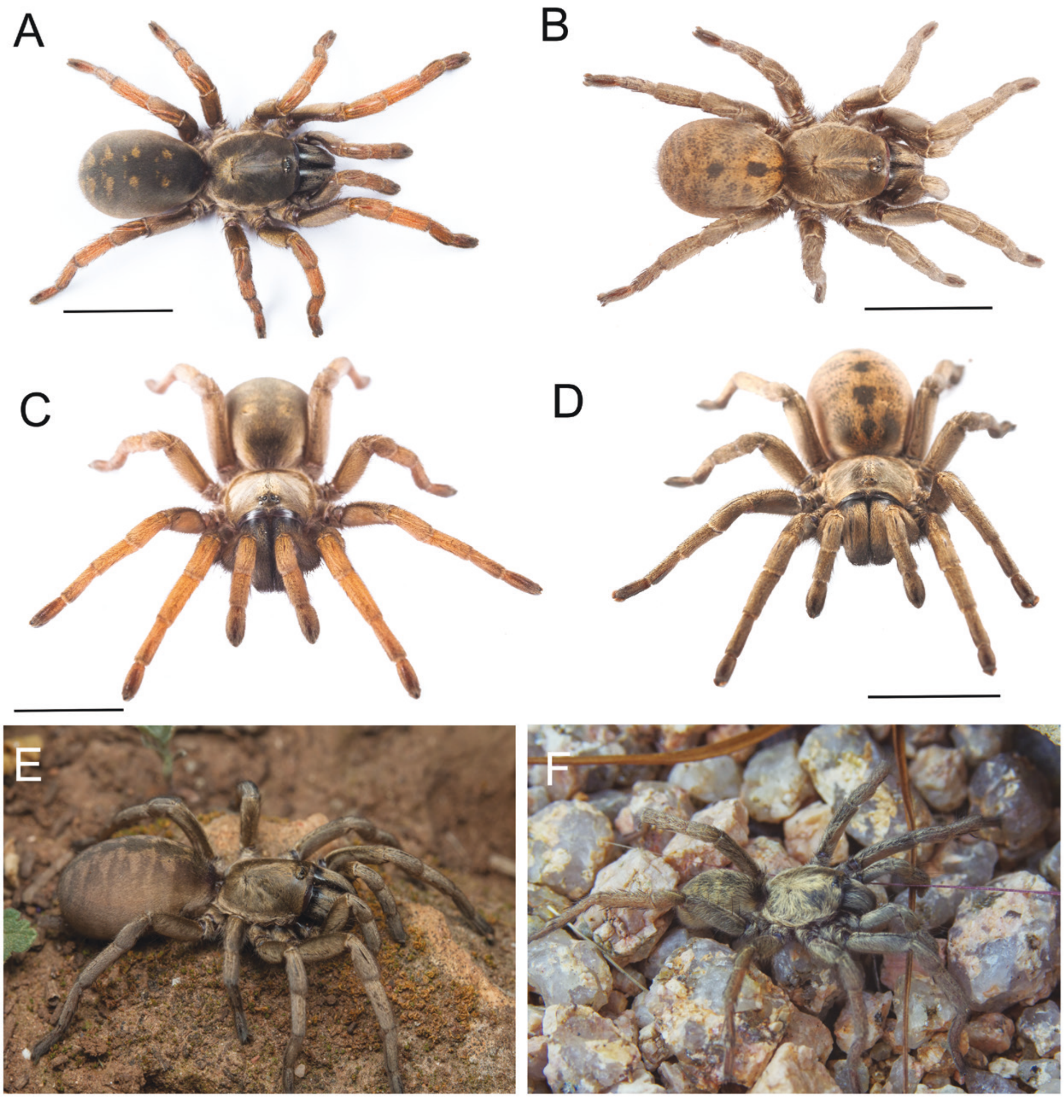

Figure 23. Habitus of *I. elongatus* from different regions of Morocco. A, adult female from Tafraout (south); B, subadult female from Ksar el Kebir (north); C, adult female from Imgoune (south); D, adult female from Benslimane (north); E, adult female from Ounagha (central); F, adult male from Tafraout (south). Scale bar = 10 mm. Photo credits: J. Korba (A, C, E), A. Sánchez-Vialas (B, D), S. Vogler (F).

the patella of each leg. Abdomen beige-golden with black spots (Fig. 23C). Southern populations have orange legs with black setae, carapace golden brown, chelicerae black with golden brown setae. Abdomen light to dark-brown with golden spot pattern (Fig. 23A, B). **Carapace:** 7.74 long, 6.39 wide (Fig. 22A); cephalic region raised from lateral view; eye tubercle strongly elevated (Fig. 22E), 0.99 long, 1.40 wide; fovea deep, straight to slightly procurved (Fig. 22A); clypeus 0.29. **Eyes** (Fig. 22C): AME 0.20, PME 0.21, ALE 0.26, PLE 0.23; PME-PME 0.89, ALE-AME 0.31, ALE-PLE 0.43, AME-PLE 0.54, AME-AME 0.47, ALE-ALE 1.01. **Sternum, labium and maxillae:** sternum 3.87 long, 3.44 wide; labium 1.14 long, 1.63 wide, with approx. 20 cuspules; maxillae with approx. 70 cuspules (Fig. 22B). **Abdomen:** oval, 12.87 long, 6.77 wide (Fig. 22E); PLS basal segment 1.30 long, median segment 0.63 long, apical segment 0.84 long, triangular (Fig. 22G). **Vulva:** formed by two widely separated triangular receptacles without lobes (Fig. 22F). **Chelicerae**: robust, 4.20 mm long; basal article with nine teeth; rastellum *sensu* Raven (1994) absent, but a group of strong black bristles is present on the margin (Fig. 22D). **Pedipalps:** length: 11.61 (femur 4.26, patella 2.66, tibia 2.52, tarsus 2.17). Spination: femur (p)ap1, tibia, (v)1-1-2, (p)1-2-1.

Legs: scopula on all tarsi divided by a thick band of setae. Scopula on ventral metatarsus I entirely occupied, II four-fifths occupied, III three-quarters occupied, IV three-quarters occupied. Leg measurement: length of legs IV > I > II > III. leg IV: 21.1 (femur 6.05, patella 3.36, tibia 4.58, metatarsus 4.45, tarsus 2.66), leg III: 14.52 (femur 4.59, patella 2.61, tibia 2.60, metatarsus 2.72, tarsus 2.00), leg II: 17.19 (femur 5.21, patella 3.07, tibia 3.59, metatarsus 3.08, tarsus 2.24), leg I: 19.44 (femur 5.99, patella 3.65, tibia 4.13, metatarsus 3.34, tarsus 2.33). Spines: I femur (p)ap1, tibia (v)1-1, tarsus (v)1-0; II femur (p)ap1, tibia (r)0-0-1, (v)1-1-2, tarsus (v)1-1; III femur (r)ap1, (p)ap1, patella (r)1, (p)2, tibia (r)1-1, (p)2-2, (v)1-1-2, metatarsus (r)1, (p)2-2-2, (v)1-1-2; IV femur (r)ap1, patella (r)ap1, tibia (r)1-1-1, (v)2-1-2-1-2 metatarsus (r)1-2-1, (p)1-1, (v)2-2-2-3. Tarsus IV without pseudosegmentation.

Distribution: The species is currently known only from Morocco, where it ranges from Larache in the north to Mesti in the south. Distribution in Algeria is highly probable.

Natural history: Ischnocolus elongatus constructs a 20–30 cm deep tube burrow with an open entrance and a palisade build from surrounding material resembling that of wolf spider genus *Lycosa*, but with more dense and compact silk lining (Fig. 24E–H). Burrows in southern populations (~20 observed) consist of a single, slightly inclined underground tube, sometimes connected to the surface by side exits. Burrows in northern populations seemed to be more complex (~ten burrows observed). A tube vertically extending from the entrance ends after approximately 5–10 cm, forming a chamber where the spider deposits prey remnants and old exuviae. The main burrow connects laterally to the vertical tube few cm below the entrance. The opening to the lateral tube is small and often closed by a dense web. After a short distance, the horizontally oriented side tube turns vertical and continues approx. for another 20 cm.

The species occurs in a wide variety of habitats and climates, also in sympatry with either *I. valentinus* or *I. mogadorensis.* It has been found in humid localities in northern Morocco, in Aleppo pine (*Pinus halepensis*) or cork-oak (*Quercus suber* L.) forest with Mediterranean fan palm (*Chamaerops humilis*) (Fig. 24C), in the central coast on light sandy soil with Berber thuja (*Tetraclinis articulata*) (Fig. 24B) and in semi-arid localities in southern Morocco among argan stands [*Argania spinosa* (L.) Skeels] (Fig. 24D) or in Macaronesian vegetation with *Euphorbia balsamifera* Aiton and *E. officinarum* L. on hard sandstone bedrock (24A). In Atlas and Anti-Atlas Mountains, the localities do not exceed 2000 m a. s. l.

DISCUSSION

Theraphosidae colonized the Mediterranean region twice, independently

The results of our phylogenetic analyses of the family Theraphosidae did not recover the presumed close relationship between *Ischnocolus* and *Chaetopelma* based on their geographic proximity and morphological similarities (Smith, 1990; Longhorn & Hamilton, 2020). *Chaetopelma* was originally described as a subgenus of *Ischnocolus* (Ausserer, 1871), but it was later elevated to genus level (Pocock, 1897) because of the differences in its foveal shape and the number of tarsi with divided scopula. Based on similar morphological traits in the theraphosid subfamilies Ischnocolinae (comprising both *Ischnocolus* and *Chaetopelma*) and Eumenophorinae, Smith (1990) hypothesized that the ancestor of *Ischnocolus*/*Chaetopelma* split from Eumenophorinae and lost its ancestral stridulatory organ. Our results support *Chaetopelma* (represented by specimens from Israel and Cyprus) as the sister-group to Eumenophorinae, together forming a clade sister to the rest of the sampled Theraphosidae, alternatively suggesting that the stridulatory organ evolved after the separation of the *Chaetopelma* clade. The early branching position of Eumenophorinae recovered in our analyses is also in agreement with the transcriptomic analysis of Foley *et al.* (2019, 2021). However, both studies are based on a limited sampling of the whole Theraphosidae diversity.

The three western Mediterranean *Ischnocolus* species were recovered as a monophyletic group, thus contradicting a former hypothesis suggesting a close relationship between some Moroccan taxa and South African *Harpactirella*. *Ischnocolus* was repeatedly recovered as a sister-group to some or all Neotropical subfamilies in our analyses, although with low support. Similarly, Foley *et al.* (2019) recovered the Neotropical genus *Trichopelma* (Ischnocolinae *s.s.*) (Guadanucci, 2014) as a sister-clade to all New World Theraphosidae. Unfortunately, our analyses did not include any New World Ischnocolinae *s.s.* genera, but the same phylogenetic position of *Trichopelma* (Foley *et al.*, 2019) and *Ischnocolus* (our results) supports the position of Ischnocolinae *s.s.* and the divergence into the Old and New World taxa through the vicariant event of the Africa–South America split (Guadanucci, 2014). Our time-calibrated phylogeny provided marginal support for this hypothesis, as the split between *Ischnocolus* and Neotropical clades was dated to the Late Cretaceous (95% HPD = 72.08–94.28 Mya), which is slightly younger than the geological estimates for the split between South America and Africa (102.5–120.0 Mya) (Iturralde-Vinent, 2006; Blakey, 2008, Matthews *et al.*, 2016). Similar divergence times between Ischnocolinae *s.s.* taxa and the rest of New

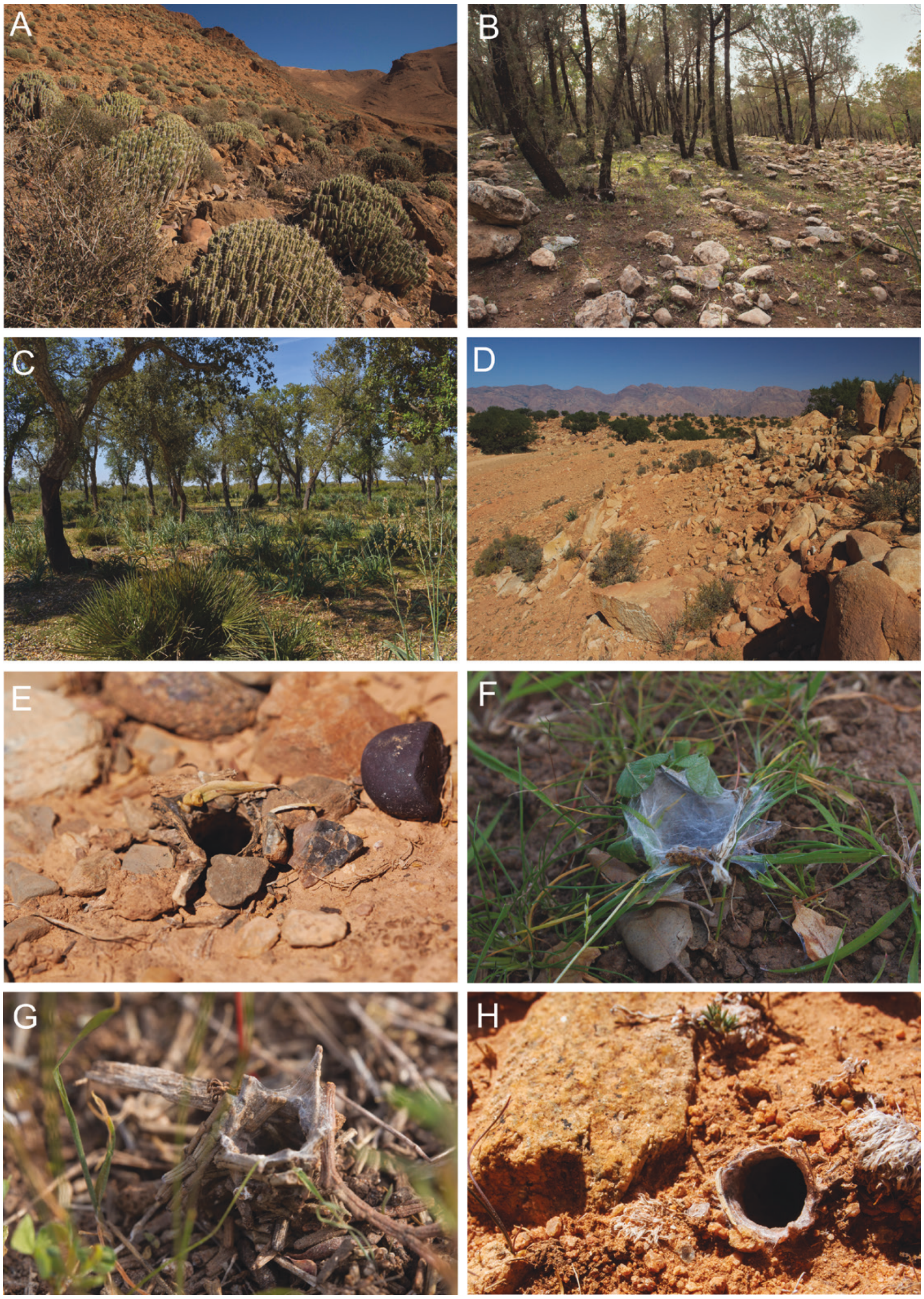

Figure 24. Habitats and burrow entrances of *I. elongatus*. A, locality Imgoune, semi-arid valley with *Euphorbia officinarum*. B, locality Ounagha, coastal plain on sandy soil with stands of *Tetraclinis articulata*. C, locality Benslimane, *Quercus suber* stands with *Chamaerops humilis.* D, locality Tafraout, Anti-Atlas Mountains, semi-arid habitat with *Argania spinosa.* E, locality Imgoune, burrow entrance in a hard rocky habitat. F, locality Benslimane; some burrows were found closed by dense web. G, locality Ounagha; where there is available material around, spiders construct conspicuous above ground turrets. H, locality Tafraout, burrow entrance in hard bedrock. Photo credits: J. Korba (A, B, D, E, G, H), A. Sánchez-Vialas (C, F).

World Theraphosidae were recently inferred at 100 Mya for *Trichoplema* (Foley *et al.*, 2021) and at 92 Mya for *Ischnocolus* (Ortiz *et al.*, 2018). Interestingly, the placement of *Ischnocolus* recovered in our analyses contrasts with the results of genomic analyses of Opatova *et al.* (2020) that inferred *Ischnocolus* either as sister to Asian *Cyriopagopus* (Ornithoctoninae) or to a clade formed by the last species and the South

African *Brachionopus* (Harpacterinae), but the sampling across Theraphosidae in these analyses was too limited to be informative.

Our findings suggest two independent colonization events of the Mediterranean Basin by the family Theraphosidae, probably from western Gondwana (Foley *et al.*, 2021). The distribution of these two genera in the Mediterranean is almost disjunct. *Ischnocolus* is mostly restricted to the west (Spain, Morocco, Algeria, Tunisia, Sicily and Libya) and *Chaetopelma* to the east (Crete, Cyprus, Turkey, Israel and Lebanon). Partial overlap occurs in the Middle East, from where only one species of *Ischnocolus* is reported (Guadanucci & Wendt, 2014; Zonstein, 2018). Although Africa has been inferred as the ancestral area for Eumenophorinae, emerging around 58–55.5 Mya (Foley *et al.*, 2021), the split between *Chaetopelma* and Eumenophorinae is much older according to our analysis (83.17 Mya, 70–97 Mya). At that time, Africa was already disconnected from South America (Matthews *et al.*, 2016), thus an African origin of *Chaetopelma* is more likely.

A lifestyle shift in *Ischnocolus*

Our results revealed a deep evolutionary split within the western Mediterranean *Ischnocolus*, corresponding to the two different lifestyles reported in this group. While the sister-taxa *I. valentinus* and *I. mogadorensis* show opportunistic behaviour and inhabit natural cavities, *I. elongatus* constructs deep, complicated tube burrows, often with a palisade around its entrance. These contrasting ecological strategies are reflected in their morphology: *I. elongatus* has an oval opisthosoma, strong, black bristles on the chelicerae, a more elevated caput and stouter legs that probably evolved as adaptations for digging (Pérez-Miles & Perafán, 2017), while the opportunistic *Ischnocolus* species display a more generalized morphology, with flat opisthosoma and longer PLS. Although these morphological differences (see Figs 9, 10, 11B) may have evolved as a response to specific evolutionary pressure, assessing the evolutionary polarity of the lifestyle shift and concomitant changes in morphology will require a more complete phylogenetic assessment of the genus *Ischnocolus*.

Drivers of overlooked diversity in western Mediterranean *Ischnocolus*

Our molecular analyses revealed that western Mediterranean *Ischnocolus* consists of two geographically overlapping, yet deeply divergent clades (i.e. morphotypes '*valentinus*' and '*elongatus*'), with differences in morphology and spinning structures. Each clade was further structured into several allopatric lineages. Deep divergences among populations of sedentary organisms, such as mygalomorph spiders, are common (Bond *et al.*, 2001; Bond & Stockman, 2008; Rix *et al.*, 2018) and have been documented in other Mediterranean taxa (Opatova & Arnedo, 2014; Opatova *et al.*, 2016). Distinguishing a population structure from cryptic diversity is often challenging, because the results of the delimitation process can be biased by both the methodological approach (Sukumaran & Knowles, 2017; Leaché *et al.*, 2019) and the insufficient taxon sampling (Hamilton, 2014; Chambers & Hillis, 2020). Therefore, an integration of several independent lines of evidence and broad geographic sampling is usually needed to achieve a reliable outcome (Edwards & Knowles, 2014).

The presence of overlooked diversity seems to be the rule rather than an exception in Theraphosidae (Hendrixson *et al.*, 2013) and integrative approaches have proven to be useful for detecting cryptic species within many genera (Hamilton, 2014, 2016b; Montes de Oca *et al.*, 2016; Ortiz & Francke, 2016; Candia-Ramírez & Francke, 2020). In the case of the opportunistic *valentinus* clade, the deep genetic divergence between its two main lineages was further corroborated by genitalic as well as ecological differences. The combination of different sources of evidence justified the revalidation of *I. mogadorensis*, endemic to semi-arid southern Morocco, as a different species from *I. valentinus*. Conversely, the geographic structuring of the burrowing *I. elongatus* clade into four allopatric lineages ('north', 'north-east', 'central' and 'south'), was not accompanied by obvious morphological or ecological differences. The morphological comparisons relied exclusively on females in this case, which may be problematic. Spermathecae have been reported to either show strong intraspecific variation, as, for example, in North American *Aphonopelma* Pocock, 1901 species (Hamilton *et al.*, 2016b), or hardly possess any interspecific differences (Harvey, 2015). Among *I. elongatus*, the 'north-east', 'central' and 'south' spermatheca shapes were similar, but the 'north' lineage differed from the rest. Interestingly, significant differences in the shape of the apical segment of PLS were found between the 'south' lineage and both the 'north' and 'north-east' lineages, but not with the 'central' one. More data, especially male morphology, will be necessary to support, or reject, the species status of the divergent lineages within *I. elongatus* revealed here.

While the opportunistic and burrowing *Ischnocolus* was mostly sympatric across its range, our results indicate an allopatric pattern among the lineages within each morphotype. However, two lineages of each clade overlapped at the northern slopes of the High Atlas Mountains. The sympatry was also predicted by the SDM, along the lines of the existence of a transition zone between humid sclerophyllous Mediterranean forest habitat and semi-arid habitats of western High Atlas. The westernmost part of the Atlas Mountains close to the Atlantic Ocean is relatively low (< 2000 m) and probably did not act as a barrier between the Essaouira plains and parts of the northern slopes of High Atlas, as *I. mogadorensis* was found in elevations up to 2000 m. The time of the uplift of the High Atlas is uncertain, but it is generally accepted that some minor deformations had already occurred during the Late Eocene–Oligocene (Ellero *et al.*, 2012), but the main uplift phase probably did not occur earlier than Mid to Late Miocene (El Harfi *et al.*, 1996; Gomez *et al.*, 2000). According to the most recent study, the tectonic deformation did not significantly change the mean elevation of the mountain range during the Late Miocene period (the mean height was 1200 ± 500 m) and it was not until the Plio-Quaternary when the increased uplift of the High Atlas occurred (gain approx. 1000 m) (Boulton *et al.*, 2016). On the other hand, the climate was significantly cooler (Herbert *et al.*, 2016) and mid-elevation habitats may not have been suitable for these thermophilic organisms. Similar biogeographic patterns roughly concordant with Late Miocene uplift have been reported in other animals, such as agamid lizards (Brown *et al.*, 2002) and *Buthus* scorpions (Klesser *et al.*, 2021), which suggest that the uplift acted as an effective geographic barrier.

Based on substitution rate priors, the estimated time of the divergence of 'south' and 'central' lineages of *I. elongatus* (9.6 Mya, 5.1–17.0) suggests that the Atlas orogeny may have driven population structuring in the latter group. However, our divergence-time estimates between *I. valentinus* and *I. mogadorensis*, and among the 'north' and the remaining *I. elongatus* lineages, predated the Atlas formation. In this case, divergences may have been driven by adaptation to distinct environmental conditions, as suggested by the SDM predictions.

Our evidence suggests that *I. valentinus* colonized Europe at least twice independently, since the populations in Iberia and Sicily did not form a clade and were both nested in the 'north' lineage. Our time estimates suggest that the colonization occurred during the Messinian salinity crisis (MSC) (5.96–5.33 Mya), when the sea level of the Mediterranean Sea dropped significantly and created land bridges, facilitating the taxa exchange (Agustí *et al.*, 2006; García *et al.*, 2016; Klesser *et al.*, 2021). The latitude of the northernmost occurrence of *I. valentinus* in the Iberian Peninsula (north-east of Serra de Aitana, province of Valencia, Spain) matches the distribution of other thermophilic organisms (Husemann *et al.*, 2012). Interestingly, although the SDM also predicted the presence of the 'north' lineage of *I. elongatus* in the southern Iberian Peninsula, the species has never been reported there.

On a cautionary note, we should emphasize that the former discussion was based on the time estimates derived from prior information on substitution rates. However, these values were consistently younger (about half the estimated age) than the estimates based on the secondary calibration points for the *All_Theraphosidae* matrix. The use of the time estimates derived from the theraphosid analyses to the *Ischnocolus* biogeographic history, would result in much older splitting events, in some cases difficult to reconcile with the geochronology of the region. For instance, the split of the Iberian and North African populations would correspond to the Late Oligocene to Early Miocene, a time when the northern part of Morocco (Rif) was still part of the Iberian Peninsula (Rosenbaum *et al.*, 2002). It has been suggested that the use of fossil constraints on deep nodes may result in the overestimation of time divergences at shallow nodes, because of the inability of current models to completely account for rate heterogeneity or substitution saturation (Van Tuinen & Torres, 2015). Interestingly, the estimated value for the substitution rate of the *COI* derived from the theraphosid analysis (ucdl.mean = 0.127), was half the rate estimated for other spiders (ucdl.mean = 0.0199) (Bidegaray-Batista & Arnedo, 2011), yet similar to what has been inferred on other theraphosid taxa (ucld.mean = 0.0124) (Ortiz *et al.*, 2018). However, when the value was used as prior for estimating divergence time in *Ischnocolus*, the posterior estimates were twice higher (ucld.mean = 0.024, SD = 0.006). Surprisingly, when we used the faster rate (0.0199) instead, results converged in almost identical posteriors (0.245, 0.0045). Additional data and new time estimates based on a more balanced distribution of calibration points along the tree will be required to either confirm or reject the evolutionary scenario for the diversification of western Mediterranean *Ischnocolus* put forward in the present study.

CONCLUSIONS

The only two theraphosid genera currently inhabiting the Mediterranean Basin, *Ischnocolus* and *Chaetopelma*, are not sister-taxa and have their closest relatives on different continents. The integration of molecular evidence with morphology and ecological data has revealed the existence of two main clades with contrasting lifestyles within *Ischnocolus* in the western Mediterranean. In each of these clades, additional lineages with mostly allopatric distribution could be delimited. The geographic structuring most likely reflects barriers to gene flow imposed by the orography and climatic changes in the region since the Mid-Miocene. Our data supports the revalidation of *I. mogadorensis* to include the southern lineage of the *valentinus* morphotype. Additional lineages were also delimited within *I. elongatus*. However, low clade support, their ecological interchangeability and the lack of males for morphological comparison precluded clarifying their taxonomic status.

ACKNOWLEDGEMENTS

We are grateful to R. Kaderka and F. Polakovič for providing photos of a type specimen of *I. valentinus* from BMNH, to I. Wendt (Stuggart Museum) and P. Just for providing additional material of *Ischnocolus.* We thank D. Ortiz, J. P. L. Guadanucci, J. Wilson and D. Candia-Ramírez for advice concerning taxonomy and morphology of Theraphosidae T. Kudláček for advice concerning phylogenetic methods, T. Hamřík and O. Zimmerman are thanked for help with IT issues and P. Fabiánek, E. Hijmensen, T. Romanoff, R. Calvacante and S. Vogler are thanked for permission to use their photos in this work. We thank E. Kosnicki for grammatical review of the manuscript. We also thank three anonymous reviewers for their valuable comments that greatly improved the manuscript.

FUNDING

This work was funded by Spanish Ministry of Science and Innovation (MICINN) grant CGL 2009-07639, the Ministry of Economy and Competitiveness (MINECO) grant CGL 2016-80651-P (M.A.) and BES-2017-080538 scholarship (A.B.). Additional support was provided by 2017SGR73 from the Catalan Government (M.A.), AP 2008-01841 scholarship (MICINN) and Charles University Research Centre program UNCE 204069 (V.O.).

DATA AVAILABILITY

The sequence data that support the findings of this study are available at GenBank (https://www.ncbi.nlm.nih.gov/) under the following accession numbers: OK428700-OK428793, OM618647-OM618695, OM618640-OM618646, OM618635-OM618639, OM618696-OM618701, OM618702-OM618707 and OM654548-OM654553.

REFERENCES

Adams BJ, **Burnell AM**, **Powers TO. 1998.** A phylogenetic analysis of *Heterorhabditis* (Nemata: Rhabditidae) based on internal transcribed spacer 1 DNA sequence data. *Journal of Nematology* **30:** 22–39.

Adams DC, **Glynne E**, **Kaliontzopoulou A. 2020.** Interspecific allometry for sexual shape dimorphism: macroevolution of multivariate sexual phenotypes with application to Rensch's rule. *Evolution* **74:** 1908–1922.

Adams DC, **Collyer ML**, **Kaliontzopoulou A**, **Baken EK. 2021.** *Geomorph: software for geometric morphometric analyses*. R package v.4.0. https://cran.r-project.org/web/packages/geomorph/index.html (date last accessed 14 August 2020).

Agustí J, **Garcés M**, **Krijgsman W. 2006.** Evidence for African–Iberian exchanges during the Messinian in the Spanish mammalian record. *Palaeogeography, Palaeoclimatology, Palaeoecology* **238:** 5–14.

Ali FS, **Ismail M**, **Mamoon A. 2019.** Comparative molecular identification of genus *Dicentrarchus* using mitochondrial genes and internal transcribed spacer region. *Egyptian Journal of Aquatic Biology and Fisheries* **23:** 371–384.

Álvarez-Padilla F, **Hormiga G. 2008.** A protocol for digesting internal soft tissues and mounting spiders for scanning electron microscopy. *Journal of Arachnology* **35:** 538–542.

Anslan S, **Tedersoo L. 2015.** Performance of cytochrome c oxidase subunit I (COI), ribosomal DNA Large Subunit (LSU) and Internal Transcribed Spacer 2 (ITS2) in DNA barcoding of Collembola. *European Journal of Soil Biology* **69:** 1–7.

Ausserer A. 1871. Beiträge zur Kenntniss der Arachniden-Familie der Territelariae Thorell (Mygalidae Autor). *Verhandlungen der Kaiserlich-Königlichen Zoologisch-Botanischen Gesellschaft in Wien* **21:** 117–224.

Ausserer A. 1875. Zweiter Beitrag zur Kenntniss der Arachniden-Familie der Territelariae Thorell (Mygalidae Autor.). *Verhandlungen der Kaiserlich-Königlichen Zoologisch-Botanischen Gesellschaft in Wien* **25:** 125–206.

Baken EK, **Collyer ML**, **Kaliontzopoulou A**, **Adams DC. 2021.** Geomorph v.4.0 and gmShiny: enhanced analytics and a new graphical interface for a comprehensive morphometric experience. *Methods in Ecology and Evolution* **12:** 2355–2363.

Benoit PLG. 1965. Études sur les Barychelidae du Centre Africain (Araneae – Orthognatha) II. – Leptopelmatinae nouveaux. *Revue de Zoologie et de Botanique Africaines* **71:** 297–303.

Berland L. 1932. Les Arachnides (Scorpions, Araignées, etc. *Encyclopédie Entomologique* **16:** 1–485.

Bertani R. 2001. Revision, cladistic analysis, and zoogeography of *Vitalius, Nhandu*, and *Proshapalopus*; with notes on other theraphosine genera (Araneae, Theraphosidae). *Arquivos de Zoologia* **36:** 265–356.

Bidegaray-Batista L, **Arnedo MA. 2011.** Gone with the plate: the opening of the western Mediterranean Basin drove the diversification of ground-dweller spiders. *BMC Evolutionary Biology* **11:** 3171–3115.

Blakey RC. 2008. Gondwana paleogeography from assembly to breakup – a 500 m.y. odyssey. *Geological Society of America Special Papers* **441:** 1–28.

Bond JE. 2012. Phylogenetic treatment and taxonomic revision of the trapdoor spider genus *Aptostichus* Simon (Araneae, Mygalomorphae, Euctenizidae). *ZooKeys* **252:** 1–209.

Bond JE, **Stockman AK. 2008.** An integrative method for delimiting cohesion species: finding the population-species interface in a group of Californian trapdoor spiders with extreme genetic divergence and geographic structuring. *Systematic Biology* **57:** 628–646.

Bond JE, **Hedin MC**, **Ramirez MG**, **Opell BD. 2001.** Deep molecular divergence in the absence of morphological and ecological change in the Californian coastal dune endemic trapdoor spider *Aptostichus simus*. *Molecular Ecology* **10:** 899–910.

Bonnet P. 1957. *Bibliographia araneorum. Analyse méthodique de toute la littérature aranéologique jusqu'en 1939. Tome II. Systématique des araignées (Étude par ordre alphabétique) (3me partie: G-M)*. Toulouse: Douladoure, 1927–3026.

Boulton SJ, **Vandevelde J**, **Mather AE**, **Stokes M. 2016.** When did the Moroccan High Atlas Mountains get high? Constraints on neo-and active tectonics from fluvial geomorphology and palaeoaltimetry. 7th International INQUA Workshop on Paleoseismology, Active Tectonics and Archaeoseismology, Vol. 7. Crestone, Colorado: PATA.

Brown RP, **Suárez NM**, **Pestano J. 2002.** The Atlas Mountains as a biogeographical divide in North-West Africa: evidence from mtDNA evolution in the Agamid lizard *Agama impalearis*. *Molecular Phylogenetics and Evolution* **24:** 324–332.

Caeiro-Dias G, **Luís C**, **Pinho C**, **Crochet PA**, **Sillero N**, **Kaliontzopoulou A. 2018.** Lack of congruence of genetic and niche divergence in *Podarcis hispanicus* complex. *Journal of Zoological Systematics and Evolutionary Research* **56:** 479–492.

Calatayud-Mascarell A, **Sánchez-Vialas A. 2020.** Range extension of *Harpactirella insidiosa* (Denis, 1960) (Araneae: Mygalomorphae: Theraphosidae): a poorly known endemic spider from Morocco. *Graellsia* **76:** 113.

Candia-Ramírez DT, **Francke O. 2020.** Another stripe on the tiger makes no difference? Unexpected diversity in the widespread tiger tarantula *Davus pentaloris* (Araneae: Theraphosidae: Theraphosinae). *Zoological Journal of the Linnean Society* **192:** 75–104.

Cao X, **Liu J**, **Chen J**, **Zheng G**, **Kuntner M**, **Agnarson I. 2016.** Rapid dissemination of taxonomic discoveries based on DNA barcoding and morphology. *Scientific Reports* **6:** 1–13.

di Caporiacco L. 1937. Un manipolo di araneidi della Tripolitania costiera. *Monitore Zoologico Italiano* **48:** 57–60.

Carstens BC, **Pelletier A**, **Reid NM**, **Satler JD. 2013.** How to fail at species delimitation. *Molecular Ecology* **22:** 4369–4383.

Chambers EA, **Hillis DM. 2020.** The multispecies coalescent over-splits species in the case of geographically widespread taxa. *Systematic Biology* **69:** 184–193.

Cicero C, **Mason NA**, **Jiménez RA**, **Wang-Claypool CY**, **Bowie RCK. 2021.** Integrative taxonomy and geographic sampling underlie successful species delimitation. *Ornithology* **138:** 1–15.

Cooper SJB, **Harvey MS**, **Saint KM**, **Main BY. 2011.** Deep phylogeographic structuring of populations of the trapdoor spider *Moggridgea tingle* (Migidae) from southwestern Australia: evidence for long-term refugia within refugia. *Molecular Ecology* **20:** 3219–3236.

Denis J. 1960. Notes d'aranéologie marocaine. VIII. Un barychélide nouveau du Maroc. *Bulletin de la Société des Sciences Naturelles du Maroc* **39:** 185–189.

de Oca LM, **D'Elía G**, **Pérez-Miles F. 2016.** An integrative approach for species delimitation in the spider genus *Grammostola* (Theraphosidae, Mygalomorphae). *Zoologica Scripta* **45:** 322–333.

Drummond AJ, **Suchard MA**, **Rambaut A. 2012.** Bayesian phylogenetics with BEAUti and the BEAST 1.7. *Molecular Biology and Evolution* **29:** 1969–1973.

Dufour L. 1820. Observations sur quelques arachnides quadripulmonaires. *Annales Générales des Sciences Physiques* **5:** 96–116.

Edwards DL, **Knowles LL. 2014.** Species detection and individual assignment in species delimitation: can integrative data increase efficacy? *Proceedings of the Royale Society* **2811777:** 20132765.

El Harfi A, **Lang J**, **Salomon J. 1996.** Le remplissage continental cénozoïque du bassin d'avant pays de Ouarzazate. Implications sur l'évolution géodynamique du Haut-Atlas Central (Maroc). *Comptes Rendus de l´Académie des Sciences. Série 2. Sciences de la Terre et des Planètes* **323:** 623–630.

Ellero A, **Ottria G**, **Malusa MG**, **Ouanaimi H. 2012.** Structural geological analysis of the High Atlas (Morocco): evidence of a transpressional fold-thrust belt. In: Sharkov E, ed. *Tectonics – recent advances*. London: IntechOpen.

Ferretti N, **Soresi D**, **González A**, **Arnedo MA. 2019.** An integrative approach unveils speciation within the threatened spider *Calathotarsus simoni* (Araneae: Mygalomorphae: Migidae). *Systematics and Biodiversity* **17:** 439–457.

Fick SE, **Hijmans RJ. 2017.** WorldClim 2: new 1-km spatial resolution climate surfaces for global land areas. *International Journal of Climatology* **37:** 4302–4315.

Foley S, **Lüddecke T**, **Dong-Chiang C**, **Krehenwinkel H**, **Künzel S**, **Longhorn SJ**, **Wendt I**, **von Wirth V**, **Tänzler R**, **Vences M**, **Piel WH. 2019.** Tarantula phylogenomics: a robust phylogeny of multiple tarantula lineages inferred from transcriptome data sheds light on the prickly issue of urticating setae evolution. *Molecular Phylogenetics and Evolution* **140:** 106573.

Foley S, **Krehenwinkel H**, **Cheng DQ**, **Piel WH. 2021**. Phylogenomic analyses reveal a Gondwanan origin and repeated out of India colonization into Asia by tarantulas (Araneae: Theraphosidae). *PeerJ* **9e:** 11162.

Fujisawa T, **Barraclough TG. 2013.** Delimiting species using single-locus data and the generalized mixed yule coalescent approach: a revised method and evaluation on simulated data sets. *Systematic Biology* **62:** 707–724.

García-Alix A, **Minwer-Barakat R**, **Martín Suárez E**, **Freudenthal M**, **Aguirre J**, **Kaya F. 2016.** Updating the Europe–Africa small mammal exchange during the late Messinian. *Journal of Biogeography* **43:** 1336–1348.

Gomez F, **Barazangi M**, **Beauchamp W. 2000.** Role of the Atlas Mountains (northwest Africa) within African-Eurasian plate-boundary zone. *Geology* **28:** 769–864.

Gower JC. 1975. Generalized procrustes analysis. *Psychometrika* **40:** 33–51.

Grooten M, Almond REA, eds. 2018. *Living planet report 2018: aiming higher*. Gland: WWF.

Guadanucci JPL. 2014. Theraphosidae phylogeny: relationships of the Ischnocolinae genera (Araneae, Mygalomorphae). *Zoologica Scripta* **43:** 508–518.

Guadanucci JPL, Wendt I. 2014. Revision of the spider genus *Ischnocolus* Ausserer, 1871 (Mygalomorphae: Theraphosidae: Ischnocolinae). *Journal of Natural History* **48:** 387–402.

Hamilton CA, Formanowicz DR, Bond JE. 2011. Species delimitation and phylogeography of *Aphonopelma hentzi* (Araneae, Mygalomorphae, Theraphosidae): cryptic diversity in North American tarantulas. *PLoS One* **6:** e26207.

Hamilton CA, Hendrixson BE, Brewer MS, Bond JE. 2014. An evaluation of sampling effects on multiple DNA barcoding methods leads to an integrative approach for delimiting species: a case study of the North American tarantula genus *Aphonopelma* (Araneae, Mygalomorphae, Theraphosidae). *Molecular Phylogenetics and Evolution* **71:** 79–93.

Hamilton CA, Lemmon AR, Lemmon EM, Bond JE. 2016a. Expanding anchored hybrid enrichment to resolve both deep and shallow relationships within the spider tree of life. *BMC Evolutionary Biology* **16:** 1–20.

Hamilton CA, Hendrixson BE, Bond JE. 2016b. Taxonomic revision of the tarantula genus *Aphonopelma* Pocock, 1901 (Araneae, Mygalomorphae, Theraphosidae) within the United States. *ZooKeys* **560:** 1–340.

Harvey M, Main BY, Rix M, Cooper SJB. 2015. Refugia within refugia: In situ speciation and conservation of threatened *Bertmainius* (Araneae: Migidae), a new genus of relictual trapdoor spiders endemic to the mesic zone of south-western Australia. *Invertebrate Systematics* **29:** 511–553.

Hebert PD, Cywinska A, Ball SL, De Waard JR. 2003. Biological identifications through DNA barcodes. *Proceedings of the Royal Society of London. Series B: Biological Sciences* **270:** 313–321.

Hedin M, Starrett J, Hayashi C. 2013. Crossing the uncrossable: novel trans-valley biogeographic patterns revealed in the genetic history of low-dispersal mygalomorph spiders (Antrodiaetidae, *Antrodiaetus*) from California. *Molecular Ecology* **22:** 508–526.

Hendrixson BE, Guice AV, Bond JE. 2015. Integrative species delimitation and conservation of tarantulas (Araneae, Mygalomorphae, Theraphosidae) from a North American biodiversity hotspot. *Insect Conservation and Diversity* **8:** 120–131.

Herbert T, Lawrence K, Tzanova A, Peterson LC, Caballero-Gill R, Kelly CS. 2016. Late Miocene global cooling and the rise of modern ecosystems. *Nature Geoscience* **9:** 843–847.

Hewitt G. 2000. The genetic legacy of the Quaternary ice ages. *Nature* **405:** 907–913.

Hoang DT, Chernomor O, von Haeseler A, Minh BQ, Vinh LS. 2018. UFBoot2: improving the ultrafast bootstrap approximation. *Molecular Biology and Evolution* **35:** 518–522.

Husemann M, Schmitt T, Stathi I, Habel JC. 2012. Evolution and radiation in the scorpion *Buthus elmoutaouakili* Lourenço and Qi 2006 (Scorpiones: Buthidae) at the foothills of the Atlas Mountains (North Africa). *Journal of Heredity* **103:** 221–229.

Irwin DE. 2002. Phylogeographic breaks without geographic barriers to gene flow. *Evolution* **56:** 2383–2394.

Iturralde-Vinent AM. 2006. Meso-Cenozoic Caribbean paleogeography: implications for the historical biogeography of the region. *International Geology Review* **48:** 791–827.

Kalyaanamoorthy S, Minh BQ, Wong TKF, von Haeseler A, Jermiin LS. 2017. ModelFinder: fast model selection for accurate phylogenetic estimates. *Nature Methods* **14:** 587–589.

Kapli P, Lutteropp S, Zhang J, Kobert K, Pavlidis P, Stamatakis A, Flouri T. 2017. Multi-rate Poisson tree processes for single-locus species delimitation under maximum likelihood and Markov chain Monte Carlo. *Bioinformatics* **33:** 1630–1638.

Karsch F. 1879. Arachnologische Beiträge. *Zeitschrift für die Gesammten Naturwissenschaften* **52:** 534–562.

Katoh K, Misawa K, Kuma K, Miyata T. 2002. MAFFT: a novel method for rapid multiple sequence alignment based on fast Fourier transform. *Nucleic Acids Research* **30:** 3059–3066.

Klesser R, Husemann M, Schmitt T, Sousa P, Moussi A, Habel JC. 2021. Molecular biogeography of the Mediterranean *Buthus* species complex (Scorpiones: Buthidae) at its southern Palaearctic margin. *Biological Journal of the Linnean Society* **133:** 166–178.

Koch L. 1875. *Aegyptische und abyssinische Arachniden gesammelt von Herrn C. Jickeli*. Nürnberg: Bauer & Raspe.

Kress WJ, García-Robledo C, Uriarte M, Erickson DL. 2015. DNA barcodes for ecology, evolution, and conservation. *Trends in Ecology & Evolution* **30:** 25–35.

Kumar S, Stecher G, Tamura K. 2015. MEGA 7: molecular evolution genetics analysis v.7.0 for bigger datasets. *Molecular Biology and Evolution* **33:** 1870–1874.

Lanfear R, Calcott B, Ho SY, Guindon S. 2017. PartitionFinder: combined selection of partitioning schemes and substitution models for phylogenetic analyses. *Molecular Biology and Evolution* **29:** 1695–1701.

Leaché AD, Zhu T, Rannala B, Yang Z. 2019. The spectre of too many species. *Systematic Biology* **68:** 168–181.

Leavitt DH, Starrett J, Westphal MF, Hedin M. 2015. Multilocus sequence data reveal dozens of putative cryptic species in a radiation of endemic Californian mygalomorph spiders (Araneae, Mygalomorphae, Nemesiidae). *Molecular Phylogenetics and Evolution* **91:** 56–67.

Longhorn SJ, Nicholas M, Chuter J, Vogler AP. 2007. The utility of molecular markers from non-lethal DNA samples of the CITES II protected" tarantula" *Brachypelma vagans* (Araneae, Theraphosidae). *Journal of Arachnology* **35:** 278–292.

Longhorn SJ, Hamilton Ch. 2020. A molecular approach to the phylogeny of Theraphosidae and their kin. In: Pérez-Miles F, eds. *New World tarantulas – taxonomy, biogeography and evolutionary biology of Theraphosidae (Zoological Monographs 6)*. Heidelberg: Springer.

Lüddecke T, Krehenwinkel H, Canning G, Glaw F, Longhorn SJ, Taenzler R, Wendt I, Vences M. 2018.

Discovering the silk road: nuclear and mitochondrial sequence data resolve the phylogenetic relationships among theraphosid spider subfamilies. *Molecular Phylogenetics and Evolution* **119:** 63–70.

Lukhtanov VA. 2019. Species delimitation and analysis of cryptic species diversity in the XXI century. *Entomological Review* **99:** 463–472.

Matthews KJ, **Maloney KT**, **Zahirovic S**, **Williams SE**, **Seton M**, **Mueller RD. 2016.** Global plate boundary evolution and kinematics since the late Paleozoic. *Global and Planetary Change* **146:** 226–250.

Mayden RL. 1997. A hierarchy of species concepts: the denouement in the saga of the species problem. In: Claridge MF, Dawah HA, Wilson MR, eds. *Species: the units of diversity*. London: Chapman & Hall, 381–423.

Mayr E. 1982. Speciation and macroevolution. *Evolution* **36:** 1119–1132.

Mendoza J. 2016. Las tarántulas endémicas: problemática y conservación. *Conabio/Sedema* **2:** 245–248.

Mendoza J, **Francke OF. 2017.** Systematic revision of *Brachypelma* red-kneed tarantulas (Araneae: Theraphosidae), and the use of DNA barcodes to assist in the identification and conservation of CITES-listed species. *Invertebrate Systematics* **31:** 157–179.

Mittermeier RA, **Turner WR**, **Larsen FW**, **Brooks TM**, **Gascon C. 2011.** Global biodiversity conservation: the critical role of hotspots. In: Zachos FE, Habel JC, eds. *Biodiversity hotspots*. Berlin, Heidelberg: Springer, 3–22.

Moggridge JT. 1874. *Supplement to harvesting ants and trap-door spiders*. London: Reeve & Co.

Montemor VM, **West RC**, **Zamani A**, **Moradmand M**, **von Wirth V**, **Wendt I**, **Huber S**, **Guadanucci JPL. 2020.** Taxonomy of the genus *Ischnocolus* in the Middle East, with description of a new species from Oman and Iran (Araneae: Theraphosidae). *Zoology in the Middle East* **66:** 76–90.

Mora E, **Paspati A**, **Decae AE**, **Arnedo MA. 2017.** Rafting spiders or drifting islands? Origins and diversification of the endemic trapdoor spiders from the Balearic Islands, Western Mediterranean. *Journal of Biogeography* **44:** 924–936.

Nentwig W, **Blick T**, **Bosmans R**, **Gloor D**, **Hänggi A**, **Kropf C. 2020.** *Spiders of Europe, v.12*. Available at: https://www.araneae.nmbe.ch (accessed 20 December 2020) https://doi.org/10.24436/1.

Nguyen LT, **Schmidt HA**, **von Haeseler A**, **Minh BQ. 2015.** IQTREE: a fast and effective stochastic algorithm for estimating maximum-likelihood phylogenies. *Molecular Biology and Evolution* **32:** 268–274.

Opatova V, **Arnedo MA. 2014.** Spiders on a hot volcanic roof: colonisation pathways and phylogeography of the Canary Islands endemic trap-door spider *Titanidiops canariensis* (Araneae, Idiopidae). *PLoS One* **9:** e115078.

Opatova V, **Bond JE**, **Arnedo MA. 2013.** Ancient origins of the Mediterranean trap-door spiders of the family Ctenizidae (Araneae, Mygalomorphae). *Molecular Phylogenetics and Evolution* **69:** 1135–1145.

Opatova V, **Bond JE**, **Arnedo MA. 2016.** Uncovering the role of the western Mediterranean tectonics in shaping the diversity and distribution of the trap-door spider genus *Ummidia* (Araneae, Ctenizidae). *Journal of Biogeography* **43:** 1955–1966.

Opatova V, **Hamilton, CA**, **Hedin M**, **de Oca LM**, **Král J**, **Bond JE. 2020.** Phylogenetic systematics and evolution of the spider infraorder Mygalomorphae using genomic scale data. *Systematic Biology* **69:** 4671–4707.

Ortiz D, **Francke OF. 2016.** Two DNA barcodes and morphology for multi-method species delimitation in *Bonnetina* tarantulas (Araneae: Theraphosidae). *Molecular Phylogenetics and Evolution* **101:** 176–193.

Ortiz D, **Francke OF. 2017.** Reconciling morphological and molecular systematics in tarantulas (Araneae: Theraphosidae): revision of the Mexican endemic genus *Bonnetina*. *Zoological Journal of the Linnean Society* **180:** 819–886.

Ortiz D, **Francke OF**, **Bond JE. 2018.** A tangle of forms and phylogeny: extensive morphological homoplasy and molecular clock heterogeneity in *Bonnetina* and related tarantulas. *Molecular Phylogenetics and Evolution* **27:** 55–73.

Pappalardo AM, **Federico C**, **Sabella G**, **Saccone S**, **Ferrito V. 2015.** A COI nonsynonymous mutation as diagnostic tool for intraspecific discrimination in the European anchovy *Engraulis encrasicolus* (Linnaeus). *PLoS One* **10:** e0143297.

Paradis E, **Claude J**, **Strimmer K. 2004.** APE: analyses of phylogenetics and evolution in R language. *Bioinformatics* **20:** 289–290.

Pérez-Miles F, **Perafán C. 2017.** Behavior and biology of Mygalomorphae. In: Viera C, Gonzaga MO, eds. *Behaviour and ecology of spiders*. Cham: Springer International Publishing, 29–54.

Phillips SJ, **Anderson RP**, **Schapire RE. 2006.** Maximum entropy modeling for species geographic distribution. . *Ecological Modeling* **190:** 231–259.

Phillips SJ, **Dudík M**, **Schapire RE. 2017.** *Maxent software for modeling species niches and distributions (v.3.4.1)*. Available at: http://biodiversityinformatics.amnh.org/open_source/maxent/ (accessed 11 December 2020).

Pickard-Cambridge FO. 1897. Arachnida – Araneida and Opiliones. *Biologia Centrali-Americana, Zoology* **2:** 89–192.

Pocock RI. 1897. On the spiders of the suborder Mygalomorphae from the Ethiopian Region, contained in the collection of the British Museum. *Proceedings of the Zoological Society of London* **65:** 724–774.

Pons J, **Barraclough TG**, **Gomez-Zurita J**, **Cardoso A**, **Duran DP**, **Hazell S**, **Kamoun S**, **Sumlin WD**, **Vogler AP. 2006.** Sequence-based species delimitation for the DNA taxonomy of undescribed insects. *Systematic Biology* **55:** 595–609.

Puillandre N, **Lambert A**, **Brouillet S**, **Achaz G. 2012.** ABGD, automatic barcode gap discovery for primary species delimitation. *Molecular Ecology* **21:** 1864–1877.

Purcell WF. 1902. On the South African Theraphosidae or 'baviaan' spiders, in the collection of the South African Museum. *Transactions of the South African Philosophical Society* **11:** 319–347.

QGIS Development Team. **2020.** *QGIS Geographic Information System*. Open Source Geospatial Foundation

Project. Available at: http://qgis.osgeo.org (date last accessed 4 October 2020).

de Queiroz K. 1998. The general lineage concept of species, species criteria, and the process of speciation: a conceptual unification and terminological recommendations. In: Howard DJ, Berlocher SH, eds. *Endless forms: species and speciation*. Oxford: Oxford University Press.

de Queiroz K. 2007. Species concepts and species delimitation. *Systematic Biology* **56:** 879–886.

RStudio Team. 2019. *RStudio: Integrated Development Environment for R*. Boston, MA. Available at: http://www.rstudio.com/.

R Core Team. 2021. *R: a language and environment for statistical computing*. Vienna: R Foundation for Statistical Computing. Available at: https://www.R-project.org/ (date last accessed 20 October 2020).

Rambaut A. 2009. *FigTree, v.1.3.1*. Available at: http://tree.bio.ed.ac.uk/software/figtree/ (date last accessed 26 June 2020).

Rambaut A, Drummond AJ, Xie D, Baele G, Suchard MA. 2018. Posterior summarization in Bayesian phylogenetics using Tracer 1.7. *Systematic Biology* **67:** 901–904.

Raven RJ. 1985. The spider infraorder Mygalomorphae (Araneae): cladistics and systematics. *Bulletin of American Museum of Natural History* **182:** 1–180.

Raven RJ. 1994. Mygalomorph spiders of the Barychelidae in Australia and the western Pacific. *Memoirs of the Queensland Museum* **35:** 291–706.

Reimoser E. 1919. Katalog der echten Spinnen (Araneae) des Paläarktischen Gebietes. *Abhandlungen der Zoologisch-Botanischen Gesellschaft in Wien* **10:** 1–280.

Rix MG, Raven RJ, Austin AD, Cooper SJB, Harvey MS. 2018. Systematics of the spiny trapdoor spider genus *Bungulla* (Mygalomorphae: Idiopidae): revealing a remarkable radiation of mygalomorph spiders from the Western Australian arid zone. *Journal of Arachnology* **46:** 249–344.

Rix MG, Wilson JD, Harvey MS. 2020. First phylogenetic assessment and taxonomic synopsis of the open-holed trapdoor spiders (Mygalomorphae: Anamidae): a highly diverse mygalomorph lineage from Australia′s tropical eastern rainforests. *Invertebrate Systematics* **34:** 679–726.

Roewer CF. 1942. Katalog der Araneae von 1758 bis 1940. 1. Band (Mesothelae, Orthognatha, Labidognatha: Dysderaeformia, Scytodiformia, Pholciformia, Zodariiformia, Hersiliaeformia, Argyopiformia). *Natura, Bremen* **1:** 1–1040.

Rohlf FJ. 2008. *TPSUTIL, v.1.40*. New York: Department of Ecology and Evolution, State University of New York.

Rohlf FJ, Slice DE. 1990. Extensions of the Procrustes method for optimal superimposition of landmarks. *Systematic Zoology* **39:** 40–59.

Ronquist F, Huelsenbeck JP. 2003. MRBAYES 3: Bayesian phylogenetic inference under mixed models. *Bioinformatics* **19:** 1572–1574.

Rosenbaum G, Lister GS, Duboz C. 2002. Reconstruction of the tectonic evolution of the western Mediterranean since the Oligocene. In: Rosenbaum G, Lister GS, eds. Reconstruction of the evolution of the Alpine-Himalayan Orogen. *Journal of the Virtual Explorer* **8:** 107–130.

Roy V, Constantino R, Chassany V, Giusti-Miller S, Diouf M, Mora P, Harry M. 2014. Species delimitation and phylogeny in the genus *Nasutitermes* (Termitidae: Nasutitermitinae) in French Guiana. *Molecular Ecology* **23:** 902–920.

Rudloff JP. 2001. Anmerkungen zur systematischen Stellung von *Acanthopelma rufescens* F.O.P.-Cambridge, 1897 und *Acanthopelma annae* Reichling, 1997 (Ischnocolinae: Theraphosidae: Mygalomorphae), sowie die Einrichtung einer neuen Gattung *Reichlingia* gen. nov. (Mygalomorphae: Barychelidae: Trichopelmatinae). *Arthropoda* **9:** 14–20.

Satler JD, Carstens BC, Hedin M. 2013. Multilocus species delimitation in a complex of morphologically conserved trapdoor spiders (Mygalomorphae, Antrodiaetidae, *Aliatypus*). *Systematic Biology* **62:** 805–823.

Savory TH. 1928. *The biology of spiders*. London: Sidgwick & Jackson Ltd, 376.

Schlick-Steiner B, Steiner FM, Seifert B, Christian S, Crozier R. 2010. Integrative taxonomy: a multisource approach to exploring biodiversity. *Annual Review of Entomology* **55:** 421–438.

Schoch CL, Seifert KA, Huhndorf S, Robert V, Spouge JL, Levesque CA, Chen W, Fungal Barcoding Consortium. 2012. Nuclear ribosomal internal transcribed spacer (ITS) region as a universal DNA barcode marker for Fungi. *Proceedings of the National Academy of Sciences of the USA* **109:** 6241–6246.

Selden PA. 2002. First British Mesozoic spider, from Cretaceous amber of the Isle of Wight, southern England. *Palaeontology* **45:** 973–983.

Simon E. 1873. Aranéides nouveaux ou peu connus du midi de l'Europe. (2e mémoire). *Mémoires de la Société Royale des Sciences de Liège* **5:** 187–351.

Simon E. 1885. Études sur les Arachnides recueillis en Tunisie en 1883 et 1884 par MM. A. Letourneux, M. Sédillot et Valéry Mayet, membres de la mission de l'Exploration scientifique de la Tunisie. In: *Exploration scientifique de la Tunisie, publiée sous les auspices du Ministère de l'instruction publique. Zoologie – Arachnides*. Paris, 55.

Simon E. 1888. Études arachnologiques. 21e Mémoire. XXIX. Descriptions d'espèces et de genres nouveaux de l'Amérique centrale et des Antilles. *Annales de la Société Entomologique de France* **8:** 203–216.

Simon E. 1889. Étude sur les espèces de la famille des Aviculariidae qui habitent le nord de l'Afrique. *Actes de la Société Linnéenne de Bordeaux* **42:** 379–397.

Simon E. 1892. *Histoire naturelle des araignées. Deuxième édition, tome premier*. Paris: Roret, 1–256.

Simon E. 1903. *Histoire naturelle des araignées. Deuxième édition, tome second.* Paris: Roret, 669–1080.

Simon E. 1909. Étude sur les arachnides recueillis au Maroc par M. Martinez de la Escalera en 1907. *Memorias de la Real Sociedad Española de Historia Natural* **1:** 5–43.

Smith AM. 1990. *Baboon spiders: tarantulas of Africa and the Middle East*. London: Fitzgerald Publishing, 1–142.

Starrett J, Derkarabetian S, Hedin M, Bryson RW Jr, McCormack JE, Faircloth BC. 2017. High phylogenetic utility of an ultraconserved element probe set designed for Arachnida. *Molecular Ecology Resources* **17:** 812–823.

Sukumaran J, Knowles LL. 2017. Multispecies coalescent delimits structure, not species. *Proceedings of the National Academy of Sciences of the USA* **114:** 1607–1612.

Swofford DL. 2003. *PAUP*. Phylogenetic analysis using parsimony (* and other methods), v.4.* Sunderland: Sinauer Associates.

Tamajón Gómez R, Pertegal Pérez C, Rodríguez Castilla G. 2020. Primeros registros de *Ischnocolus valentinus* (Dufour, 1820) (Araneae: Theraphosidae) en la provincia de Córdoba (Andalucía, España). *Revista Ibérica de Aracnología* **36:** 165–166.

Turner SP, Longhorn SJ, Hamilton CA, Gabriel R, Pérez-Miles F, Vogler AP. 2018. Re-evaluating conservation priorities of New World tarantulas (Araneae: Theraphosidae) in a molecular framework indicates non-monophyly of the genera, *Aphonopelma* and *Brachypelma*. *Systematics and Biodiversity* **16:** 89–107.

Van Tuinen M, Torres CR. 2015. Potential for bias and low precision in molecular divergence time estimation of the Canopy of Life: an example from aquatic bird families. *Frontiers in Genetics* **6:** 203.

Vences M, Thomas M, Bonett RM, Vieites DR. 2005. Deciphering amphibian diversity through DNA barcoding: chances and challenges. *Philosophical Transactions of the Royal Society B: Biological Sciences* **360:** 1859–1868.

Walckenaer CA. 1805. *Tableau des aranéides ou caractères essentiels des tribus, genres, familles et races que renferme le genre Aranea de Linné, avec la désignation des espèces comprises dans chacune de ces divisions*. Paris: De L´Imprimerie de Dentu, 88.

Warren DL, Glor RE, Turelli M. 2010. ENMTools: a toolbox for comparative studies of environmental niche models. *Ecography* **33:** 607–611.

Wheeler WC, Coddington JA, Crowley LM, Dimitrov D, Goloboff PA, Griswold CE, Hormiga G, Prendini L, Ramirez MJ, Sierwald P, Almeida-Silva L, Alvarez-Padilla F, Arnedo MA, B, enavides Silva LR, Benjamin SP, Bond JE, Grismado CJ, Hasan E, Hedin M, Izquierdo MA, Labarque FM, Ledford J, Lopardo L, Maddison WP, Miller JA, Piacentini LN, Platnick NI, Polotow D, Silva-Davila D, Scharff N, Szuts T, Ubick D, Vink CJ, Wood HM, Zhang J. 2017. The spider tree of life: phylogeny of Araneae based on target-gene analyses from an extensive taxon sampling. *Cladistics* **33:** 574–616.

Wooten JA, Gibbs HL. 2012. Niche divergence and lineage diversification among closely related *Sistrurus* rattlesnakes. *Journal of Evolutionary Biology* **25:** 317–328.

World Spider Catalog. 2021. *World spider catalog, v.22.0*. Bern: Natural History Museum Bern. Available at: http://wsc.nmbe.ch (accessed 14 June 2021).

Wright K. 2006. *Corrgram: plot a correlogram, R package, v.1.1*. Available at: http://CRAN.R-project.org/package=corrgram (accessed 14 August 2020).

WWF. 2021. *Northern Africa: along the coast of Morocco and on the two easternmost Canary Islands in the eastern Atlantic*. Available at: https://www.worldwildlife.org/ecoregions/pa1212 (accessed 20 April 2021).

Xu X, Kuntner M, Bond JE, Hirotsugu O, Fengxiang L, Long Y, Daiqin L. 2019. Multi-tier species delimitation approach resolves conflicts in delineating the primitively segmented spider genus *Heptathela* endemic to Japanese islands. *Molecular Phylogenetics and Evolution* **151:** 106900.

Yao H, Song J, Liu C, Luo K, Han J, Li Y, Pang X, Xu H, Zhu Y, Xiao P, Chen S. 2010. Use of ITS2 region as the universal DNA barcode for plants and animals. *PLoS One* **5:** e13102.

Zonstein SL. 2018. Complementary data on the genus *Ischnocolus* (Araneae: Theraphosidae). *Israel Journal of Entomology* **48:** 105–118.

SUPPORTING INFORMATION

Additional Supporting Information may be found in the online version of this article at the publisher's web-site.

Table S1. Detailed locality information and GenBank accession codes for samples used in this study.
Table S2. Primers and PCR conditions for all loci used in this study.
Table S3. Partitions and evolutionary models found by PartitionFinder for both matrices.
Table S4. Niche overlap values (Schoener's D).
Table S5. Summarized ANOVA results of the character state 'prosoma lateral' between lineages. Significant values are highlighted.
Table S6. Summarized ANOVA results of the character state 'prosoma dorsal' between lineages. Significant values are highlighted.
Table S7. Summarized ANOVA results of the character state 'spinnerets lateral' between lineages. Significant values are highlighted.
Table S8. Summarized ANOVA results of the character state 'spinnerets dorsal' between lineages. Significant values are highlighted.
Figure S1. Bayesian BEAST tree of the family Theraphosidae with posterior probability values.
Figure S2. Bayesian consensus tree of the family Theraphosidae recovered from MrBayes with values of posterior probability values.
Figure S3. Maximum likelihood tree of the family Theraphosidae recovered from IQTREE with ultrafast bootstrap supports.
Figure S4. Maximum parsimony tree of the family Theraphosidae recovered by PAUP with bootstrap supports.
Figure S5. Bayesian BEAST tree of *Ischnocolus* with posterior probability values.

Figure S6. Maximum likelihood tree of *Ischnocolus* recovered by IQTREE with ultrafast bootstrap supports.
Figure S7. Bayesian consensus tree of *Ischnocolus* recovered by MrBayes with posterior probability values.
Figure S8. Results from niche identity tests conducted on 100 pseudoreplicates of randomized pairs of taxa. Values near 1.0 are considered as highly interchangeable models, values near 0.0 are considered as completely different. Black: *I. valentinus* and *I. mogadorensis*; dark grey: *I. elongatus* 'north' and 'south'; light grey: *I. elongatus* 'north' and 'central'; white *I. elongatus* 'south' and 'central'; stars: Schoener's D-values of niche overlap.